Chapter 5

Mixed-Phase Clouds: Progress and Challenges

A. Korolev,[a] G. McFarquhar,[b,r] P. R. Field,[c,d] C. Franklin,[e] P. Lawson,[f] Z. Wang,[g]
E. Williams,[h] S. J. Abel,[c] D. Axisa,[i,s] S. Borrmann,[j] J. Crosier,[k,l] J. Fugal,[m]
M. Krämer,[n] U. Lohmann,[o] O. Schlenczek,[m] M. Schnaiter,[p] and M. Wendisch[q]

[a] Environment and Climate Change Canada, Toronto, Ontario, Canada
[b] University of Illinois at Urbana–Champaign, Urbana, Illinois
[c] Met Office, Exeter, United Kingdom
[d] University of Leeds, Leeds, United Kingdom
[e] Bureau of Meteorology, Melbourne, Victoria, Australia
[f] Stratton Park Engineering Corporation, Boulder, Colorado
[g] University of Wyoming, Laramie, Wyoming
[h] Massachusetts Institute of Technology, Cambridge, Massachusetts
[i] National Center for Atmospheric Research, Boulder, Colorado
[j] Max Planck Institute for Chemistry, Mainz, Germany
[k] School of Earth and Environment, University of Manchester, Manchester, United Kingdom
[l] National Centre for Atmospheric Science, University of Manchester, Manchester, United Kingdom
[m] Institute for Atmospheric Physics, University of Mainz, Mainz, Germany
[n] Forschungszentrum Jülich, Jülich, Germany
[o] ETH Zurich, Institute for Atmospheric and Climate Science, Zurich, Switzerland
[p] Karlsruhe Institute of Technology, Karlsruhe, Germany
[q] University of Leipzig, Leipzig, Germany

ABSTRACT

Mixed-phase clouds represent a three-phase colloidal system consisting of water vapor, ice particles, and coexisting supercooled liquid droplets. Mixed-phase clouds are ubiquitous in the troposphere, occurring at all latitudes from the polar regions to the tropics. Because of their widespread nature, mixed-phase processes play critical roles in the life cycle of clouds, precipitation formation, cloud electrification, and the radiative energy balance on both regional and global scales. Yet, in spite of many decades of observations and theoretical studies, our knowledge and understanding of mixed-phase cloud processes remains incomplete. Mixed-phase clouds are notoriously difficult to represent in numerical weather prediction and climate models, and their description in theoretical cloud physics still presents complicated challenges. In this chapter, the current status of our knowledge on mixed-phase clouds, obtained from theoretical studies and observations, is reviewed. Recent progress, along with a discussion of problems and gaps in understanding the mixed-phase environment is summarized. Specific steps to improve our knowledge of mixed-phase clouds and their role in the climate and weather system are proposed.

[r] Current affiliation: Cooperative Institute for Mesoscale Meteorological Studies, School of Meteorology, University of Oklahoma, Norman, Oklahoma.

[s] Current affiliation: Droplet Measurement Technologies, Longmont, Colorado.

Corresponding author: Alexei Korolev, alexei.korolev@canada.ca

1. Introduction

a. Brief history of studies of mixed-phase clouds

The first documented laboratory observation of supercooled liquid water dates back to Gabriel Daniel Fahrenheit in 1724 (Fahrenheit 1724). Half a century later, in 1783, Horase Benedict de Saussure discovered

that small water droplets could remain in the liquid state at temperatures below 0°C. In a famous balloon flight in 1850, another French researcher, Jean-Augustin Barral, confirmed the existence of supercooled cloud droplets at temperatures as low as −10°C (Strangeways 2006). By the early twentieth century, Wegener (1911) pointed out that, where ice crystals and supercooled liquid droplets coexist, crystals grow at the expense of the droplets because the equilibrium water vapor pressure is lower over ice crystals than over liquid droplets. Subsequently, Bergeron used Wegener's ideas as a basis of his "ice crystal precipitation theory," originally described in his doctoral thesis (Bergeron 1928), which recognizes that the number concentration of ice particles in mixed-phase clouds must be much smaller than that of cloud droplets. Only then can ice particles grow to sizes sufficient to release precipitation (Bergeron 1935). Findeisen (1938) then contributed to the "ice crystal precipitation theory" with the experimental confirmation of enhanced growth of ice in the mixed phase, theoretical calculations, and in situ observations. The "ice crystal precipitation" theory is usually referred to as the Wegener–Bergeron–Findeisen (WBF; or the Bergeron–Findeisen) process and is one of the cornerstones of cloud physics. Early airborne in situ observations utilizing primitive replicator and impactor techniques showed that mixed-phase clouds are ubiquitous and that ice particles and liquid droplets can coexist at cloud temperatures as low as −40°C (Peppler 1940; Findeisen 1942; Weickmann 1945; Byers and Braham 1949; Zak 1949; Borovikov et al. 1963).

Significant progress in the measurement and development of the theory of mixed-phase environments has been achieved over the past 20 yr. Despite this progress, there are many gaps that still remain in the experimental and theoretical description of mixed-phase clouds and their effect on weather, the hydrological cycle, and regional and global climate. In the following sections, the main accomplishments of studies of mixed-phase clouds are summarized along with the formulation of questions and problems that still remain to be solved in future studies.

b. Significance of mixed-phase for clouds and climate

Airborne in situ (e.g., Korolev et al. 2003; Korolev 2008; McFarquhar and Cober 2004), ground (e.g., Shupe et al. 2001; Hogan et al. 2003b; Dong and Mace 2003), and aircraft-based remote sensing (e.g., Baum et al. 2000; Wang et al. 2012; Plummer et al. 2014) and satellite studies (e.g., Mioche et al. 2015; Tan et al. 2014) have shown that clouds with both liquid water and ice can occur in a wide variety of locations from the tropics to the poles, are associated with multiple cloud types and meteorological conditions, and can occur throughout the year in all seasons. Global quantitative estimates of the prevalence of mixed-phase clouds are difficult because of the limited data from airborne probes, the small geographic coverage of ground-based remote sensing sites, and the uncertainty in phase detection from satellite remote sensors, especially over high latitudes. Nevertheless, depolarization measurements from the spaceborne CALIOP (acronyms are defined in Table 5-1) lidar have shown that supercooled water is frequently observed near storm tracks in high-latitude regions and also over continental areas (e.g., Hu et al. 2010).

Studies in the Arctic and over the Southern Ocean have especially highlighted the importance of mixed-phase clouds. Given the prevalence of mixed-phase clouds over the Arctic (Shupe et al. 2001, 2005; Intrieri et al. 2002), they exert a major influence on both the surface and the top-of-atmosphere radiative budget there (e.g., Dong and Mace 2003; Zuidema et al. 2005). Supercooled water and mixed-phase clouds are also common over the Southern Ocean (e.g., Hu et al. 2010; Kanitz et al. 2011; A. E. Morrison et al. 2011; Huang et al. 2012). It has been hypothesized that the inability of models to represent the frequent occurrence of supercooled water and the mixed phase is one of the main reasons why climate models (Bodas-Salcedo et al. 2016) and reanalysis products (Naud et al. 2014) reveal large errors in the annual mean downwelling solar (shortwave) absorbed radiation at the surface in this region. Even if models exhibit the correct total condensed water content, the same amount of condensed water in the ice phase rather than in the liquid phase has a lower albedo. The reason for that is that ice particles would be fewer and larger than the corresponding liquid droplets, and thus the optical thickness of the glaciated cloud is less. Therefore, it is important to know what controls the phase of clouds not only because the radiative properties of water and ice are different (e.g., Sun and Shine 1994) but also because the development of precipitation (e.g., Field and Heymsfield 2015; Mülmenstädt et al. 2015), and hence the lifetime of the clouds, is controlled by the ice phase. In addition, Tsushima et al. (2006) found the amount of cloud ice in the mixed-phase layer determined how much the cloud water distribution changed for experiments with doubled carbon dioxide.

Despite their importance for Earth's climate, large uncertainties remain in the representation of mixed-phase clouds in global climate models (e.g., McCoy et al. 2016). This is problematic because, among others, Gregory and Morris (1996) and Li and Le Treut (1992) showed that modeled fields of important cloud properties such as cloud cover, cloud water content, cloud albedo, outgoing terrestrial (longwave) radiation, and the sensitivity parameter of Cess and Potter (1988) depend significantly on the temperature range where liquid water and ice are

TABLE 5-1. Abbreviations.

2D-S	2D stereo probe
AIDA	Aerosol Interaction and Dynamics in the Atmosphere
AIRS	Atmospheric Infrared Sounder
BCPD	Backscatter Cloud Probe with Polarization Detection
BWER	Bounded weak echo region
CALIOP	Cloud–Aerosol Lidar with Orthogonal Polarization
CALIPSO	*Cloud–Aerosol Lidar and Infrared Pathfinder Satellite Observations*
CAPE	Convective available potential energy
CAS	Cloud and Aerosol Spectrometer
CAS-DPOL	Cloud and Aerosol Spectrometer with Detection Polarization
CCN	Cloud condensation nuclei
CDP	Cloud Droplet Probe
CERN	Conseil Européen pour la Recherche Nucléaire (European Organization for Nuclear Research)
CLOUD	Cosmics Leaving Outdoor Droplets
CMIP	Coupled Model Intercomparison Project
CPI	Cloud particle imager
CPL	Cloud physics lidar
CPSPD	Cloud Particle Spectrometer with Polarization Detection
ECMWF	European Centre for Medium-Range Weather Forecasts
FCDP	Fast Cloud Droplet Probe
FSSP	Forward Scattering Spectrometer Probe
HALO	High Altitude and Long Range Research Aircraft
HALOHOLO	HALO Holographic probe
HOLODEC	Holographic Detector for Clouds probe
HSI	High Speed Imager
INP	Ice nucleating particles
IR	Infrared
IWC	Ice water content
IWP	Ice water path
LWP	Liquid water path
MMCR	Millimeter wavelength cloud radar
MODIS	Moderate Resolution Imaging Spectroradiometer
MPL	Micropulse lidar
MWR	Microwave radiometer
NIR	Near-infrared
NSA	North Slope of Alaska
OAP	Optical array probe
PDI	Phase Doppler interferometer
PDL	Polarization diversity lidar
PDPA	Phase Doppler Particle Analyzer
PHIPS-HALO	Particle Habit Imaging and Polar Scattering probe for the HALO aircraft
PMS	Particle Measuring Systems
POLDER	Polarization and Directionality of the Earth's Reflectances
PPD-2K	Particle Phase Discriminator, mark 2
RICE	Rosemount Icing Detector
SEA	Science Engineering Associates
SHEBA	Surface Heat Budget of the Arctic Ocean
SID	Small Ice Detector
TWC	Total water content
VHF	Very high frequency
VIPS	Video ice particle sampler
WBF	Wegener–Bergeron–Findeisen
WCL	Wyoming Cloud Lidar
WCR	Wyoming Cloud Radar

assumed to coexist. Even when separate variables are used to predict the ice and liquid contents (Komurcu et al. 2014; Cesana et al. 2015), all climate models from phase 5 of the Coupled Model Intercomparison Project (CMIP5) examined by McCoy et al. (2015) effectively partitioned the liquid water ratio only as a function of temperature. However, the temperature at which ice and liquid are equally mixed, and the glaciation temperature, varied by as much as 40°C. Large impacts of the mixed phase on cloud albedo (McCoy et al. 2014) were also found.

Understanding mixed-phase cloud processes is also important for quantifying aerosol indirect effects. Although it is recognized that changes in aerosol number concentration can change liquid cloud droplet concentrations and cloud radiative effects through different indirect effects (Twomey 1974; Albrecht 1989; Hansen et al. 1997) and dynamical responses (Pincus and Baker 1994; Boers and Mitchell 1994), the response of ice-phase and mixed-phase clouds to such changes are not as well known. Three indirect effects that act in mixed-phase clouds have been proposed: (i) the glaciation indirect effect, where increases in ice crystal concentrations are associated with increases in the number of ice nucleating particles (Lohmann 2002); (ii) the riming indirect effect, where decreased droplet sizes are associated with increases in cloud condensation nuclei (CCN), which consequently decrease the ice water content (IWC) by inhibiting riming growth (Borys et al. 2003); and (iii) a cold second indirect effect, where increases in CCN increase the droplet number concentration, decrease liquid drop sizes, and inhibit ice crystal formation through less efficient secondary ice crystal production (Rangno and Hobbs 2001). Lance et al. (2010) and Jackson et al. (2012) have examined the importance of these effects in Arctic mixed-phase clouds but have not categorically determined the relative importance of each effect because of the need to acquire data in a large variety of surface, meteorological, and cloud conditions.

In addition to impacts on climate, the hydrological cycle and radiative energy balance, and the hydrological cycle, mixed-phase clouds are important for the understanding of cloud electrification and how cloud seeding might act to increase or inhibit precipitation. However, much is still unknown about the role of mixed-phase clouds in these processes. For example, it is recognized that the presence of supercooled water plays an important role in the charge separation in a cloud (section 5), but the exact mechanism by which charges are transferred between different sizes and phases of particles is still under debate. Further, although it is known that artificially seeded clouds can promote the development of the ice-phase through the supply of ice nucleating particles (e.g., Tessendorf et al. 2012, 2015), it is not clear how the evolution of the system or the amount and distribution of precipitation is affected by this seeding, or by the time and place at which the seeding agent is added.

2. Definition of mixed-phase clouds

The measurement of the microphysical properties of mixed-phase clouds continues to be a challenging task. During the last two decades, a variety of instruments have been developed for characterizing mixed-phase clouds. These instruments can be sorted into three main categories: 1) in situ, 2) active remote sensing, and 3) passive remote sensing. Each class of instrument has fundamentally different scales for spatial averaging, utilizes different metrics to describe cloud microstructure, and applies different definitions of cloud phase composition. Unfortunately, there is no consensus regarding what defines "liquid," "mixed phase," and "ice" conditions. For instance, should a cloud be defined as mixed phase if it has one ice particle per 10 or per 10^{12} liquid droplets? Should a cloud be considered glaciated if it contains one liquid droplet per 10^{12} ice particles, or is it still mixed phase?

The absence of a common definition of the mixed phase complicates intercomparisons of cloud phase measurements performed by in situ and remote sensing techniques. The results of cloud phase measurements are used in cloud and climate modeling studies for evaluation of simulations. Such comparisons require the model definition of mixed-phase clouds to also be consistent with the in situ or remote sensing definitions. The strong need for further improvement of cloud and climate models motivates the development of a well-defined commonly accepted definition of the mixed phase, which should be consistent with the remote sensing and in situ studies. In this section, the definitions of mixed phase used by in situ and remote sensing techniques are outlined.

a. In situ definition

In measurements of cloud microstructure, different investigators have used various definitions of the mixed phase. In many ways, these definitions depend on the type, resolution, and accuracy of the instruments or techniques being utilized to measure the cloud particles.

Early in situ observations of the phase composition of clouds were based on a visual assessment of images of cloud particles collected by a replicator. A sampled cloud was categorized as mixed phase if the replicator's sample contained images of both ice crystals and liquid cloud droplets (e.g., Peppler 1940; Weickmann 1945; Zak 1949; Borovikov et al. 1963; Mossop et al. 1970). Subsequently, if the sample contained only ice crystals or only liquid droplets, then the cloud was considered either ice or liquid, respectively. Basically, the replicator identification of the phase composition was based on an assessment of some minimum concentration of ice and liquid water particles present in the replicator's sampled volume. The accuracy of such cloud phase identification was low, and, furthermore, it was biased because of the different collection efficiencies of ice particles and liquid droplets, low sampling statistics, a sparsity of data points, and other issues.

The development of airborne optical and hot-wire probes resulted in a more complex set of rules for phase identification. For example, Hobbs and Radke

(1975) used a combination of an ice crystal counter, a replicator, and a hot-wire Johnson–Williams probe to determine the phase composition of clouds. Moss and Johnson (1994) applied an ice-to-water mass ratio deduced from image recognition of particle images measured by the PMS Optical Array Probes OAP-2DC and OAP-2DP (Brenguier et al. 2013) to characterize the cloud phase. Cober et al. (2001b) used a complex set of rules based on measurements from a Forward Scattering Spectrometer Probe (FSSP), OAP-2DC, Nevzorov probe, and Rosemount (Brenguier et al. 2013) Icing Cylinder to determine phase composition. McFarquhar et al. (2013) used measures of particle morphology derived from particles with dimensions smaller than $100\,\mu$m imaged by a cloud particle imager (CPI) to define the cloud phase.

A generic way of describing the mixed phase was proposed by Korolev et al. (1998), who defined an ice (or liquid) phase fraction coefficient as

$$\mu_{\mathrm{ice}} = \frac{\alpha_{\mathrm{ice}}}{\alpha_{\mathrm{ice}} + \alpha_{\mathrm{liq}}}, \qquad (5\text{-}1)$$

where α_{ice} and α_{liq} are based on the specific cloud microphysical metric characterizing ice and liquid components of the cloud, respectively, such as N_i and N_w, the number concentration of ice particles and liquid droplets; β_{ice} and β_{liq}, the extinction coefficient associated with ice and liquid phase; and IWC and liquid water content (LWC). The advantage of the use of the phase fraction coefficient μ_{ice} is that it varies in a limited range $0 \le \mu_{\mathrm{ice}} \le 1$, where $\mu_{\mathrm{ice}} = 0$ corresponds to liquid phase, and $\mu_{\mathrm{ice}} = 1$ corresponds to ice phase. Some studies choose to use the liquid-phase fraction coefficient μ_{liq}, which is related to the ice fraction as $\mu_{\mathrm{liq}} = 1 - \mu_{\mathrm{ice}}$. The decision of which metric to use for α_{ice} and α_{liq} depends on the utilized instrumentation and application. Thus, for analysis of the radiative transfer in mixed-phase clouds it would be most appropriate to use α metrics based on β_{ice} and β_{liq}. In recent studies, most in situ characterization of mixed-phase clouds has been based on measurements of IWC and LWC (i.e., $\alpha_{\mathrm{ice}} = $ IWC and $\alpha_{\mathrm{liq}} = $ LWC).

An important aspect in the definition of the mixed phase is related to what values of $\mu_{\mathrm{ice}}^{(l)}$ and $\mu_{\mathrm{ice}}^{(i)}$ should be assigned for the separation of liquid $[0 \le \mu_{\mathrm{ice}} \le \mu_{\mathrm{ice}}^{(l)}]$, ice $[\mu_{\mathrm{ice}}^{(i)} \le \mu_{\mathrm{ice}} \le 1]$), and mixed-phase $[\mu_{\mathrm{ice}}^{(l)} < \mu_{\mathrm{ice}} \le \mu_{\mathrm{ice}}^{(i)}]$ conditions. Currently, there is no physical basis for a particular choice of $\mu_{\mathrm{ice}}^{(l)}$ and $\mu_{\mathrm{ice}}^{(i)}$. In many studies ,the choice of $\mu_{\mathrm{ice}}^{(l)}$ and $\mu_{\mathrm{ice}}^{(i)}$ is dictated by the type and accuracy of the airborne instrumentation, such as $\mu_{\mathrm{ice}}^{(l)} = 0.1$ and $\mu_{\mathrm{ice}}^{(i)} = 0.9$ (Korolev et al. 2003; Field et al. 2004; and others).

Another important aspect in the definition of cloud phase is related to the spatial (or volumetric) averaging scale Δx.
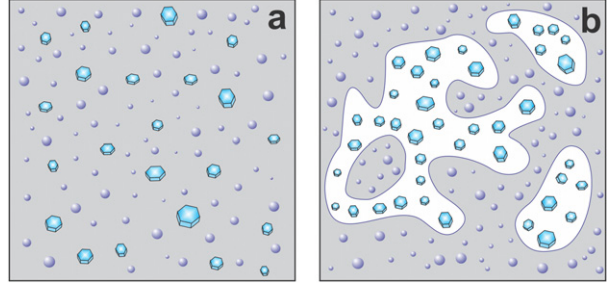

FIG. 5-1. Conceptual diagrams of the phase inhomogeneity in mixed clouds: (a) droplets and ice particles are mixed homogeneously (genuinely mixed-phase clouds); (b) droplets and ice particles are inhomogeneously mixed, and they are forming single-phase clusters (conditionally mixed-phase clouds).

If $\Delta x \to 0$, the state of the mixed-phase colloidal system will be either liquid or ice. However, for $\Delta x \to \infty$, all clouds within the temperature range -40°C $< T < 0^\circ$C will be mixed phase. In between these two extremes of Δx, ice particles and liquid droplets may form a homogeneous mixture of ice and liquid (Fig. 5-1a) or an inhomogeneous mixture when ice particles and liquid droplets are clustered in single-phase liquid or ice cloud regions (Fig. 5-1b). The first type of mixed-phase clouds will be referred to as ''genuine'' mixed-phase and the second type as ''conditional'' mixed phase. In the conditionally mixed-phase clouds, the interaction between ice crystals and liquid droplets is hindered because of their spatial separation. As a result, the thermodynamic and radiative properties of genuine and conditional mixed-phase clouds might be different. Therefore, it is important to properly adjust Δx, $\mu_{\mathrm{ice}}^{(l)}$, and $\mu_{\mathrm{ice}}^{(i)}$ in order to segregate during observations genuine and conditionally mixed-phase clouds.

At the present stage, the choice of Δx is selected based on instrumental characteristics and requirements of statistically significant sampling. Most airborne in situ measurements are integrated at scales of $\Delta x \approx 100$ m (i.e., $\Delta t = 1$ s at airspeed $100\,\mathrm{m\,s}^{-1}$).

It is important to note that the definition of a mixed-phase cloud is part of a more general definition of a cloud regardless of its thermodynamic phase. As in the case of the definition of the mixed phase, there is no commonly accepted definition of a cloud. For example, McFarquhar et al. (2007) showed that the fraction of mixed-phase cloud observations varied depending on whether a threshold TWC of 0.001 or 0.005 g m^{-3} was used to define clouds. Presently the cloud definition depends on the equipment used to identify and study cloud. As equipment sensitivity varies, so does each research teams' ability to detect the presence of a cloud. In other words, the community is currently relying on instrument-subjective definitions of clouds and

their thermodynamic phase, rather than on physically based concepts.

b. Remote sensing definition based on radar, lidar, and radiometer measurements

Cloud phase identification is a necessary step to remotely sense cloud microphysical properties because liquid droplets and ice crystals have different scattering, absorption, and emission properties. Compared with in situ measurements, which usually have very small sampling volumes and with averaging along flight paths, remote sensors have much larger sampling volumes involving both vertical and horizontal averaging. However, sampling volumes of remote sensors vary strongly with instrument type (active versus passive, visible compared to IR and microwave) and also evolve with time as sensor technology advances. Therefore, remote sensing–based cloud phase definition is more dependent on instrumentation than is in situ measured phase.

Passive sensor measurements offer mainly cloud-layer phase discrimination along the sensors view field (e.g., vertical column) or more weighted on the cloud top, rather than vertically resolved discrimination of cloud-layer phase, which can be provided by active sensor measurements. Passive satellite-based sensors measure column-integrated radiance over a wide-range swath to categorize a cloudy pixel by thermodynamic phase based on its radiative signatures and are usually dominated by the cloud-top characteristics. Therefore, geometrically thick and multilayer clouds present a challenging situation for passive retrievals.

Active sensors (i.e., lidars and cloud radars) provide vertically resolved cloud signals (from a few meters to a few hundred meters), which offer height-dependent cloud phase discrimination. However, lidars are limited by their penetration depth and, thus, provide vertical profile measurements for optically thin clouds. Active remote sensors can be deployed on ground-based fixed sites, aircraft, or satellites (*CloudSat* and *CALIPSO*).

The definition of cloud thermodynamic phase from remote sensor measurements, especially for passive sensors, is a radiative-equivalent cloud phase (based on β_{ice} and β_{liq} or τ_{ice} and τ_{liq}, where τ is the cloud-layer optical depth). As indicated by in situ measurements, mixed-phase regions are dominated either by liquid phase or ice phase; therefore, identifying mixed-phase clouds from radiative measurements has been a challenging task. The Moderate Resolution Imaging Spectroradiometer (MODIS), a passive sensor that observes clouds and aerosol particles from space, categorizes a cloudy pixel as only liquid, ice or undetermined phase (Platnick et al. 2017). With additional measurements of polarization properties of the cloud-reflected solar radiance, such as

those provided from the Polarization and Directionality of the Earth's Reflectances (POLDER) instrument (Buriez et al. 1997), improved information for each cloudy pixel can be assigned (e.g., mixed-phase clouds can be identified for each cloudy pixel). Although the radiative signals of different phases of clouds are linked with τ_{ice} and τ_{liq}, the phase determinations for passive sensors are not based on the phase fraction coefficient [Eq. (5-1)] using τ_{ice} and τ_{liq}. By taking advantage of the different sensitivities of lidar and cloud radar to liquid droplets and ice crystals, combined lidar–radar and passive microwave measurements offer reliable identification of mixed-phase clouds, as discussed in detail in section 4b.

Although there are challenges in providing microphysically consistent definitions of mixed-phase clouds for in situ and remote sensing techniques, remote sensing measurements from space are critical in providing the global distribution of mixed-phase clouds. Understanding the limitations of the remotely sensed cloud phase is a necessary step to more efficient use of these global measurements. One of the caveats of the remote sensing techniques is that they may artificially enhance the occurrence of mixed-phase clouds because of mixing viewing spatially separated pure ice and pure liquid cloud regions in their large sampling volumes. As illustrated in Fig. 5-1b, such clouds will be identified as conditionally mixed-phase clouds. However, the airborne and ground-based lidar and radar measurements have the potential to identify genuine and conditional mixed-phase clouds at a spatial scale of 10 m or smaller. In the future, the synergy of in situ measurements with different platform remote sensing will lead to an advanced understanding of mixed-phase clouds across the globe, even though applying the same definition of mixed-phase cloud may not be possible.

c. Physically based definition of cloud phase

In this section, the basic principles of a physically based definition of cloud phase are discussed. The first approach is based on a comparison between the characteristic lifetime of a cloud τ_{cl} and characteristic time of changes of the phase fraction τ_{pf} inside a cloud parcel. Since the mixed phase is a colloidally unstable system, the phase fraction is a function of time $\mu_{\text{ice}}(t)$, which changes from 0 at the beginning of glaciation to 1 at the final stage of glaciation. The characteristic time change of μ_{ice} can be estimated as $\tau_{\text{pf}} \sim \mu_{\text{ice}}(t)/(\partial\mu_{\text{ice}}/\partial t)$. If $\mu_{\text{ice}}(t) \ll 1$, and the characteristic cloud lifetime $\tau_{\text{cl}} \ll \tau_{\text{pf}}$, the cloud may be considered as liquid. In this case, ice crystals will have only a minor effect on the cloud microstructure before the cloud dissipates. If $\mu_{\text{ice}}(t) \cong 1$, and $\tau_{\text{pf}} \to \infty$, the cloud is in the ice phase. In this case, the cloud is glaciated and the phase fraction has reached a steady state. In all intermediate cases, it is the mixed phase.
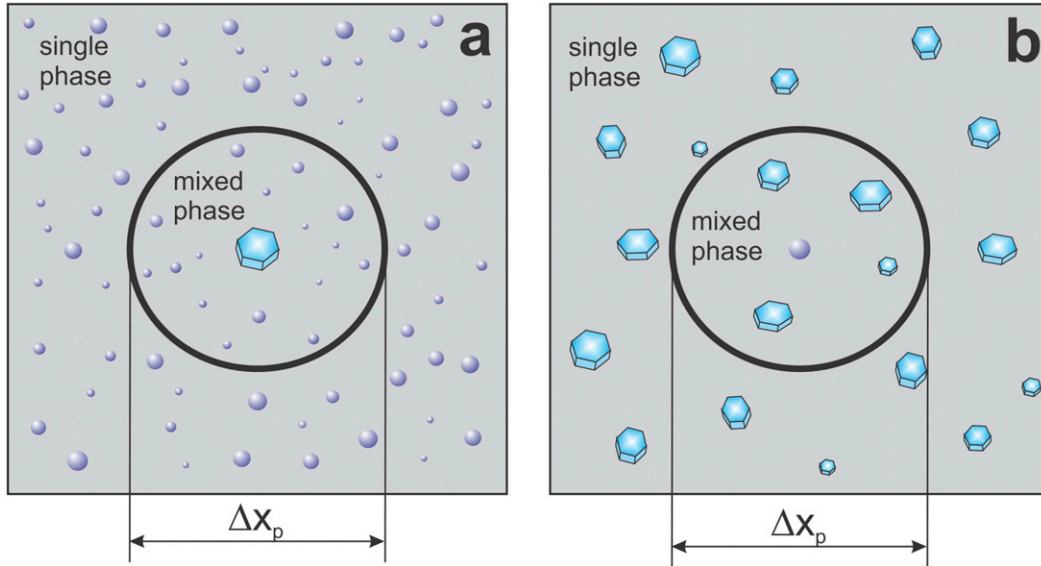
FIG. 5-2. Conceptual diagram of the spatial distribution of cloud particles in a mixed-phase cloud showing cloud space with characteristic size Δx_p beyond which the colloidal system may be considered as a single-phase: (a) liquid or (b) ice.

Another aspect of a physically based definition of the mixed phase is related to the spatial phase scale Δx_p. Figure 5-2 shows a conceptual diagram of (i) an ice crystal surrounded by liquid droplets and (ii) a cloud droplet surrounded by ice crystals in a mixed-phase cloud. These diagrams mimic the spatial distribution of cloud particles in mixed-phase clouds at different stages of glaciation. Of fundamental importance is determining the characteristic distance Δx_p around an ice particle (Fig. 5-2a) or liquid droplet (Fig. 5-1b) such that at distances $x < \Delta x_p/2$ the cloud is considered a mixed phase, and at $x > \Delta x_p/2$ it is considered single-phase [i.e., liquid (Fig. 5-2a) or ice (Fig. 5-2b)]. The definition of Δx_p should be based on consideration of the distances up to which the ice particle can affect the surrounding liquid droplets (Fig. 5-2a) and the distances over which ice particles may affect the droplet that they surround (Fig. 5-2b). In other words, cloud particles at $x > \Delta x_p/2$ are not sensitive to the cloud particles of the opposite phase and behave as a single phase. The definition of Δx_p should be related to some predetermined time scale τ, which may be a function of the characteristic time such as turbulent mixing τ_t, water vapor diffusion τ_d, phase relaxation τ_p, particle residence time in the cloud volume τ_r related to its fall velocity, or glaciation time τ_g.

d. General principles of cloud phase definition

It may not be possible to develop a single definition of the phase composition of a colloidal system that is universally applicable. In each particular study, the definition

of cloud phase should be governed by the problem being considered (e.g., radiation and climate, precipitation formation, cloud glaciation, aircraft icing, cloud electrification, cloud seeding, remote sensing). The definition of cloud phase in each particular case should be based on the choice of (i) cloud phase metrics μ_{ice}; (ii) thresholds separating liquid, mixed, and ice phase $\mu_{ice}^{(l)}$ and $\mu_{ice}^{(i)}$; and (3) the spatial averaging scale Δx. The choice of instrumentation should be tailored to address the requirements related to μ_{ice}, $\mu_{ice}^{(l)}$, $\mu_{ice}^{(i)}$, and Δx.

3. Theoretical description of mixed-phase clouds

Theoretical analysis of the behavior of mixed-phase clouds has been performed in a number of studies (e.g., Shifrin and Perelman 1960; Mazin 1986; van der Hage 1995; Korolev and Mazin 2003; Castellano et al. 2004, 2008; Korolev 2007, 2008; Korolev and Field 2008; Yang et al. 2013, 2014; Hill et al. 2014; Field et al. 2014; Pinsky et al. 2014, 2015). Below we discuss the main achievements in the theoretical investigations of mixed-phase clouds.

a. Basic equations

This section focuses on describing the interaction of liquid droplets and ice particles in a mixed-phase environment through the gaseous phase. The water vapor pressure ultimately determines the growth rates of the ice and liquid phases and their partitioning. Therefore, the equation describing the rate of change of water

vapor is one of the central equations in the theory of mixed-phase clouds.

For a vertically moving adiabatic mixed-phase parcel initially at a liquid water vapor supersaturation S_w, the change to the supersaturation dS_w can be described as (Korolev and Mazin 2003)

$$\frac{1}{S_w + 1} \frac{dS_w}{dt} = a_0 u_z - a_2 B_i^* N_i \bar{r}_i + (a_1 B_w N_w \bar{r}_w + a_2 B_i N_i \bar{r}_i) S_w.$$

$$(5\text{-}2)$$

Here $\bar{r}_w$, $\bar{r}_i$, N_w, and N_i are the average liquid droplet and ice particle radii and number concentrations, respectively; u_z is the vertical velocity; and a_0, a_1, a_2, B_w, B_i, and B_i^* are coefficients that depend weakly on the air temperature T and pressure P. With a high level of accuracy, the effect of the temperature and pressure dependence of these coefficients on S_w can be disregarded within a few hundred meters of vertical displacement. Several other forms of Eq. (5-2) can be found in Korolev and Mazin (2003) and Pinsky et al. (2014). After expanding dependencies of $\bar{r}_w$ and $\bar{r}_i$ on S_w Eq. (5-2) turns into an integro-differential equation that does not have a known analytical solution. However, Eq. (5-2) can be integrated analytically under the assumption that $\bar{r}_w =$ const. and $\bar{r}_i =$ const. In this case, the solution of Eq. (5-2) yields the limiting supersaturation

$$S_{\mathrm{qs},w} = \frac{a_0 u_z - b_i^* N_i \bar{r}_i}{b_w N_w \bar{r}_w + b_i N_i \bar{r}_i},$$

$$(5\text{-}3)$$

to which $S_w(t)$ asymptotically approaches with a characteristic time τ_p given by

$$\frac{1}{\tau_p} \cong \frac{1}{\tau_{pw}} + \frac{1}{\tau_{pi}},$$

$$(5\text{-}4)$$

where $\tau_{pw} = 1/(c_w N_w \bar{r}_w)$ and $\tau_{pi} = 1/(c_i N_i \bar{r}_i)$ are the times of phase relaxation associated with the liquid droplets and ice particles composing the mixed-phase cloud, respectively; and b_w, b_i, b_i^*, c_w, and b_i are coefficients depending on T and P. The value $S_{\mathrm{qs},w}$ is usually referred to as the quasi-steady supersaturation, and τ_p is the time of phase relaxation. A notable property of the quasi-steady approximation is that $S_{\mathrm{qs},w}$ approaches $S_w(t)$ within the characteristic time $t < 3\tau_p$ (Korolev and Mazin 2003).

Typically, the time of phase relaxation in liquid τ_{pw} and mixed-phase τ_p clouds ranges from one-tenth of a second to several seconds, whereas in ice clouds, τ_{pi} ranges from tens of seconds to tens of minutes. Since the measurement of in-cloud supersaturation remains a challenging task in experimental cloud physics, the quasi-steady supersaturation $S_{\mathrm{qs},w}$ can be used to estimate the humidity inside clouds from the measurements of $N_w \bar{r}_w$, $N_i \bar{r}_i$, and u_z.

The main outcomes from the analysis of Eqs. (5-2)–(5-4) are as follows: (i) the quasi-steady humidity in mixed-phase and liquid clouds is close to saturation over liquid water; (ii) because of a typically short relaxation time, mixed-phase clouds will rapidly (within seconds) adjust to their nearly saturated over liquid quasi-steady value; and (iii) because of the long relaxation time, humidity in ice clouds can be both supersaturated and subsaturated with respect to ice, and the maximum supersaturation is limited to that of the saturation over water.

The theoretical prediction of RH_w in different types of clouds was verified by in situ observations by Korolev and Isaac (2006). Humidity in ice clouds requires an extended time to adjust to its quasi-equilibrium value because of the long phase relaxation times, which in many cases is comparable to the lifetime of the entire cloud (Krämer et al. 2009; Rollins et al. 2016).

b. Glaciation time

Another important parameter characterizing mixed-phase clouds is the time it takes to convert all liquid water into ice because of the WBF mechanism. The process of the liquid to ice conversion is usually called "glaciation." After the glaciation process has completed the cloud becomes optically thin and its radiative properties change significantly. Along with radiative transfer, the glaciation time is also important for precipitation formation, and it plays an important role in the effectiveness of cloud seeding.

Theoretical analysis of the glaciation time was conducted by Shifrin and Perelman (1960), Mazin (1986), Korolev and Isaac (2003), Korolev and Mazin (2003), and Pinsky et al. (2014).

For $u_z = 0$, the glaciation time of a mixed-phase cloud can be estimated as (Korolev and Mazin 2003)

$$\tau_{\mathrm{gl}} = \frac{1}{4\pi c A_i S_i} \left(\frac{9\pi \rho_i}{2\rho_a^2}\right)^{1/3} \left[\left(\frac{q_{w0} + q_{i0}}{N_i}\right)^{2/3} - \left(\frac{q_{i0}}{N_i}\right)^{2/3}\right],$$

$$(5\text{-}5)$$

where q_{w0} and q_{i0} are the initial liquid and ice water mixing ratios, respectively; S_i is the supersaturation over ice at the saturation vapor pressure over liquid; ρ_i and ρ_a are the densities of the air and ice, respectively; A_i is a coefficient dependent on T and P; and c is a constant "capacitance" representing the ice crystal habit in the diffusional growth equation. Depending on the air temperature T, for typical values of N_i, q_{w0}, and q_{i0}, the glaciation time may vary from hundreds of seconds to hours.

The effect of u_z on τ_{gl} was studied in Korolev and Isaac (2003) and Pinsky et al. (2014). Pinsky et al. (2014)

showed that, if the mixed-phase cloud volume has moved a vertical distance Δz, and the following condition $|\bar{u}_z| \tau_{gl} \geq \Delta z \geq -q_{w0} a_1/a_0$ is satisfied, then the glaciation time does not depend on the cloud parcel trajectory and its vertical velocity $u_z(t)$. For this case, the glaciation time can be presented as

$$\tau_{gl} = \frac{3}{2(\varphi-1)} \left\{ \frac{1}{C_i N_i^{2/3}} \left[\left(q_{i0} + \frac{a_1}{a_2} q_{w0} + \frac{a_0}{a_2} \Delta z \right)^{2/3} - q_{i0}^{2/3} \right] \right. $$
$$\left. + \frac{\varphi}{C_w N_w^{2/3}} q_{w0}^{2/3} \right\}. $$

$$(5\text{-}6)$$

Here C_w, C_i, φ are coefficients dependent on T and P.

c. Three basic equilibrium points and the WBF regime

The first term on the right-hand side of Eq. (5-2) corresponds to an external dynamic forcing, which may result in increased or decreased supersaturation depending on the amplitude of u_z. The external dynamic forcing plays a major role in the direction and rate of the partitioning of ice ($\dot{q}_i$), liquid ($\dot{q}_w$), and water vapor ($\dot{q}_v$) mixing ratios in mixed-phase clouds. Analysis of Eq. (5-2) suggests the existence of three phase-equilibrium points in mixed-phase clouds (Korolev 2008). The first point corresponds to ice equilibrium, namely, $\dot{q}_i = 0$ and $S_i = 0$. The vertical velocity corresponding to this condition is equal to

$$u_z^o = \frac{e_{is} - e_{ws}}{e_{ws}} \chi N_w \bar{r}_w, \qquad (5\text{-}7)$$

where e_{ws} and e_{is} are the saturation vapor pressure over liquid and ice, respectively.

The second point corresponds to the equilibrium of liquid water, namely, $\dot{q}_w = 0$ and $S_w = 0$. The corresponding vertical velocity is equal to

$$u_z^* = \frac{e_{ws} - e_{is}}{e_{is}} \eta N_i \bar{r}_i. \qquad (5\text{-}8)$$

The third equilibrium point corresponds to water vapor, namely, $\dot{q}_v = 0$. This condition corresponds to the vertical velocity

$$u_z^+ = \frac{(\xi - 1)(B_w b_i - b_w B_i) N_w \bar{r}_w N_i \bar{r}_i}{a_0 \xi (B_w N_w \bar{r}_w + B_i N_i \bar{r}_i)} \qquad (5\text{-}9)$$

and the equilibrium supersaturation

$$S_w^{(v)} = -\frac{B_i^* N_i \bar{r}_i}{B_w N_w \bar{r}_w + B_i N_i \bar{r}_i}. \qquad (5\text{-}10)$$

Here ξ, χ and η are coefficients dependent on T and P.

For any mixed-phase cloud, the equilibrium velocities are related through

$$u_z^o < u_z^+ < u_z^*. \qquad (5\text{-}11)$$

The inequality in Eq. (5-11) splits the phase transformation in mixed clouds into the four regimes shown in the conceptual diagram in Fig. 5-3 (Korolev 2008).

1) Figure 5-3a: If $u_z < u_z^o$, then $\dot{q}_v > 0$, $\dot{q}_i < 0$, and $\dot{q}_w < 0$. Here, both ice particles and droplets evaporate, whereas the mass of the vapor increases. In terms of the vapor pressure, this corresponds to the condition when $e < e_{is} < e_{ws}$.

2) Figure 5-3b: If $u_z^o < u_z < u_z^+$, then $\dot{q}_v > 0$, $\dot{q}_i > 0$, and $\dot{q}_w < 0$. Under these conditions ice particles grow, droplets evaporate, and the water vapor mixing ratio increases. The water vapor pressure in this case is in the range of $e_{is} < e < e_v < e_{ws}$. Here, $e_v = [1 + S_w^v] e_{ws}$, is the equilibrium vapor pressure.

3) Figure 5-3c: If $u_z^+ < u_z < u_z^*$, then $\dot{q}_v > 0$, $\dot{q}_i > 0$, and $\dot{q}_w < 0$. In this situation, ice particles grow, droplets evaporate, and the water vapor mass decreases. This case corresponds to the water vapor pressure $e_{is} < e_v < e < e_{ws}$.

4) Figure 5-3d: If $u_z > u_z^*$, then $\dot{q}_v > 0$, $\dot{q}_i > 0$, and $\dot{q}_w > 0$. At this point, both ice particles and liquid droplets grow, and the water vapor mass decreases. Under this condition, the water vapor pressure will be $e_{is} < e_{ws} < e$.

One of the important outcomes of the analysis of the water mass partitioning during phase transformation is that only conditions in Figs. 5-3b,c correspond to the formal definition of the WBF process, when ''ice particles are growing at the expense of evaporating droplets.'' Therefore, the WBF process presents a simplistic description of the water partitioning in mixed-phase clouds. Comparisons of $\dot{q}_w$, $\dot{q}_i$, and $\dot{q}_v$ show that for the condition in Fig. 5-3b, the evaporating droplets contribute more to the vapor mass increase than to the growth of ice. On the other hand, for the condition in Fig. 5-3c, the ice particles grow mainly at the expense of water vapor with minor contributions from evaporating droplets. Regimes in Figs. 5-3a and 5-3d do not satisfy the definition of the WBF process since both droplets and ice crystals are either evaporating or growing simultaneously.

Numerical simulations suggest that in persistent stratiform mixed-phase clouds, the WBF process is active only in approximately half of the cloud volume, and that in the other half both ice particles and liquid droplets are growing simultaneously (Fan et al. 2011). In
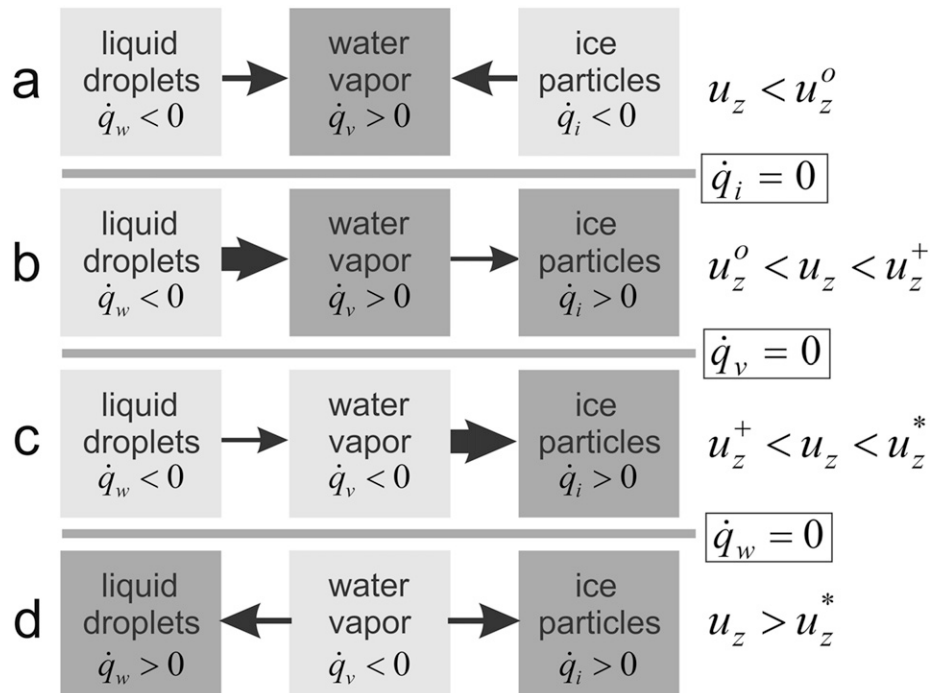
Fig. 5-3. Conceptual diagram of four different scenarios of phase transformation in mixed-phase clouds: (a) $u_z < u_z^o$; (b) $u_z^o < u_z < u_z^+$; (c) $u_z^+ < u_z < u_z^*$; (d) $u_z^* > u_z$. Thickness and direction of the arrows indicate the rate and direction of the mass transfer. A darker color indicates the water phase where the water mass is accumulating.

convective clouds, even in moderate updrafts the WBF process is not active in mixed-phase regions (Korolev 2007). Climate model simulations also suggest that the WBF process occurs at most half of the time (Lohmann and Hoose 2009).

d. Dynamic forcing and maintenance of mixed-phase clouds

Rauber and Tokay (1991) and Pinto (1998) have described long-lived narrow layers of supercooled water overlying mixed and ice layers with cloud tops as cold as −30°C. Later on, persistent mixed-phase layers with lifetimes from several hours to several days were reported in a number of studies (e.g., McFarquhar et al. 2011; Shupe et al. 2008, 2011; and others). The existence of such layers appears to conflict with the outcome expected from the WBF mechanism. Rauber and Tokay (1991), Pinto (1998), Harrington et al. (1999), and Harrington and Olsson (2001) attempted to explain the existence of such layers by an imbalance between the condensate supply rate, the bulk ice crystal mass growth rate and the removal of ice freezing nuclei (IFN) by precipitating ice particles. Field et al. (2004) suggested that observations of embedded liquid water regions with horizontal extents as short as 100 m may be the result of turbulent motions leading to the intermittent

production of liquid water. Korolev and Isaac (2003) found that a cloud parcel undergoing vertical oscillations may be subject to an indefinitely long periodic evaporation and activation of liquid droplets in the presence of ice particles. After a certain amount of time, the average IWC and LWC reaches a steady state. This phenomenon may explain the existence of long-lived mixed phase in stratiform layers.

While it has long been recognized that the WBF mechanism is a major process in precipitation formation in cold clouds, most theoretical efforts have focused on studies of the transition of mixed phase into ice clouds. Heymsfield (1977) was the first to recognize that ice clouds could be turned into mixed phase through the activation of liquid water in updrafts. Since then, a few studies have investigated the minimum updraft required to maintain steady-state mixed-phase conditions (e.g., Mazin 1986; Tremblay et al. 1996; Zawadzki et al. 2001). Korolev and Mazin (2003) developed a simple analytical expression for a critical vertical velocity [Eq. (5-8)] such that, if $u_z > u_z^*$, liquid water will be activated in a preexisting ice cloud. The second condition defines the minimum vertical travel $\Delta Z_{min} = (1/a_0) \ln(E_w/e_0)$, which the vertically moving cloud parcel should exceed in order to activate liquid, that is, $Z > Z_{min}$. These two conditions make up a set of necessary and sufficient
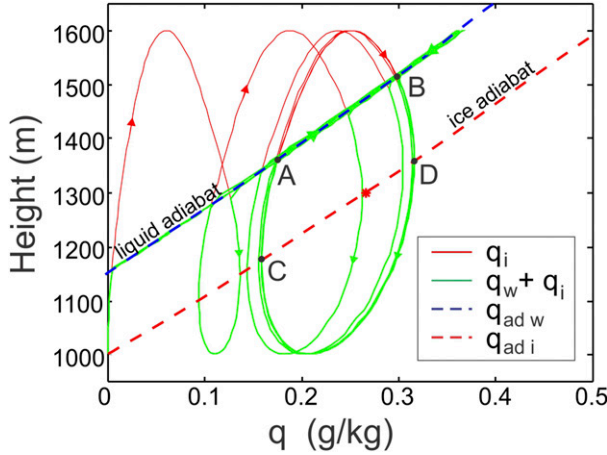
FIG. 5-4. Effect of vertical velocity on the formation of mixed-phase during harmonic oscillations. Magnitude of sinusoidal vertical velocity = 0.1 m s^{-1}. After a few cycles $q(z)$ reaches the limit cycle. Activation of liquid water occurs at point A during ascent, and complete evaporation at point B during descent. Ice evaporates below CD line (ice adiabat) and it grows above it. Numerical simulation was conducted for $T = -10°$C, initial ice crystal radius of $r_{i0} = 10\,\mu$m and ice concentration of $100\,$L^{-1}. [Adapted from Korolev and Field (2008).]

conditions for turning an ice cloud into a mixed-phase cloud during vertical motion (Korolev and Field 2008).

When an ice cloud parcel undergoes continuous cyclical motions, by being driven by a sinusoidal vertical motion, liquid water can be repeatedly formed and lost. The repeated formation of mixed-phase cloud occurs if the vertical extent of motions and the maximum vertical velocity satisfy analogous necessary and sufficient conditions for the formation of mixed-phase clouds (Korolev and Field 2008). Specifically, these conditions

are that the vertical extent of the cyclical motion must be large enough to bring the parcel to water saturation and that the vertical velocity is able to provide a source of supersaturation that exceeds the loss due to the presence of ice. Under these conditions a mixed-phase cloud can be long-lived (Fig. 5-4).

Vertical motions in clouds are not only constant or cyclic but are often turbulent. Rapid fluctuations of a parcel containing ice may be able to bring the parcel to water saturation and maintain a source of saturation against the sink of vapor to ice, thereby allowing the activation of droplets and creating a mixed-phase cloud. This scenario was explored in large-eddy simulation (LES) modeling (Hill et al. 2014) by varying turbulence strength (initial shear of 0.2–0.3 s^{-1} allowed to decay over time) and ice concentration (1–100 L^{-1}). The simulations used a high-resolution (10 m) grid where over 95% of the turbulence was explicitly represented. It was found that instantaneous snapshots of model microphysical and dynamical fields satisfied the necessary and sufficient conditions (Korolev and Field 2008) for converting ice into mixed-phase cloud (Figs. 5-5a,b).

An analytic approach was developed by Field et al. (2014) that was able to reproduce the domain mean results of the LES simulations. The approach is based on the solution of a stochastic differential equation that describes the evolution of ice supersaturation as

$$dS_i = a_0 \sigma_w \xi \tau_d^{1/2} dt - a_2 B_i^* N_i \bar{r}_i dt - \left(\frac{\varepsilon}{L^2}\right)^{1/3}(S_i - S_E)dt. \tag{5-12}$$

Here, the vertical velocity u_z is replaced by a Gaussian white noise vertical motion (ξ) whose magnitude is
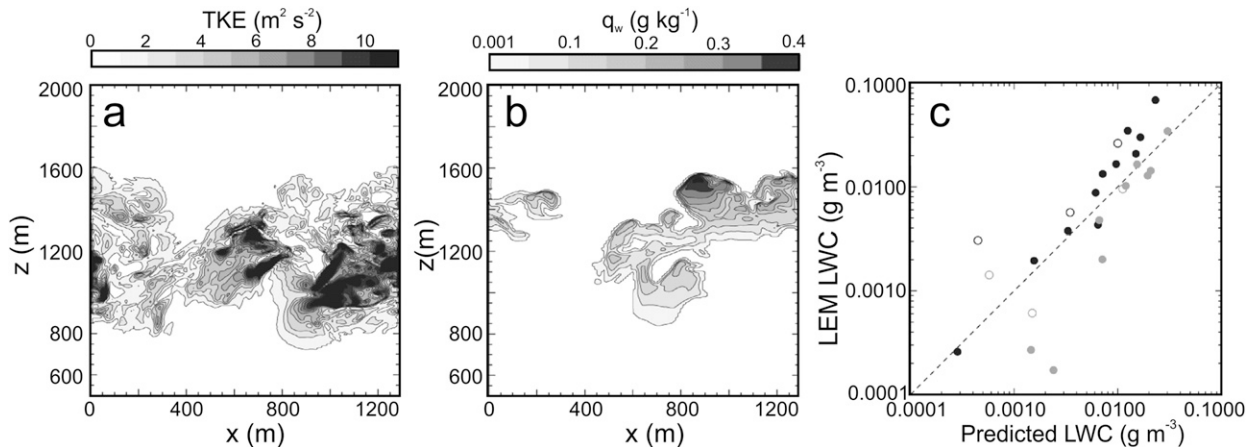
FIG. 5-5. (a) Cross sections through LES ($dx = dy = 10$ m, $dz = 5$ m) of TKE. (b) Liquid water mixing ratio for background ice conditions of 0.1 g kg^{-1} and 10 L^{-1} at $-9°$C. (c) Comparison of turbulent domain mean liquid water content from the LES and the analytic solution for a range of TKE and ice concentrations. [Adapted from Hill et al. (2014) and Field et al. (2014).]

characterized by the standard deviation of vertical velocity σ_w and eddy dissipation rate ε through the turbulent decorrelation time scale $\tau_d = 2\sigma_w^2/\varepsilon C_0$, C_0 is the Lagrangian structure function constant, σ_w is the standard deviation of vertical velocity distribution, S_i is the supersaturation over ice for the ensemble of turbulent parcels, and S_E is the environmental supersaturation over ice. For the Gaussian vertical velocity noise term, the steady-state solution is also Gaussian with the mean ice supersaturation S_i and supersaturation variance σ_s given by

$$S_i = S_E \frac{(\varepsilon/L^2)^{1/3}}{a_2 B_i^* N_i \bar{r}_i + (\varepsilon/L^2)^{1/3}} = S_E \frac{\tau_{pi}}{k\tau_t + \tau_{pi}}, \quad \text{and} \quad (5\text{-}13)$$

$$\sigma_s^2 = \frac{a_0^2 \sigma_w^2 \tau_d}{2[a_2 B_i^* N_i \bar{r}_i + (\varepsilon/L^2)^{1/3}]} = \frac{a_0^2 \sigma_w^2}{2} \frac{\tau_d \tau_t \tau_{pi}}{k\tau_t + \tau_{pi}}. \quad (5\text{-}14)$$

Here, $\tau_t = L^{2/3}/\varepsilon^{1/3}$ is the characteristic mixing time of turbulent eddies with the spatial scale L, τ_{pi} is the time of phase relaxation associated with ice fraction (section 3a), and k is a coefficient dependent on T and P.

Given the mean and variance of the saturation within the turbulent region, the liquid fraction and water content are found by integrating the distribution above water saturation. We note that to keep the problem tractable and analytically solvable, this approach ignores latent heating effects. The comparisons of the LWC predicted from Eq. (5-13) and that derived from the LES simulation is shown in Fig. 5-5c.

It follows from Eq. (5-13) that if $k\tau_t \gg \tau_{pi}$, the sink of vapor to ice is a much stronger effect on the vapor field in the turbulent region than mixing to the region outside. For this case, $S_i \rightarrow 0$ and the microphysical sink of vapor drives the saturation environment to ice saturation. In the converse case, if $k\tau_t \ll \tau_{pi}$, the mixing with the surrounding environment dominates and $S_i \rightarrow S_E$. The steady-state solution for the distribution of ice supersaturation (in the absence of liquid water) indicates that supercooled liquid water content, when diagnosed from the liquid water supersaturated part of the saturation distribution, increases with increasing vertical velocity variance, but is reduced by increasing the sink of vapor to the ice phase, which is controlled by the integral ice radius $N_i \bar{r}_i$ in Eq. (5-14).

4. Observations of mixed-phase clouds

a. In situ observations

Until recently, the bulk of knowledge on the microstructure of mixed-phase clouds has been collected using airborne in situ observations. Airborne measurements provide insights into aspects of microphysical properties and the processes governing the evolution of mixed-phase clouds. These insights include diagnostics of early ice initiation in liquid clouds, effects of aerosols on the phase composition, dynamic forcing of the mixed phase, and intermittency of cloud phase on small scales. One of the limitations of in situ measurements is related to the relatively low sampling statistics due to small sampling volumes of microphysical probes. Nevertheless, in situ measurements remain one of the main tools for studying mixed-phase clouds and evaluation of remote sensing techniques.

1) MAIN INSTRUMENTATION FOR IN SITU OBSERVATION OF THE MIXED PHASE: PRINCIPLES, ALGORITHMS, CHALLENGES, AND LIMITATIONS

Airborne investigations of mixed-phase clouds date back over 75 yr (i.e., Peppler 1940; Findeisen 1942; Weickmann 1945; Zak 1949; Byers and Braham 1949). Yet despite this long history of airborne observations, microphysical characterization of mixed-phase clouds remains an ongoing challenge. The quantification of microphysical properties of such clouds from in situ measurements incorporates problems in measuring of both pure ice and pure liquid clouds (Baumgardner et al. 2017, chapter 9). The difficulties of such quantifications are compounded by the problem of phase identification of liquid and ice particles, since liquid and ice can be confused with one another. This results in errors in the assessment of phase composition. In this section, we provide a list of instruments that are used in mixed cloud studies and identify their limitations.

For the sake of discussion, we separate the various instruments used to investigate mixed-phase clouds into the following categories (there are other possible classification schemes):

1) Icing rods: Rosemount Icing Detector (Baumgardner and Rodi 1989).
2) Hot-wire probes: Johnson–Williams (J-W) probe (Neel 1955); King probe (King et al. 1978); Nevzorov probe (Korolev et al. 1998); Droplet Measurement Technologies (DMT) hot-wire (www.dropletmeasurement.com); Science Engineering Associates (SEA) hot wire and hot cylinder (Steen et al. 2016).
3) Evaporators: TWC evaporator (Nicholls et al. 1990); counterflow virtual impactor (CVI; Noone et al. 1988); isokinetic probe (IKP; Davison et al. 2012).
4) Scattering probes: FSSP (Knollenberg 1981); Fast FSSP (FFSSP; Brenguier et al. 1998; O'Connor et al. 2008); Cloud Droplet Probe (CDP; Lance et al. 2010); Fast CDP (FCDP; Lawson et al. 2017); Cloud Aerosol Spectrometer (CAS; Baumgardner et al. 2002).
5) Scattering probes with phase-discriminating capabilities: Small Ice Detector (SID; Cotton et al. 2010;

Nichman et al. 2016); CAS with Polarization (CAS-POL; Baumgardner et al. 2014); BCPD with Polarization (Freer et al. 2014); Phase Doppler Particle Analyzer (PDPA; Bachalo and Houser 1984).

6) Particle imaging probes: 2D-C optical array probe (Knollenberg 1970); Cloud Imaging Probe (CIP; Baumgardner et al. 2001); 2D-S stereo probe (Lawson et al. 2006); CPI (Lawson et al. 2001); High Speed Imaging (HSI) probe (Bachalo et al. 2015); video ice particle sampler (VIPS; Heymsfield and McFarquhar 1996); Hydrometeor Videosonde (HyVis; Murakami and Matsuo 1990); HOLODEC (Fugal and Shaw 2009); PHIPS-HALO (Abdelmonem et al. 2016; Schnaiter et al. 2017).

(i) Icing rods

The Rosemount Icing Rod (RICE) was designed to detect the presence of supercooled water in clouds. The principle of its operation is based on measurements of the natural frequency of a vibrating rod. Ice particles are expected to bounce off the rod's surface, whereas supercooled droplets will form a liquid film on impact, which will rapidly turn into ice. The vibrating frequency changes as ice builds up on the rod's surface. The frequency change is converted into voltage, which may be used to identify the presence of supercooled liquid water. A relationship between icing rate and LWC was derived by Baumgardner and Rodi (1989) from data collected in an icing tunnel. Subsequent icing tunnel tests and comparisons with other sensors in mixed-phase clouds showed that the icing rate is a function of droplet size, and that it may also be sensitive to ice crystals. The threshold sensitivity to supercooled water of the RICE is estimated as 0.002–0.01 $\mathrm{g\,m}^{-3}$ depending on airspeed, droplet size, and temperature (Heymsfield and Miloshevich 1989; Mazin et al. 2001). Because of its low accuracy, the RICE should not be used for a quantitative assessment of LWC in mixed-phase clouds (Mazin et al. 2001) but rather only for its identification. It should be noted that accretion of ice occurs on the surface of the icing rod only if the total air temperature T_{tot} is below the freezing point, and when LWC is lower than the Ludlam limit (Mazin et al. 2001; Cober et al. 2001a). Thus, at an airspeed of $150\,\mathrm{m\,s}^{-1}$ the total air temperature is approximately 15°C higher than the air static temperature. This is a serious limitation for the RICE in studying phase composition, since a large fraction of mixed-phase clouds occur at $T_{\mathrm{air}} > -15$°C. Other limitations of the RICE are related to (i) erosion of accreted ice by ice particles, (ii) deicing cycle dead time, and (iii) limited response to short time exposure to liquid clouds. Until recently these limitations of RICE observations have not received much

attention in the literature and their effects are not quantified.

The overall assessment of the RICE's performance is that it is reliable as an icing detector in clouds with a relatively high sustained LWC at $T_{\mathrm{tot}} < 0$°C (i.e., $>0.02\,\mathrm{g\,m}^{-3}$ at $100\,\mathrm{m\,s}^{-1}$, $T_{\mathrm{air}} < -5$°C). However, the RICE does not detect very small amounts of supercooled liquid water ($<0.005\,\mathrm{g\,m}^{-3}$) in mixed-phase clouds. In the case shown in Fig. 5-6 (right panel) where the cloud is dominated by ice with some embedded droplets, this liquid water would not be detected by the RICE.

(ii) Hot-wire probes

The family of hot-wire devices rely on the principle of measuring the electric power required for vaporizing cloud particles on impact with the heated sensor surface. The amount of evaporated water is calculated from the measured power based on first principles. LWC hot-wire sensors usually have cylindrical shapes with diameters ranging from 0.5 to 3 mm. The expectation is that ice particles will bounce off the convex cylindrical surface, whereas liquid droplets will form a thin film on the heated surface and completely evaporate. However, icing tunnel tests show that drops larger than about $50\,\mu\mathrm{m}$ do not completely evaporate and, therefore, the response of the probe rolls off as a function of drop diameter $> 50\,\mu\mathrm{m}$ (Biter et al. 1987; Strapp et al. 2003). It has also been demonstrated that LWC hot-wire sensors can erroneously respond to ice particles, detecting 10%–20% of the ice mass depending on the ice particles size distribution and airspeed (Korolev et al. 1998; Cober et al. 2001b; Field et al. 2004).

Hot-wire sensors with concave shapes (e.g., the Nevzorov TWC and SEA TWC probes) are designed to measure the total condensate amount by vaporizing both liquid water drops and ice particles. All hydrometeors are expected to be trapped and completely vaporized within the concave structures. Because of the different response to ice particles and liquid droplets, LWC and IWC in mixed-phase clouds can be separated and calculated from the LWC and TWC hot-wire sensor measurements by solving a system of linear equations (Korolev et al. 2003; Korolev and Strapp 2002). The errors in calculating LWC and IWC in mixed-phase clouds are related to uncertainties in the collection efficiencies of liquid droplets and ice crystals by the LWC and TWC sensors. High-speed video observations in icing tunnels show that some fraction of ice particles bounce off the TWC hot-wire sensor, resulting in an underestimation of IWC (Emery et al. 2004; Korolev et al. 2013c). An example of LWC and TWC measurements in a mixed-phase cloud calculated from the Nevzorov probe is shown
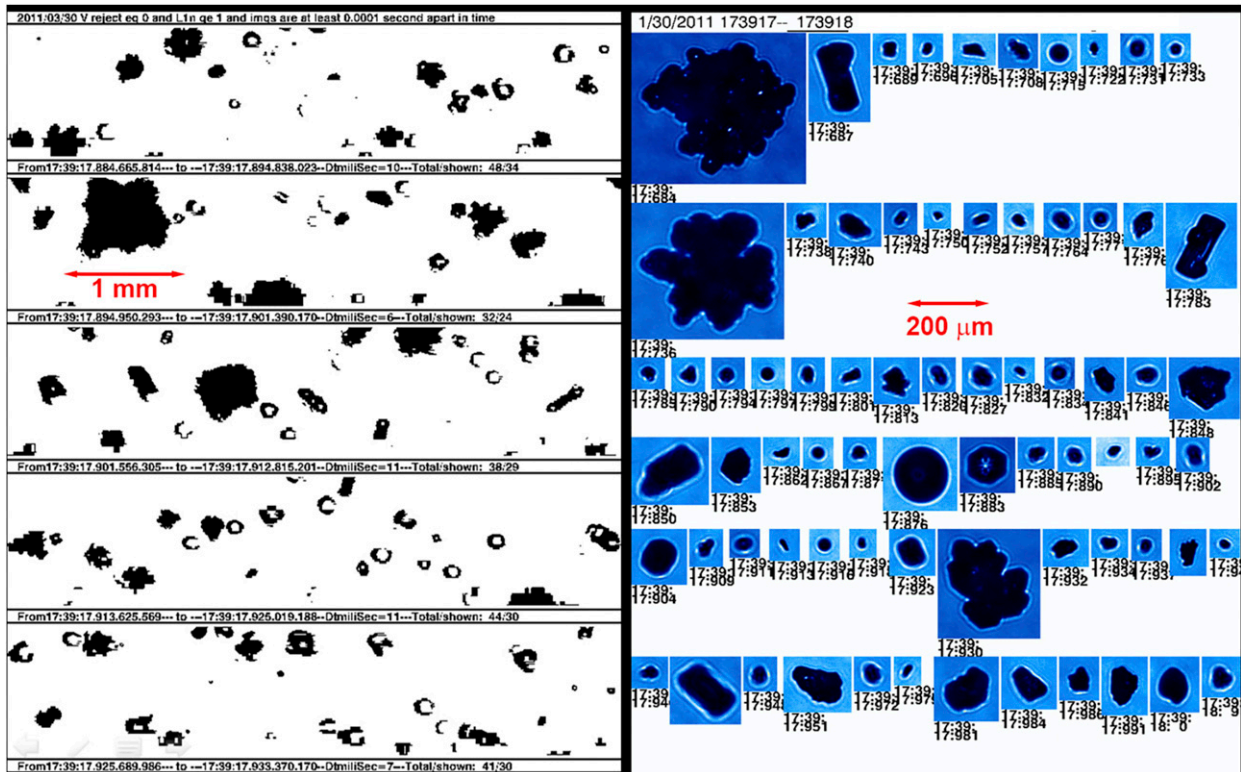
FIG. 5-6. (left) 2D-S images and (right) 3V-CPI images observed simultaneously in a tropical cumulus cloud at −24°C on 30 Jul 2011. The RICE did not indicate the presence of supercooled liquid water; however, the CPI images clearly show spherical images that are likely water drops while the 2D-S images are ambiguous.

in Fig. 5-7. When used in conjunction with RICE measurements, sensors such as the Nevzorov probe provide reasonable and consistent results.

In summary, hot-wire probes remain the main instruments for quantitative assessment of bulk LWC and IWC in mixed-phase clouds. However, the residual effect of ice on the LWC hot-wire sensors degrades the liquid–ice discrimination by the hot-wire technique for cases with $\mu_{ice} \to 1$.

(iii) Evaporators

The principle of operation of evaporators is based on the evaporation of both liquid droplets and ice particles ingested by the probe's inlet. The total water vapor of the air that experienced evaporation inside the probe is measured by a humidity sensor. The total water content is calculated by subtracting the background humidity of the cloudy air from the humidity measured inside the evaporator (e.g., Nicholls et al. 1990; Davison et al. 2012). Evaporators do not discriminate between ice and liquid, and in terms of the final product of their measurements they are equivalent to the TWC hot-wire probes. However, the advantage of evaporators is that they are capable of measurements of high values of

TWC up to $10\,\mathrm{g\,m^{-3}}$ at $200\,\mathrm{m\,s^{-1}}$ (Davison et al. 2012). The accuracy of the evaporator TWC measurements depends on the accuracy of the measurements of the evaporator's and background's humidity. Usually the TWC accuracy ranges from 0.005 to $0.1\,\mathrm{g\,m^{-3}}$ depending on the air temperature. A relatively low accuracy of the TWC measurements limits the use of evaporators for characterization of the cloud phase composition when TWC is $<(0.2\text{–}0.3)\,\mathrm{g\,m^{-3}}$.

(iv) Scattering probes

Scattering probes are designed and calibrated to measure individual water droplets. However, it is well documented that they also respond to ice particles (e.g., Gardiner and Hallett 1985; Field et al. 2003; Korolev et al. 2011). Scattering particle probes like the FSSP, CDP, FCDP, and CAS do not discriminate signals from ice particles and liquid droplets. This results in an overestimation of measured droplet concentration and LWC in mixed-phase clouds (e.g., Korolev et al. 2013c). Ice shattering contributes to further degradation of measurements from the scattering probes. For example, for scattering probes not equipped with antishattering tips, the false LWC
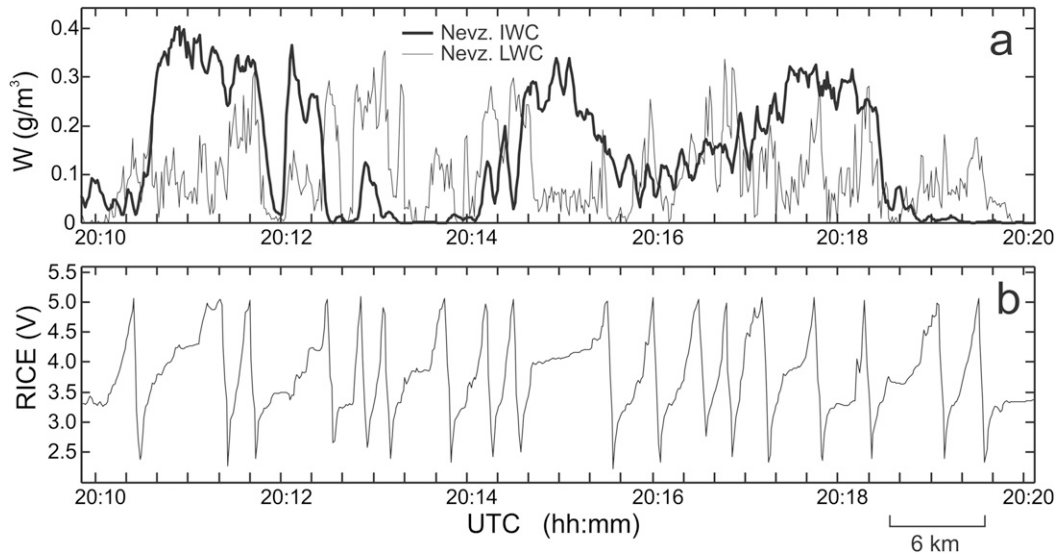
FIG. 5-7. Example showing (a) time series of LWC (gray curve) and IWC (black curve) from the Nevzorov probe, and (b) signal from the RICE in mixed phase. The slope of the RICE increases in supercooled liquid water, which corresponds well with the increases in LWC. The rapid decreases in RICE signal occur when the rod is heated to melt accreted ice and restart the measurement cycle. Data collected by the Environment Canada from the NRC Convair 580 during the Alliance Icing Research Study (AIRS), Ottawa, Ontario, 16 Dec 1999, Nimbostratus, $T = -6°C$. [Adapted from Korolev et al. (1998).]

response caused by ice particles may go up to $0.6\,\mathrm{g\,m^{-3}}$ (Korolev et al. 2013a,c). Therefore, scattering particle probes not equipped with antishattering tips cannot be used for the quantitative assessment of microphysical properties of mixed-phase clouds. The assumption that the water droplet concentration is typically a few orders of magnitude higher than that of ice particles in mixed-phase clouds may be used as an indicator of the presence of liquid if the total concentration measured by the scattering probes exceeds approximately $10–20\,\mathrm{cm^{-3}}$ (depending on the baseline concentration of ice). In addition, the shape of the measured size distribution gives some indication of phase, with peaked distributions in the presence of supercooled water and flatter distributions in the presence of ice. However, scattering probes alone cannot be used for detection of liquid in clouds when the droplet sizes are outside the nominal probes' size range or if the droplet concentration is low. An example of such a case is shown in Fig. 5-6 (right panel).

(v) Scattering probes with phase-discriminating capabilities

Single scattering particle probes have been designed to discriminate between ice particles and water droplets. Phase discrimination is based on observations of (i) polarization interactions (CAS-POL, CPSPD, BCPD), (ii) spatially resolved forward scattering patterns (SID family of instruments), and (iii) detection of certain light scattering patterns (e.g., fringes) specific to liquid droplets, which do not occur for nonspherical ice [Phase Doppler Interferometry (PDI) family of instruments].

The polarization technique uses the principle that completely spherical water drops do not change the polarization state of linearly polarized light, whereas ice will produce some degree of cross polarization. While this technique has a sound theoretical basis, it is also subject to "false irregulars" that are registered when the instrument is flown through all-liquid clouds. The false irregulars can be the result of various factors, including nonspherical water drops, drops that are partially within the viewing area, and multiple scattering from drops. Thus, the level of polarization is not zero when flying in all-liquid clouds. In addition, small quasi-spherical ice particles will cross polarize light only slightly, so flying in a mixed-phase cloud can produce cross-polarization signals from small ice and water drops that overlap (Nichman et al. 2016). The result is that interpretation of the cross-polarization signal in the mixed phase is difficult (Farrington et al. 2016). In recent work based on the analysis of the CAS-DPOL, Costa et al. (2017) showed that the polarization technique allows the detection of the fraction of cloud particles between 20 and $50\,\mu\mathrm{m}$ that are aspherical allowing clouds to be classified as liquid, mixed phase, or ice.

The SID family of instruments examines forward scattered light that is projected on a digital camera. Figure 5-8 shows signals from the Particle Phase Discriminator, mark 2 (PPD-2K), which operates on this
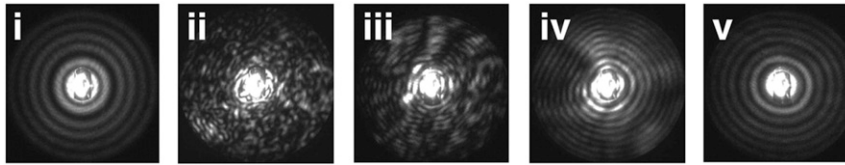
FIG. 5-8. Diffraction images of particles recorded by the PPD-2K during experiment in the AIDA chamber at different stages of the cloud formation: (i) supercooled water drop and (ii) growing frozen droplet for 2 min. Ice particles sublimating for (iii) 5, (iv) 7.5, and (v) 9 min. [Adapted from Järvinen et al. (2016).]

principle. The images were recorded in the AIDA chamber at the Karlsruhe Institute of Technology (KIT, Germany) during a rapid expansion that generates supercooled liquid drops followed by freezing and sublimation (Järvinen et al. 2016). As seen in Fig. 5-8, the pattern of a water drop (Fig. 5-8i) is very similar to that of the frozen drop after it has sublimated for several minutes (Fig. 5-8v). When flying in all-liquid clouds, Johnson et al. (2014) found that the SID-2 recorded enough "false irregulars" to compromise discrimination between water drops and ice particles in a study to identify first ice in tropical cumulus. A later version, SID-3, has been reported to produce improved results by removing "artifacts" using manual identification (Vochezer et al. 2016). However, as in the case of the cross-polarization technique, interpretation of the ratio of ice to water drops in the mixed phase is somewhat subjective. Another limitation of the SID probes is related to a low camera frame rate (30 Hz). In many mixed-phase environments with moderate cloud droplet number concentrations, the SID camera only measures only a subset of the particles and is likely to miss ice if $N_i \ll N_w$.

Theoretical calculations of light scattering performed for oblate ice spheroids (Borrmann et al. 2000; Meyer 2013) have limited value, since they cannot be applied to other ice shapes and varied ice-surface roughnesses. Furthermore, no known laboratory size calibrations by ice particles have been performed, thus far, to justify the theoretical calculations of ice scattering. Thus, even though scattering probes with phase-discriminating capability are able to segregate ice particles and liquid droplets, their accuracy in ice particle sizing remains an ongoing issue.

The PDI type of instruments are optically configured to detect only spherical particles and, therefore, only measure water drops (Bachalo 2000; Bachalo and Houser 1984). As a result, PDI measurements may provide a more reliable assessment of LWC in the mixed phase. Despite their widespread use for characterization of industrial sprays, the PDI instruments are utilized for in situ mixed-phase cloud measurements only on rare occasions. Therefore, no conclusive comments can be made regarding the phase-discriminating capabilities of cloud particle phase by PDI instruments at this stage.

(vi) Particle imaging probes

Optical imaging probes provide particle images and can be used for the identification of particle phase state. This identification is based on the two following assumptions: 1) ice particles have nonspherical shapes and, therefore, ice particles provide only noncircular images; 2) circular images are produced by spherical particles, which are associated with only liquid droplets.

The first assumption is valid for ice particles grown in clouds with the exception of frozen droplets. Depending on their size and temperature, droplets may freeze as spheres or develop bulges and spikes during freezing (e.g., Iwabuchi and C. Magono 1975; Takahashi 1975; Korolev et al. 2004; López and Ávila 2012). Spherical frozen droplets will appear as circles in the imaging probes and they may be confused with liquid droplets. On the other hand, laboratory experiments have shown that frozen water spheres produce nonspherical features during vapor deposition growth (e.g., Gliki et al. 1962; Takahashi 1979; Korolev and Isaac 2003; Bacon et al. 2003). The characteristic time of developing facets, corners, and side crystals of a frozen sphere depend on the water vapor supersaturation, temperature, and particle size. For example, at $T = -10°C$ and water saturation (typical for the mixed phase, section 3a) the growth rate of ice is on the order of a micron per second (Ryan et al. 1976). Such a growth rate suggests that the characteristic time of producing nonspherical features will range from seconds to tens of seconds depending on the droplet size. However, at low supersaturation over ice (e.g., 1%–5%), frozen droplets may maintain a quasi-spherical shape over minutes and tens of minutes (Gliki and Eliseev 1962; Gonda and Yamazaki 1984; Korolev et al. 2003). At the same time, liquid droplets at relative humidity close to saturation over ice will quickly evaporate. Thus, particle image observations would benefit from simultaneous humidity measurements. For example, the presence of circular images at water vapor saturation would be indicative of the presence of liquid. However, in a subsaturated environment, circular images most likely originate from frozen droplets or

sublimating ice, which tend to have rounded corners and an absence of facets.

A question that has been widely discussed in the literature is how many pixels and at what size resolution can the image of a spherical water drop be discriminated from the image of a nonspherical ice particle. Korolev (2007) shows typical digital images of spherical particles as a function of distance from the object plane using an OAP (Fig. 5-9). The images in Fig. 5-9 become more circular and ''doughnut'' shaped as the particle moves away from the object plane ($Z = 0$). Thus, only ''in focus'' images can be used to discriminate images of water drops from images of nonspherical ice particles. Based on the in-focus images in Fig. 5-9, one sees that only when the image contains 15 continuous pixels is there objective criteria for identifying the image as spherical. Even at 15 continuous pixels, various shapes that are nearly spherical, for example, a hexagonal plate that is viewed perpendicular to its a plane, can be interpreted as spherical. This is demonstrated in Fig. 5-10, which shows simulations of the digitization of various shapes of ice particles imaged in situ by a CIP with 2.3-μm pixels and 256 intensity levels.

Imaging probes that use linear optical arrays (such as the 2DC, CIP, and 2D-S) typically have pixel sizes on the order of 10–25 μm, whereas probes utilizing digital cameras typically have smaller pixel sizes (2–3 μm) and are able to better distinguish spherical from nonspherical particles. The group of instruments that use digital cameras includes the CPI, HSI, PHIPS-HALO, HOLODEC, and HALOHOLO. The CPI, HSI, and PHIPS-HALO were designed to register in-focus images of single particles, which are present in the sample volume. The sample volume of an in-focus imaging probe depends on particle sizes and usually it does not exceed a few mm³. Holographic probes have significantly larger sample volumes (HOLODEC: 20 cm³; HALOHOLO: 39 cm³) and provide simultaneous imaging of ensembles of particles present in the sample volume. By numerically reconstructing each hologram (Fugal et al. 2009), one obtains the three-dimensional positioning and imaging of each individual particle. An example of a particle spatial distribution, along with the size distribution and image gallery reconstructed from a single hologram, is presented in Fig. 5-11a. The particle images are classified via supervised machine learning as described in Schlenczek et al. (2017). Figure 5-11a provides insight on how ice particles and liquid droplets are distributed in the sampled mixed-phase environment on the spatial scale smaller than 15 cm.

The PHIPS-HALO uses incoherent monochromatic laser light to backlight cloud particles, which suppresses interference effects and chromatic aberrations in the images (Fig. 5-11b). A second identical imaging system acquires a second image of the same particle from a different perspective to get (i) a three-dimensional information of the ice crystal and (ii) the orientation of the crystal with respect to the light scattering laser of the instrument. Light scattered from the imaged particle is detected in the angular range from 18° to 170° to determine the angular scattering function, which can be used to deduce the phase of the cloud particle (see Fig. 5-11b). Examples of the particle images registered by the CPI are shown in Figs. 5-6 and 5-12. McFarquhar et al. (2013) quantitatively demonstrated that at the 2.3-μm pixel resolution and 256 gray levels, the CPI enables discrimination of spherical and nonspherical images with sizes as small as 30 μm. However, automated algorithms that separate ice and water images with sizes between about 30 and 60 μm generally require quality control via manual inspection, which introduces some subjectivity.

Hybrid systems such as the 3V-CPI have recently been developed. The 3V-CPI uses a 2D-S optical array to provide a measure of the particle size distribution (PSD), with high-resolution imagery from a CPI used to assess particle phase as a function of particle size. In this way, the benefit of the large sample volume of the 2D-S is preserved. Examples of ice particle and liquid droplet size distributions that have been separated using this technique are shown in Fig. 5-12.

In summary, there is no commonly accepted methodology for quantitatively separating the ice particle and water drop size distributions in mixed-phase clouds at this time. The cases with LWC $\gg$ IWC (typically the initial stage of the mixed phase) and LWC $\ll$ IWC (typically the final stage of the mixed phase) are the most problematic for identification of phase composition. Observations of a few ice crystals among a large number of cloud droplets, and vice versa (a few liquid droplets among a large number of ice crystals), remain a challenging problem because of the small sampling statistics of in situ probes. The segregation of spherical frozen and liquid drops for imaging and scattering techniques also remains an unresolved problem. In general, collecting simultaneous data using multiple measurement techniques increases the potential for estimating the ice particle and water drop size distributions and the IWC fraction in mixed-phase clouds. However, the subjectivity inherent in interpreting results from multiple techniques also introduces the potential to misinterpret results and/or introduce bias in order to find agreement with predisposed opinions.
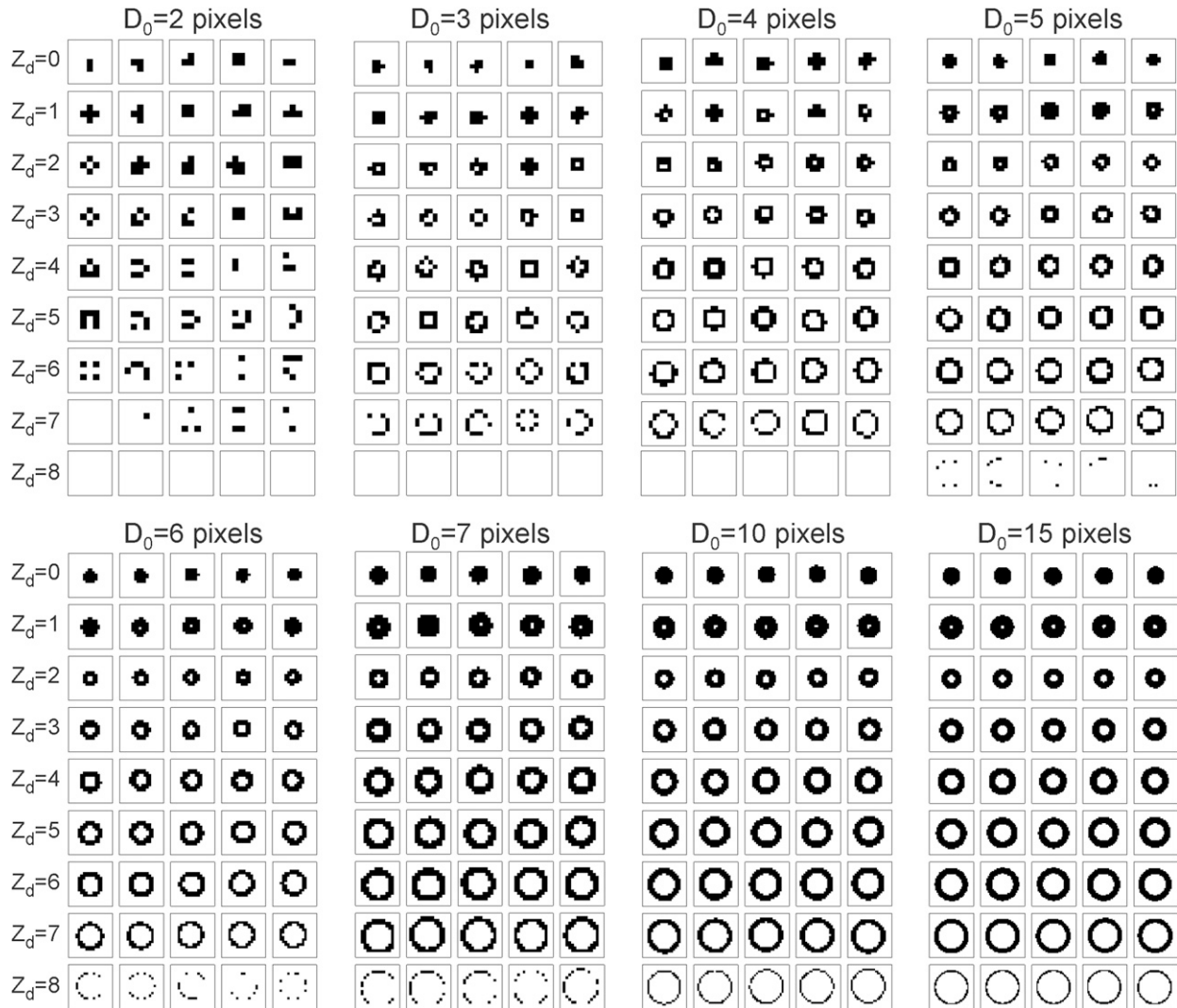
FIG. 5-9. Examples of modeled discrete binary diffraction images with different radii R [pixels from (top left) of 0 to (bottom right) of 15] and at different normalized distances $Z_d = \lambda |Z|/R^2$ from the object plane (Z is the distance from the object plane, λ is wavelength of light). The difference in the discrete images for the same Z_d is caused by shifts in particle locations as they pass over the photodiode array. [Adapted from Korolev (2007).]

2) MAIN RESULTS OF IN SITU OBSERVATIONS OF MIXED-PHASE CLOUDS

During the last three decades, there have been a number of in situ observations of mixed-phase conditions in different types of clouds. Results of studies of mixed-phase stratiform clouds (stratus, stratocumulus, altostratus, altocumulus, nimbostratus, cirrostratus, etc.) have been described by Rauber and Tokay (1991), Pinto (1998), Fleishauer et al. (2002), Gayet et al. (2002), Hogan et al. (2002), Korolev et al. (2003), Korolev and Isaac (2006), Noh et al. (2013), and others. Observations of mixed-phase clouds in the Arctic and Antarctic were presented by Hobbs and Rangno (1998), Verlinde et al. (2007), McFarquhar et al. (2007, 2011), Jackson et al. (2012), Lawson and Gettelman (2014), and others. Studies of mixed-phase convective clouds and tropical convective storms were conducted by Rosenfeld and Woodley (2000), Stith et al. (2004), Lawson et al. (2015), Leon et al. (2016), Taylor et al. (2016), and others. Mixed-phase lee-wave clouds were studied from in situ measurements in Heymsfield and Miloshevich (1993), Baker and Lawson (2006), and Field et al. (2012). In winter snowstorms, small-scale cloud-top-generating cells atop stratiform regions in the comma head have been found to generate supercooled water drops, which provide a favorable environment for
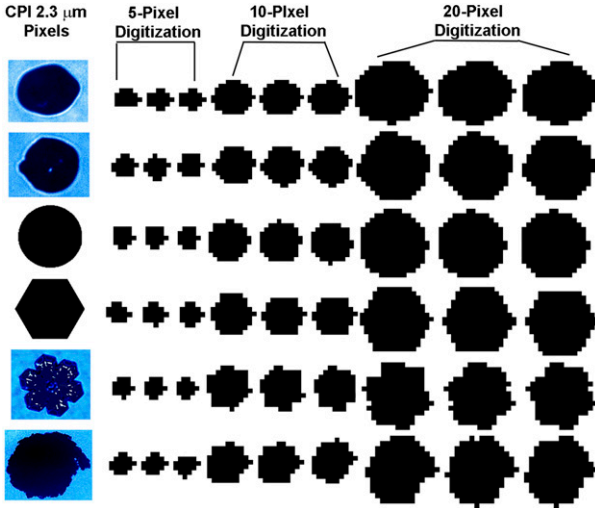
FIG. 5-10. Examples of synthetic "analog" circle and hexagonal plate (without blue background) and actual CPI particle images (with blue background). The analog images were digitized with different pixel resolution (e.g., 5, 10, and 20 pixels) and different realizations because of shifts in particle locations as they pass over the photodiode array. These examples show that at coarse pixel resolution, particles with different shapes may have a similar appearance.

enhanced concentration and growth of ice crystals (Plummer et al. 2014, 2015); elevated convection associated with such storms also provides an environment for growth of supercooled water and mixed-phase clouds (Murphy et al. 2017).

The frequency of occurrence of ice, liquid, and mixed-phase clouds was studied in a number of works (e.g., Peppler 1940; Zak 1949; Borovikov et al. 1963; Mossop et al. 1970; Isaac and Schemenauer 1979; Wallace and Hobbs 1975; Moss and Johnson 1994; Cober et al. 2001b; Korolev et al. 2003; Field et al. 2004). Comparisons of these results are hindered by the varying definitions of mixed phase, ice, and liquid clouds utilized in these studies. Despite these differences in cloud characterization, all these works found that the occurrence of mixed-phase clouds decreases toward lower temperatures.

Figure 5-13 shows spatial and mass fractions of ice, liquid, and mixed phase in midlatitude frontal and stratiform clouds. The temperature dependence of the spatial and mass fractions of mixed-phase clouds is different. This divergence is a reflection of differences in the microphysic and thermodynamic properties of ice and liquid clouds (e.g., size distributions, fall velocity, evaporation time, phase relaxation time, etc.) in different temperature intervals, which result in distinctive responses to cloud–environment interaction (turbulence, entrainment, vertical transport, radiation processes) and,

therefore, in distinctive spatial and mass distributions of liquid and ice.

Within the temperature range of $-20°C < T < -5°C$, the mass and spatial fractions of mixed-phase clouds are approximately equal to 20%. Outside this temperature range, ice and mass fractions decrease toward low and high temperatures. Ice particles require some time to melt when they fall below the freezing level, thus, mixed-phase and ice clouds may occur at $T > 0°C$.

One of the important findings on mixed-phase cloud properties obtained from in situ observations is a U shape in the frequency of occurrence of the ice water fraction $\mu_{ice} = IWC/(IWC + LWC)$ (Fig. 5-14). The U-shape distribution has its maxima at $\mu_{ice} = 0$ and $\mu_{ice} = 1$, that is, when the cloud is all liquid or all ice, respectively. It was found that the occurrence of mixed-phase clouds at $0.1 < \mu_{ice} < 0.9$ remains low and nearly constant in all temperature intervals. Such behavior of μ_{ice} is in general agreement with the theoretical description of the mixed phase as a transient stage between the metastable supercooled liquid-phase clouds and the thermodynamically stable ice phase.

It is worth noting that the statistical microphysical characteristics of mixed-phase clouds depend of the cloud dynamic forcing, sampling strategy, and instrumentation, and they may be different from those shown in Figs. 5-13 and 5-14. For example, Lohmann et al. (2016) demonstrated that there are differences in the statistics of the microphysical characteristics of mixed-phase clouds collected by different research groups in different types of clouds. Because of operational challenges of airborne sampling, the frequency of occurrence of mixed phase in convective clouds and convective storms is largely unknown.

Relative humidity (RH_w) in mixed-phase clouds determines the rate and direction of the partitioning of water mass (section 3b). As a result, RH_w is one of the important characteristics of the mixed-phase environment. In some numerical models, the water vapor pressure (e) in mixed-phase clouds is approximated as a weighted average of the respective saturation values over liquid water (e_{ws}) and ice (e_{is}), namely, $e = (1 - f)e_{ws} + f e_{is}$, where f is the weighting factor ($0 \leq f \leq 1$). The value of f in mesoscale and global circulation climate models is usually specified as a function of temperature (e.g., Fowler et al. 1996; Jakob 2002) or cloud LWC and IWC (e.g., Lord et al. 1984; Wood and Field 2000, Fu and Hollars 2004). Some models try to mimic the different stages of mixed-phase clouds by assuming water saturation provided the sum of the large-scale and turbulent vertical velocity u_z exceeds u_z^* [Eq. (5-8)] and switch to
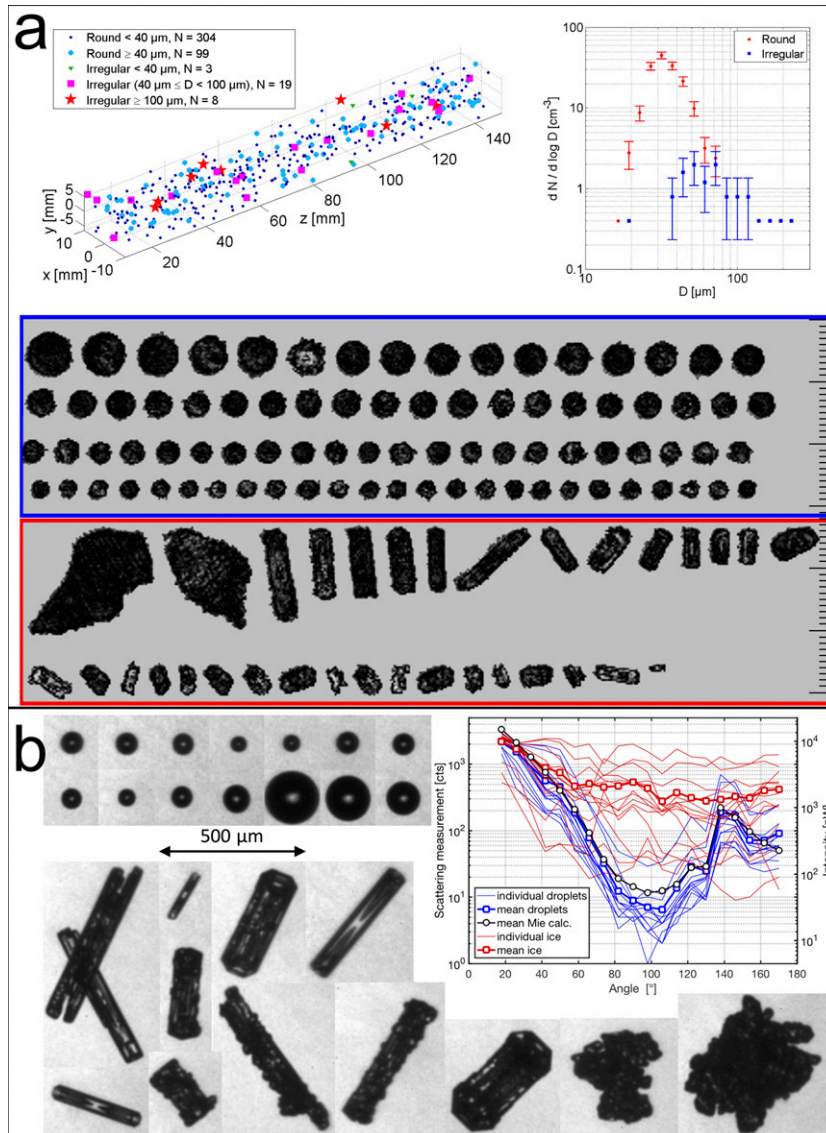
FIG. 5-11 (a) Example of data obtained from a single hologram of HALOHOLO. Shown are the (top left) spatial distribution of round and irregular particles and (top right) number-weighted size distribution. The instrument windows are located at $z = 6$ and $160\,\mathrm{mm}$. Particle images of round particles are shown in the top of the blue frame; the irregular particles are shown in the bottom and are outlined by the red rectangle. The scale bar increments are 10 and 100 microns. The habit classification segregated particle images in two categories of round and irregular. The particles were sampled in the glaciating region of a developing cumulonimbus cloud in the tropics at $T = -4°C$, $P = 508\,\mathrm{hPa}$. (b) Example of PHIPS-HALO data acquired in an Arctic mixed-phase cloud at $-1°C < T < -4°C$. Images of liquid droplets and ice particles are grouped on the left. The angular scattering functions of the corresponding droplets (blue) and ice crystals (red) are plotted on the right. Scattering functions from droplets are narrowly grouped with the primary and secondary rainbows clearly indicated at the 138° and 122° detection angles, respectively. Droplet diameters deduced from the images are used in Mie theory to calculate the averaged theoretical light scattering function (open black symbols) that nicely mimics the average of the measured functions (open blue symbols). Scattering functions from ice particles are more varying but have a rather flat angular dependence. Their averaged function (open red symbols) is clearly distinct from the corresponding function of the liquid droplets for scattering angles $> 50°$. For each individual particle, a second image is generated from a perspective 120° off the first image. [Adapted from Schnaiter et al. (2017).]
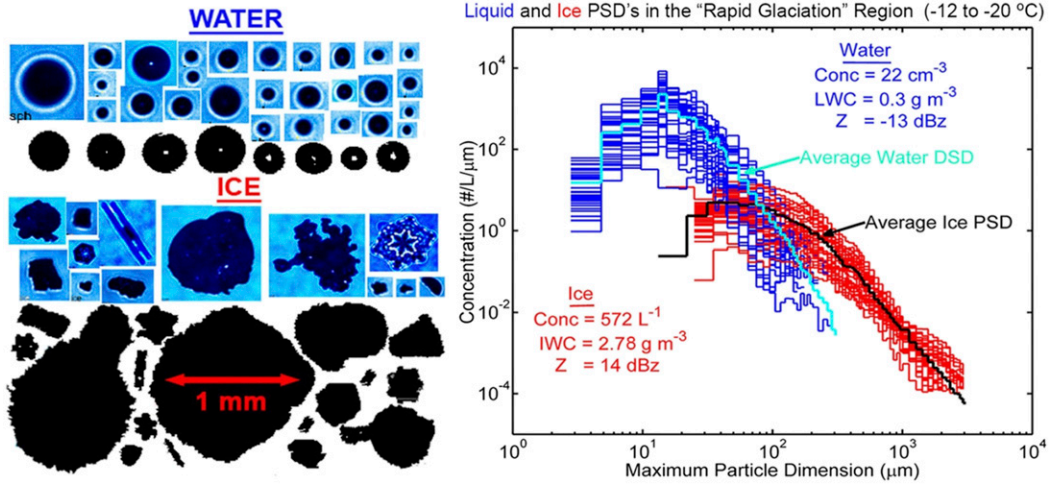
FIG. 5-12. Examples of (left) 2D-S and 3V-CPI images of water drops and ice particles and (right) water and ice PSDs. The water-to-ice PSD ratio for each size bin is determined using CPI roundness criteria for images between 30 and 400 μm, 2D-S roundness criteria for images >400 μm, and the assumption that images of <30 μm are water drops. Absolute values of water and ice size distributions are determined from 2D-S measurements. [Adapted from Lawson et al. (2015).]

saturation with respect to ice when $u_z < u_z^*$ (Storelvmo et al. 2008b; Lohmann and Hoose 2009).

Figure 5-15 shows the relative humidity over water RH_w versus μ_{ice} obtained from in situ measurements in stratiform mixed-phase clouds at a spatial averaging $\Delta x_p = 100$ m (Korolev and Isaac 2006). It was found that, on average, in all temperature intervals from 0°C down to −35°C, RH_w remains close to saturation over water (Fig. 5-15). This result is in agreement with theoretical predictions (section 3b). Therefore, in numerical simulations, RH_w in mixed-phase clouds can be assumed to be saturated over water at scales $\Delta x < 100$ m. At larger averaging scales, clouds may become conditionally mixed

(section 2a), and the average RH_w will decrease with the increase of the averaging scale (Korolev and Isaac 2006).

Zak (1949) reported observations of the high variability of the phase composition in frontal clouds. The spatial inhomogeneity of mixed-phase clouds explored in Korolev et al. (2003) and Field et al. (2004) suggests that genuine mixed-phase clouds are likely to occur at spatial scales $\Delta x < 100$ m. Analysis of humidity at different averaging scales suggested that the fraction of genuine mixed-phase clouds decreases with increasing Δx (Korolev and Isaac 2008).

As previously mentioned (section 1b), there are three indirect aerosol effects that can act in mixed-phase
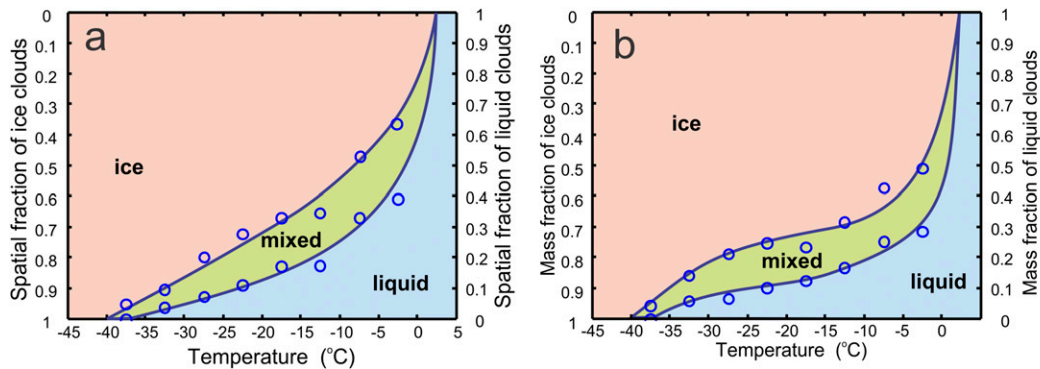
FIG. 5-13. (a) Spatial and (b) mass fractions of ice, liquid, and mixed clouds. Clouds with $\mu_{ice} \leq 0.1$ were categorized as liquid, $0.1 < \mu_{ice} < 0.9$ were categorized as mixed phase, and $\mu_{ice} \geq 0.9$ were categorized as ice. Clouds were determined as having TWC ≥ 0.01 g m^{-3}, averaging scale was 100 m, and the total length of sampled clouds was 61 765 km. Measurements were performed by Environment Canada in mid- and high-latitude continental and maritime air masses during the period 1994–2001.
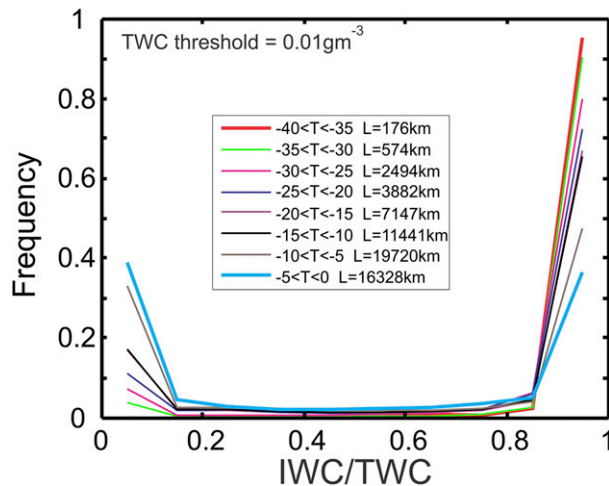
FIG. 5-14. Frequency of occurrence of ice fraction μ_{ice}, measured as the ratio of IWC to TWC, with spatial averaging of 100 m. Frequency of occurrence is provided for eight temperature intervals (see the different colors in inset), and the length of in-cloud legs for each temperature interval is also provided there. Clouds were determined as having a TWC $\geq 0.01\,\mathrm{g\,m^{-3}}$. Measurements were conducted by Environment Canada in mid- and high-latitude continental and maritime frontal clouds during the period 1994–2001. This diagram was recalculated from the data in Korolev et al. (2003) after correction of the Nevzorov measurements for the bouncing efficiency of ice (Korolev et al. 2013b).

FIG. 5-15. Dependence of the average humidity RH_w vs ice water fraction IWC/(IWC + LWC) for six different temperature intervals (see the different colors in inset) measured in mixed-phase clouds at an averaging scale of 100 m. Dashed lines correspond to the parameterization of $\mathrm{RH}_w = 100(1 - \mu_{ice} + \mu_{ice}\mathrm{RH}_{wsi})$. Vertical line on the left side represents an error bar. [Adapted from Korolev and Isaac (2006).]

clouds: the glaciation indirect effect, the riming indirect effect, and a cold second indirect effect. Jackson et al. (2012) found that, in Arctic clouds, liquid droplet concentrations were well correlated with aerosol concentrations below cloud, whereas ice crystal number concentrations were better correlated with aerosol concentrations above cloud. This observation suggests that the mixing of ice nucleating particles from above the cloud is consistent with a glaciation indirect effect. But, comparisons between cloud properties measured in the cleaner fall season against those measured in the more polluted spring season showed lower ice crystal concentrations and liquid effective radii, consistent with the thermodynamic effect. Because the majority of the observations analyzed were from the conceptually simpler single-layer mixed-phase clouds as opposed to the more complex multilayer mixed-phase clouds (e.g., Morrison et al. 2009) that occur more frequently over the Arctic, there was no statistically significant sample to categorically determine the relative importance of these indirect effects. Indeed, more detailed aerosol composition and concentration measurements in combination with in situ cloud observations in a variety of surface, meteorological, and aerosol conditions are needed to clarify the role of aerosol indirect effects in mixed-phase clouds.

In conclusion, the main outcomes from in situ studies can be formulated as follows:

1) Mixed-phase cloud regions are widespread on a global scale; they can occur in different types of clouds, over a wide range of altitudes, and at temperatures down to approximately −40°C.
2) Stratiform mixed-phase clouds may be persistent, with lifetimes significantly longer than the glaciating time.
3) The frequency distribution of the ice water fraction μ_{ice} in mixed-phase clouds averaged over the mesoscale has a U shape, with maxima at $\mu_{ice} = 0$ and $\mu_{ice} = 1$.
4) Water vapor humidity in mixed-phase clouds at an averaging scale $\Delta x_p < 100\,\mathrm{m}$ is close to saturation over water.
5) Usually the spatial correlation between LWC and IWC is poor or absent (e.g., Fig. 5-7).

b. Remote sensing of mixed-phase clouds

As indicated earlier, phase identification is a critical step in the remote sensing of cloud microphysical properties. Because of the presence of both phases, mixed-phase clouds are challenging targets for remote sensing. However, there has been significant progress in our capabilities in sensing mixed-phase clouds, mainly through new instrumentation capability, the synergy of multisensor measurements, and improved understanding of mixed-phase clouds from
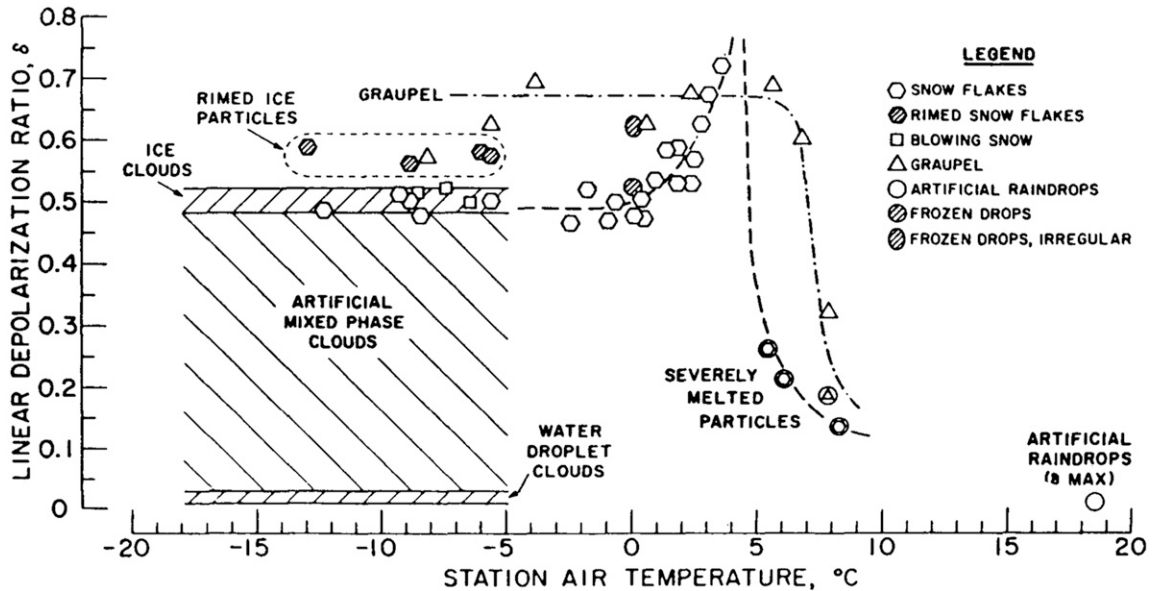
FIG. 5-16. A compilation of lidar linear depolarization ratios derived from a variety of laboratory and field studies of hydrometers using the CW laser–lidar analog approach (from Sassen 1991). The different lines highlight the ranges of the observations or mean temperature dependencies for different hydrometers.

in situ measurements. Here, we briefly summarize key instrumentation and results from ground- and space-based remote sensors.

1) MAIN INSTRUMENTATION FOR REMOTE SENSING OF MIXED-PHASE CLOUDS: PRINCIPLES, CHALLENGES, AND LIMITATIONS

There are a variety of active and passive remote sensors for mixed-phase cloud identification and quantification covering wavelengths from near-UV to millimeter wavelengths. These remote sensor observations are available from different platforms. For the convenience of discussion, we group them into the following categories: lidar, radar, moderate-spectral-resolution radiometer, high-spectral-resolution radiometer, and microwave radiometer:

(i) Lidar

Although the lidar principle was initially demonstrated in the 1930s, the rapid development of modern lidar technology started only after the invention of the laser, especially the Q-switched laser, in the early 1960s. A variety of lidar systems are now available for cloud observations with wavelengths mainly between 0.35 and 1.6 μm. Elastic lidars detect backscattering signals at the same wavelength as the transmitted laser radiation. Elastic lidars, which utilize high-power lasers (PDL, CALIOP, WCL) or low-power micropulse lasers (MPL, CPL), are widely used for cloud study from ground, aircraft, and space. Raman lidar and the high-spectral-resolution

lidar (HSRL), which offer improved cloud extinction measurements, are increasingly available for cloud observations from ground and aircraft.

Lidar, especially polarimetric lidar, is the most powerful tool to discriminate liquid and ice particles by taking advantage of the natural differences between liquid droplets and ice crystals. For backscattering, spherical droplets produce no or weak depolarization signals, while ice crystals introduce strong depolarization signals depending on ice crystal habits and orientations, as illustrated in Fig. 5-16 (Sassen 1991). Therefore, the lidar linear depolarization ratio offers a straightforward way to identify liquid and ice clouds. Water clouds have high concentrations of small water droplets, while ice clouds normally have low concentrations of ice crystals. Thus, liquid clouds produce strong peak signals and strong attenuation, while ice clouds produce weak peak signal and weak attenuation. For nonpolarimetric lidar, these signal differences can be used to discriminate liquid and ice clouds. However, the ambiguities related to this method may result in a phase misidentification at temperatures below $-30°$C (Zhang et al. 2012).

For mixed-phase clouds, the lidar signal is often dominated by the liquid phase, which makes it a challenging task to identify mixed-phase clouds with lidar measurements. Physically, ice crystals grow fast within mixed-phase clouds and fall out of the mixed-phase zone gradually. Wave clouds presented in Fig. 5-17 illustrate this process. The black contour
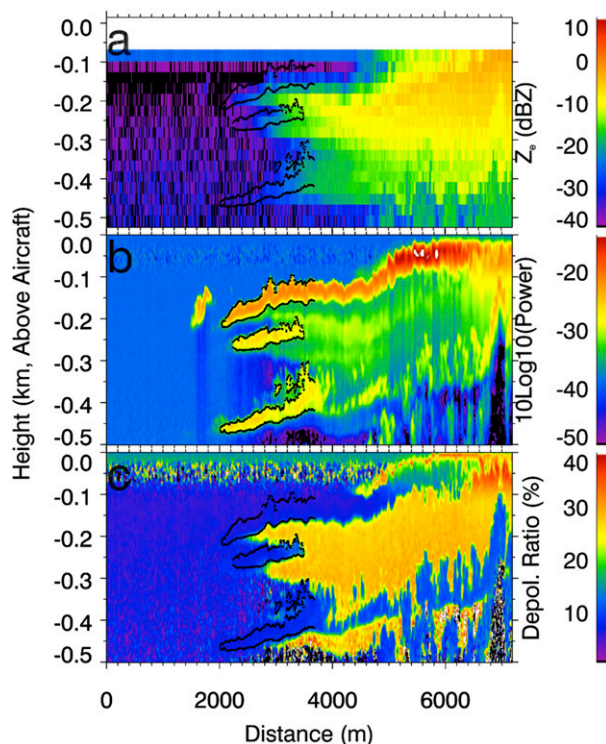
FIG. 5-17. WCR and WCL observations of ice formation in mixed-phase wave clouds on 8 Mar 2009 from the University of Wyoming King Air: (a) WCR Z_e, (b) nadir WCL power, and (c) nadir WCL depolarization ratio (uncalibrated). The black contour outlines the front ends of the three distinct wave cloud layers. [From Wang et al. (2012).]

outlines three distinct wave cloud layers. The front edges of the wave clouds are identified as a liquid-only or liquid-dominated mixed-phase environment because of their strong power (Fig. 5-17b) and low depolarization (Fig. 5-17c). After a few hundred meters, ice (high depolarization) below the supercooled-dominated region is detected and grows deeper with distance (time). Therefore, for stratiform mixed-phase clouds, the ice layer below the mixed-phase zone is always detectable with zenith-pointing lidar. By using this vertically coherent structure, polarimetric lidar can be used to effectively detect mixed-phase clouds, especially for zenith-pointed ground-based or airborne lidar (Wang and Sassen 2001). However, for nadir-pointed lidar, such as the cloud physics lidar (CPL) typically mounted on the NASA ER-2 aircraft and CALIOP mounted on a satellite, the mixed-phase layer could totally attenuate the lidar signals by the liquid-dominated top to prevent the detection of ice below. In this case, lidar measurements often classify mixed-phase cloud layers as liquid clouds. Thus, the CALIOP cloud-phase product provides only liquid or ice separations (Hu et al. 2007), and many

supercooled liquid clouds identified by CALIOP are actually mixed-phase clouds (Zhang et al. 2010). Since 2007, CALIOP was tilted 3° off nadir to reduce the impact of the specular reflection of horizontally oriented ice crystals on the CALIOP cloud-phase identification.

Additional challenges for lidar mixed-phase cloud detection include strong cloud attenuation, multiple scattering (MS), and horizontally oriented plate ice crystals. Although lidar is effective at detecting the occurrence of supercooled liquid, optically thick ice layers below or above cloud could prevent zenith- or nadir-pointing lidar to detect supercooled liquid zones. Because of the MS effect, lidar depolarization measurements from optically thick liquid clouds could be as high as those from ice clouds, especially for space-based lidar (Hu et al. 2007; Wang et al. 2009). Although ice crystals normally generate large depolarization ratios, very small depolarization ratios and strong returns can be produced by horizontally oriented plate ice crystals (Sassen 1991). Therefore, caution should be exercised when using lidar measurements for cloud phase detection.

(ii) Radar

Although precipitation radars have been used for precipitation measurements routinely for almost 60 years, W-band (~94 GHz) and Ka-band (~35 GHz) radars more suitable for cloud detection have only matured during the last 20 yr (Lhermitte 1987). Now ground-based (Moran et al. 1998; Kollias et al. 2007), airborne, and satellite (*CloudSat*; Stephens et al. 2002) millimeter-wavelength radars are available to provide cloud retrievals. The longer operating wavelength of radars makes them more sensitive than lidars to large particles. Therefore, for mixed-phase clouds, the radar reflectivity (Z_e) is dominated by ice particles. Thus, with only Z_e measurements, cloud radar is not able to detect the presence of the mixed phase because information on supercooled liquid is lacking. However, Doppler velocity spectra measurements from advanced cloud radars offer the potential to detect both the liquid and ice phase within mixed-phase clouds. Because small liquid droplets have smaller fall speeds than large ice crystals, liquid and ice contributions to the Doppler velocity spectra can be separated, as illustrated in Fig. 5-18. The overlap between ice and liquid Doppler velocity spectra is affected by the size distributions of liquid droplets and ice crystals and by turbulence. By using morphological features in Doppler spectra measured by a millimeter cloud radar (MMCR), Luke et al. (2010) developed a technique to detect supercooled liquid droplets in the
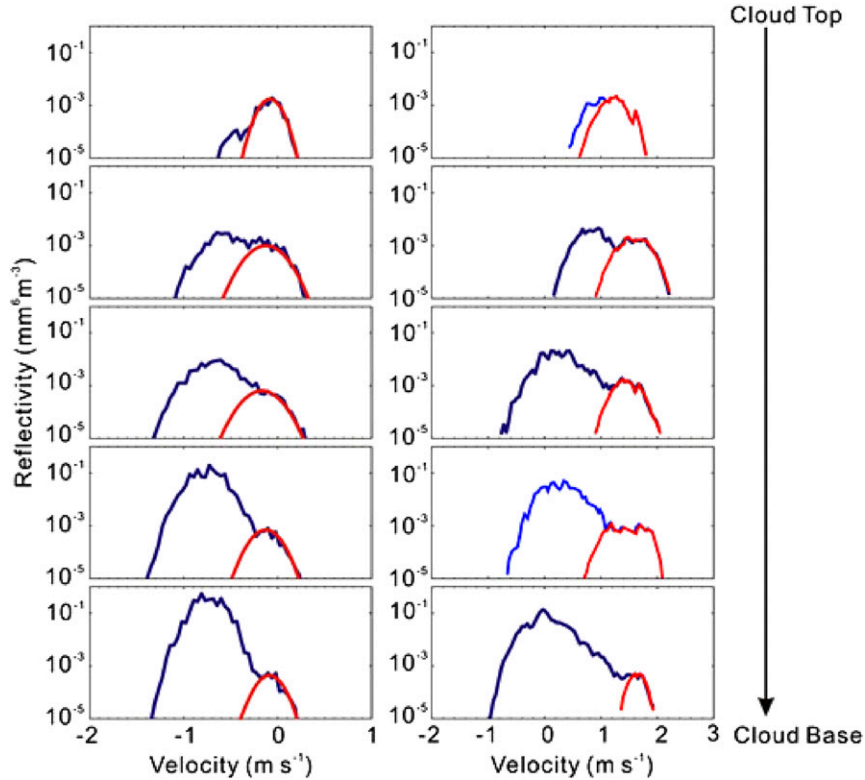
FIG. 5-18. Examples of radar Doppler spectra at different heights from cloud base to cloud top. (left) The simulated spectra based on outputs of a large-eddy simulation model for a spring season simulation. (right) Ka-band ARM zenith radar (KAZR) observations in October 2011. The red lines represent the cloud liquid drop contributions to (and retrieved from) the spectra; whereas the blue lines represent both the cloud liquid drop and ice particle contributions to the spectra. Positive velocities represent upward motion and negative velocities downward motion. [From Yu et al. (2014).]

radar sampling volume in the presence of ice particles. Yu et al. (2014) presented a technique that extracts the weak cloud liquid drop contributions from the total radar returns in Doppler velocity spectra for profiling cloud radars, and Zawadzki et al. (2001) used a vertically pointing X-band Doppler radar to infer the presence of supercooled droplets from observed bimodal Doppler spectra.

However, under strong turbulence, such as in deep convective clouds, or when Doppler spectra from cloud droplets and ice particles significantly overlap, it is not possible to reliably identify supercooled liquid from radar in Doppler velocity spectra. Other radar-based technologies were hence explored to improve supercooled liquid identifications in such mixed-phase clouds. Dual-wavelength radar approaches were developed to profile the distribution of LWC by using the differences in reflectivity and attenuation between two wavelengths (Vivekanandan et al. 1999; Huang et al. 2009). Because of the relatively weak attenuation of radar wavelengths by liquid cloud droplets and

variations of ice particle scattering, the dual-wavelength approach is mainly suitable for high LWC cases (Williams and Vivekanandan 2007). Polarimetric radar measurements offer additional information to detect supercooled liquid in convective or other deep clouds. With the National Center for Atmospheric Research S-band dual-polarization Doppler radar (S-Pol) measurements (Keeler et al. 2000), Plummer et al. (2010) showed that three polarization radar parameters—the radar reflectivity factor at horizontal polarization (ZH), the differential reflectivity (ZDR), and the specific differential phase (KDP)—are statistically distinguishable between conditions in mixed- and ice-phase clouds, even when an estimate of measurement uncertainty is included. But, the detection of mixed-phase clouds using polarimetric radar measurement is still under development partly because of the limited in situ data for evaluation and guidance. In addition, the complex and changing ice crystal sizes and habits in these vertically extended mixed-phase clouds make the retrievals very challenging.
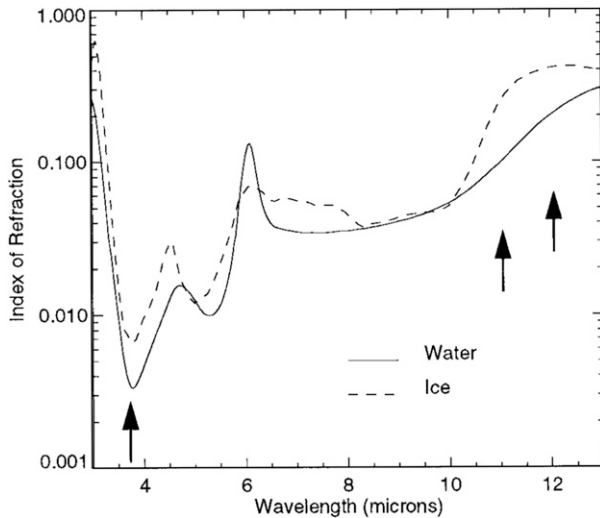
FIG. 5-19. Imaginary index of refraction for water (solid line) and ice (dashed line) from 3 to 13 μm. The three arrows correspond to the three AVHRR thermal channels (3.7, 11, and 12 μm). [From Key and Intrieri (2000).]
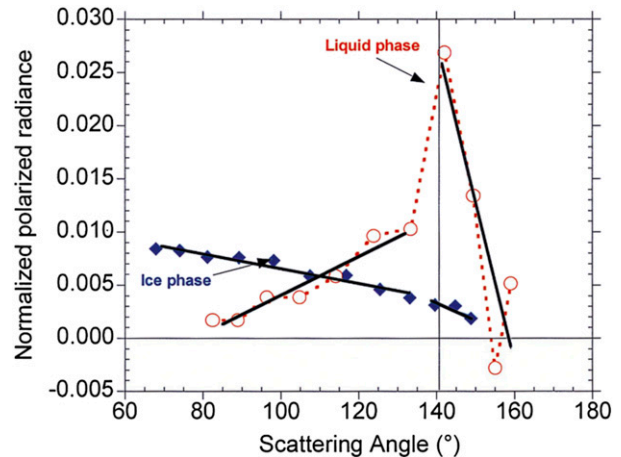
FIG. 5-20. Examples of directional polarization samples at 0.865 μm measured by POLDER over Lille (northern France) for cirrus clouds and liquid clouds. Solid lines correspond to linear fit of the measurements for the two scattering-angle ranges: 60°–140° and 140°–180°. [From Goloub et al. (2000).]

(iii) Moderate-spectral-resolution radiometer

Moderate-spectral-resolution radiometers are the main instruments for satellite passive cloud remote sensing (Stubenrauch et al. 2013). Such instruments range from 5 spectral channels in the GOES and the Advanced Very High Resolution Radiometer (AVHRR) visible and infrared radiometers to 36 spectral channels in the more advanced MODIS. Therefore, the information content available for cloud-phase determination can vary significantly.

In addition to using cloud temperature to physically determine cloud phase, passive sensors also use radiative properties for cloud-phase discrimination. Radiatively, the spectral difference between water and ice clouds occurs because of differences in absorption and scattering. As illustrated in Fig. 5-19, the absorptive properties of water and ice represented by the imaginary index of refraction have a different dependence on wavelength. Key and Intrieri (2000) demonstrated that brightness temperature differences at 3 wavelengths (3.7, 11, and 12 μm) and reflectance at 3.7 μm provide necessary, but not sufficient, information for differentiating between liquid and ice clouds. The relationship between the cloud and surface temperatures must also be considered. Because of these limitations, the IR-based cloud phase determination is further enhanced
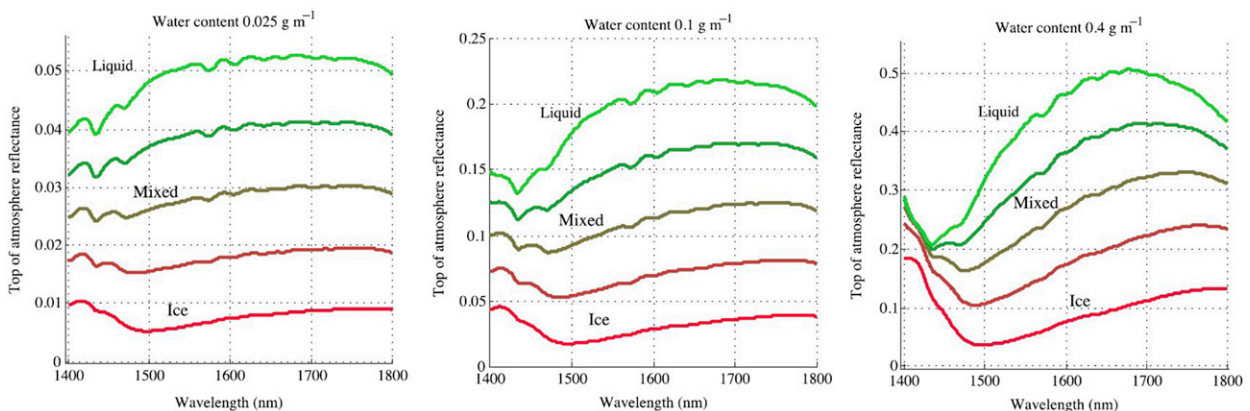
FIG. 5-21. TOA reflectance for simulated clouds of different thermodynamic phase (shown by different colors) for a single 0.5-km-thick layer at 5.5-km altitude with 30° solar zenith over a dark surface: (left to right) TWC = 0.025, 0.1, and 0.4 g m^{-3}. The particle radii are held constant at 10 and 60 μm for liquid and ice, respectively. The TWC is apportioned to one or both phases in 25% increments. [From Thompson et al. (2016).]
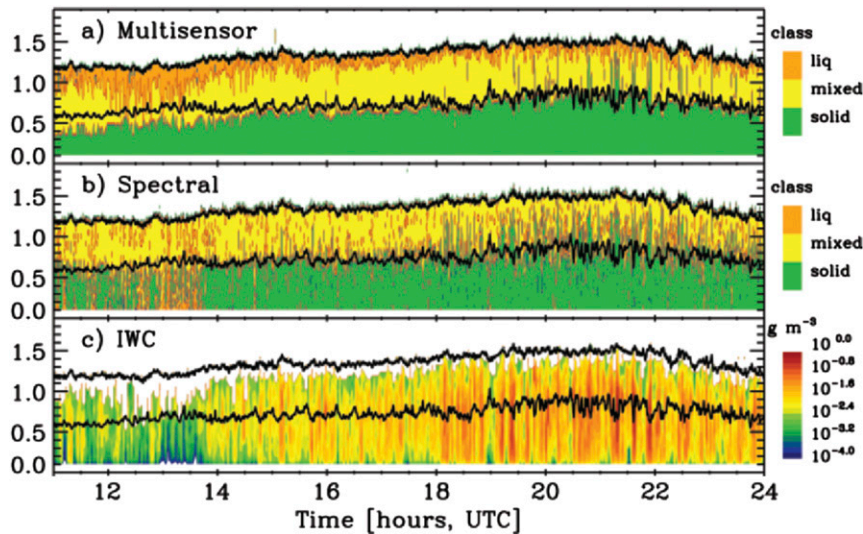
FIG. 5-22. Retrieved, vertically resolved cloud properties for 9 Oct 2004 at Barrow, Alaska:
(a) multisensor cloud-phase classification, (b) Doppler radar spectra cloud-phase classification,
(c) IWC derived from radar. [From Shupe et al. (2008).]

by using cloud emissivity ratios, as discussed in Heidinger and Pavolonis (2009) and as used in the new MODIS, version 6 (V6), product (Baum et al. 2012). Similarly, because of different imaginary indexes of refraction for liquid and ice at 1.6 and 2.1 μm (Kou et al. 1993), ice particles are more absorptive than liquid droplets at these wavelengths and thus have smaller TOA shortwave IR (SWIR) reflectances (Pilewskie and Twomey 1987; Chylek and Borel 2004). The SWIR reflectance ratio can also be used to identify liquid and ice clouds (Platnick et al. 2017). However, the accuracies of the IR and the SWIR approaches depend on many factors, such as cloud type, observing angle, atmospheric and surface properties, and optical thickness (Jäkel et al. 2013). Moreover, results can be less accurate for mixed-phase clouds and often inappropriate for multilayer clouds systems (Baum et al. 2003; Pavolonis and Heidinger 2004).

Multiangle imagers with polarization measurements, such as the POLDER satellite instrument, can provide scattering-angle-dependent polarized radiance to improve the performance of cloud-phase determination (Goloub et al. 2000). As illustrated in Fig. 5-20, cloud droplets exhibit very specific polarization features in the rainbow for scattering angles near 140°. On the other hand, theoretical studies and observations show that the rainbow characteristics disappear as soon as the particles depart from a spherical shape. Therefore, the rainbow feature can be used to improve liquid and ice separation, but it is a challenge how to handle thin cirrus clouds overlapping the liquid cloud layer (Goloub et al. 2000). POLDER visible-only measurements are not sufficient to handle this overlap cloud condition.

Based on MODIS satellite measurements (Platnick et al. 2017), passive measurements can determine only liquid or ice cloud phase. Mixed-phase cloud identification is still a challenge. To address this problem, Miller et al. (2014) proposed an approach for the detection of liquid-top mixed-phase clouds from passive satellite radiometer observations. Their algorithm makes use of reflected sunlight in narrow bands at 1.6 and 2.25 μm to optically probe below liquid-topped clouds and determine phase. Detection is predicated on differential absorption properties between liquid and ice particles, accounting for varying sun/sensor geometry and cloud optical properties. However, this approach shows strong sensitivity to ice microphysical properties.

(iv) High-spectral-resolution radiometer

As demonstrated by Nasiri and Kahn (2008), there are limitations of an approach using two infrared channels with moderate spectral resolutions for cloud-phase determination, and there is potential for improvement using channels with higher spectral resolution. Radiometers with high spectral resolution are now widely available and provide improved mixed-phase cloud determination. With high-spectral-resolution ground-based infrared measurements, Turner et al. (2003) and Lubin (2004) showed that the differences in the index of refraction of ice and water between 11 and 19 μm offer improved mixed-phase cloud identification. But such a technique is difficult to implement for high-spectral-resolution IR measurements from AIRS satellite measurements because different types and phases of clouds can occur within the large AIRS footprint.
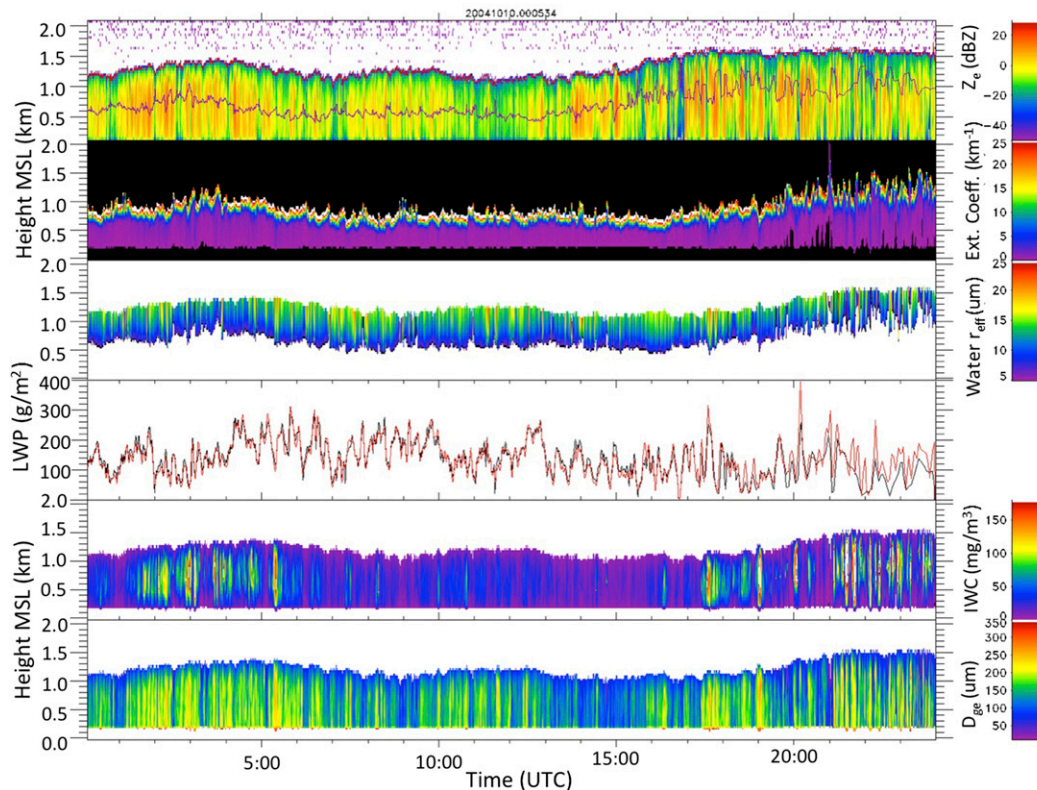
FIG. 5-23. Mixed-phase clouds observed at the Barrow site on 10 Oct 2004 by combining MMCR, MPL, MWR, and radiosonde data. (top to bottom) MMCR Z_e, MPL retrieved extinction, retrieved liquid-phase effective radius, LWP, retrieved IWC, and general effective radius. The red line superimposed on the top of the Z_e cross section indicates the mixed-phase cloud base. Cloud-top temperature $\sim -13.3°$C.

Pilewskie and Twomey (1987) showed that differences in bulk liquid water and ice absorption in the NIR (between 700 and 2500 nm) have observable consequences in cloud spectral reflectance and transmittance that can be exploited to retrieve cloud thermodynamic phase. With simulated SWIR spectra, Fig. 5-21 shows spectrum slope dependence on the mass partitioning of mixed-phase clouds. Various approaches have been developed to use this information for better cloud-phase determination (Ehrlich et al. 2008; LeBlanc et al. 2015). As illustrated by Ehrlich et al. (2008), the identification of mixed-phase clouds requires a priori knowledge of the ice crystal dimension, and uncertainties in ice microphysical properties could result in identifying boundary layer mixed-phase clouds with a pure liquid cloud-top layer as pure liquid water clouds. Thompson et al. (2016) demonstrated that combining the spectrum fitting and fast parameter estimation (Green et al. 2006; Gao and Goetz 1990) applicable to imaging spectrometers can map cloud thermodynamic phase with high fidelity and spatial resolution.

(v) Microwave radiometer

The microwave radiometer (MWR) is widely used to detect liquid water path (LWP) in liquid and mixed-phase clouds by using emitted signals from liquid drops. Therefore, the MWR can be used together with other instruments to better identify mixed-phase clouds, as discussed below. The LWPs of mixed-phase clouds are often low, especially for stratiform mixed-phase clouds in polar regions (Zhao and Wang 2010). For the traditional two-wavelength MWR, large uncertainties are present in the retrieved LWPs (Turner et al. 2007). Thus, for low LWP mixed-phase cloud measurements, either additional high frequencies (Cadeddu et al. 2013) or new processing methods (Wang 2007) are needed to improve the LWP detection accuracy of supercooled liquid within clouds. Other challenges for the MWR are the occurrence of multilayer clouds and rain. When a mixed-phase cloud layer overlies a liquid cloud layer, the lower liquid layer normally dominates the total LWP retrieved from the MWR, which makes the identification of the mixed-phase LWP difficult. The presence of rain normally dominates MWR signals to make the detection of liquid cloud challenging.

(vi) Multisensor approaches

Considering the limitations of individual instruments, the synergy of multisensor measurements is the most
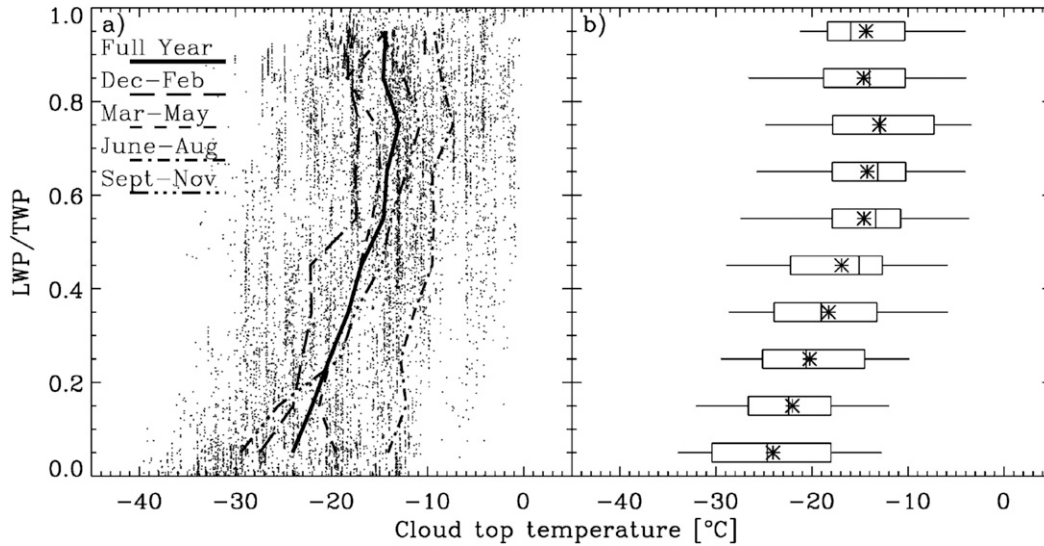
FIG. 5-24. (a) Scatterplot of the liquid fraction [LWP/(LWP + IWP)] vs cloud-top temperature for mixed-phase clouds. Plotted are the annual (solid black) and seasonal average relationships (different type lines). (b) Box-and-whisker plots summarizing the same data used in (a). The 5th, 25th, 50th, 75th, and 95th percentiles and mean value are provided for each box–whisker. [From Shupe et al. (2006).]

effective way to improve mixed-phase cloud identification. Riedi et al. (2010) demonstrated that an approach based on the synergy between the POLDER and MODIS measurements offered improved cloud-phase discrimination. As discussed above, lidar is more sensitive to cloud droplets within mixed-phase clouds, and radar is more sensitive to relatively large ice particles within mixed-phase clouds. As illustrated in Fig. 5-17, a radar clearly shows ice within supercooled liquid layers, and lidar measurements show supercooled liquid layers. Thus, the synergy of lidar and radar provides the most reliable way to identify mixed-phase clouds (Wang and Sassen 2001; Hogan et al. 2003a; Wang et al. 2004). Combined *CloudSat* radar and *CALIPSO* lidar measurements have been used to effectively identify mixed-phase clouds globally (Zhang et al. 2010; Wang et al. 2013), and to provide improved microphysical property retrievals for ice (Delanoë and Hogan 2008; Deng et al. 2010, 2013; Okamoto et al. 2010; Matus and L'Ecuyer 2017). Shupe (2007) presented a method for classifying cloud phase from a suite of ground-based sensors. The method exploits the complementary strengths of cloud radar, depolarization lidar, microwave radiometer, and temperature soundings to classify clouds observed in the vertical column as ice, snow, mixed phase, liquid, drizzle, rain, or aerosol. The comparison of a multisensor approach with a radar spectral-based approach in Fig. 5-22 shows that the multisensor approach provides more reliable identification of mixed-phase regions (see Shupe et al. 2008 for more detailed discussion).

Multisensor measurements provide effective ways not only to identify mixed-phase clouds, but also to retrieve the microphysical properties of mixed-phase clouds. As illustrated by Wang et al. (2004) and Shupe et al. (2015), combining ground-based multisensor measurements, including lidar, radar, MWR, and other measurements can provide liquid- and ice-phase microphysical properties as illustrated in Fig. 5-23. In Fig. 5-23, MPL measurements below the mixed-phase cloud layer are combined with MMCR measurements to determine properties of precipitating ice with a combined lidar–radar algorithm (Wang and Sassen 2002). Then, the MMCR measurements are used to extend ice retrievals into the mixed-phase layer. The effective radius profile of the liquid phase is determined by combining MPL-derived extinction coefficients and adiabatic liquid water content with the constraint of the retrieved LWP. With the multisensor measurements from A-Train satellites, Adhikari and Wang (2013) showed that stratiform mixed-phase cloud properties can be retrieved globally. However, retrieving mixed-phase cloud properties in deep convective clouds is still a challenging task.

2) MAIN RESULTS OF REMOTE SENSING OBSERVATIONS OF THE MIXED PHASE

As illustrated above, capabilities to remotely sense mixed-phase clouds are still very limited. So far, ground-based multisensor measurements provide the most reliable mixed-phase cloud information (Rauber and Grant 1986; Dong and Mace 2003; Shupe
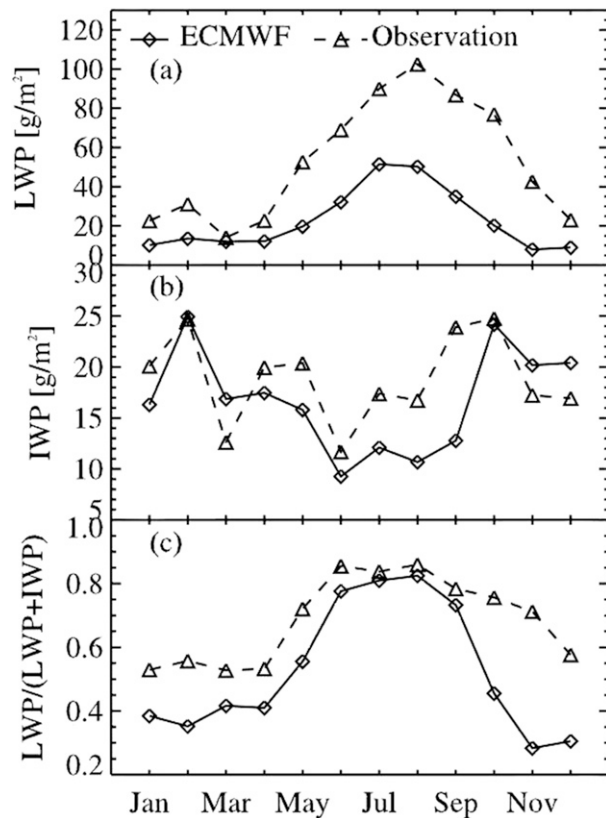
FIG. 5-25. Comparison of monthly mean (a) LWP, (b) IWP, and (c) LWP/(LWP + IWP) for the low-level clouds between the ECMWF model simulations (solid lines) and the observations (dashed lines) around the NSA site. [From Zhao and Wang (2010).]

et al. 2006, 2008, 2015; Zhao and Wang 2010). Shupe et al. (2006) presented Arctic mixed-phase cloud macro- and microphysical properties derived from a year of radar, lidar, microwave radiometer, and radiosonde observations made as part of the Surface Heat Budget of the Arctic Ocean (SHEBA) Program in the Beaufort Sea in 1997–98. During SHEBA, mixed-phase clouds occurred 41% of the time and were most frequent in the spring and fall transition seasons. These clouds often consisted of a shallow, cloud-top liquid layer from which ice particles formed and fell, although deep, multilayered mixed-phase cloud scenes were also observed. On average, individual cloud layers persisted for 12 h, while some mixed-phase cloud systems lasted for many days. Figure 5-23 shows an example of a boundary layer mixed-phase cloud that had significant temporal variations and lasted for more than one day. MMCR measurements and retrieved cloud properties showed that there are clear convective cells within these stratiform mixed-phase clouds, which lead to strong spatial variations in liquid- and ice-phase properties.

The base and top of the mixed-phase layer also vary with time. These spatial/temporal structures indicated strong couplings between dynamics and microphysical processes within Arctic stratiform mixed-phase clouds, which need to be properly treated in climate models. Similar convective generating cells have also been observed atop the comma head region of continental winter cyclones (e.g., Plummer et al. 2014; Rosenow et al. 2014).

Physically, mixed-phase clouds could be observed at temperatures as low as about $-40°C$; however, their occurrence and the liquid fraction (ratio of LWP to total condensed water path) decreases with temperature. Shupe et al. (2006) showed that the mean liquid fraction increased on average from 0 at $-24°C$ to 1 at $-14°C$ for retrievals of Arctic clouds at Barrow, Alaska (now known as Utqiaġvik), as illustrated in Fig. 5-24. The observations at $-25°C$ also show for any given liquid fraction a phase transition relationship may change moderately with season. It is important to be aware that the results in Fig. 5-24 are based on vertically integrated cloud-layer properties, including the precipitating ice, and are also dependent on the data processing algorithms (Zhao et al. 2012).

The seasonal variation of mixed-phase cloud properties can also be well characterized with ground-based measurements. With observations from the Atmospheric Radiation Measurement Climate Research Facility at the North Slope of Alaska (NSA) site during 1999–2007, Zhao and Wang (2010) showed the seasonal variation of Arctic stratiform mixed-phase clouds as presented in Fig. 5-25. The seasonal variation is mainly driven by seasonal temperature variations while other properties, such as large-scale dynamics, boundary layer structure, and surface fluxes, also impact the mixed-phase cloud properties. These observations were used to evaluate the model-simulated clouds from the European Centre for Medium-Range Weather Forecasts (ECMWF) and highlight the challenges of simulating these stratiform clouds (Klein et al. 2009).

Although it is not yet possible to provide global mixed-phase cloud microphysical properties, combined CloudSat and CALIPSO measurements do provide reliable mixed-phase cloud identification (e.g., the CloudSat 2B-CLDCLASS-lidar product; Wang et al. 2013). However, the lidar signal attenuation limits the liquid detection to a single layer near cloud top. Figure 5-26 shows global cloud phase distributions based on CloudSat- and CALIPSO-detected cloud layers. Similar to the liquid cloud distributions, stratiform mixed-phase clouds have a high frequency of occurrence over oceans caused by the more abundant water vapor supply. In the tropics, mixed-phase clouds are mainly
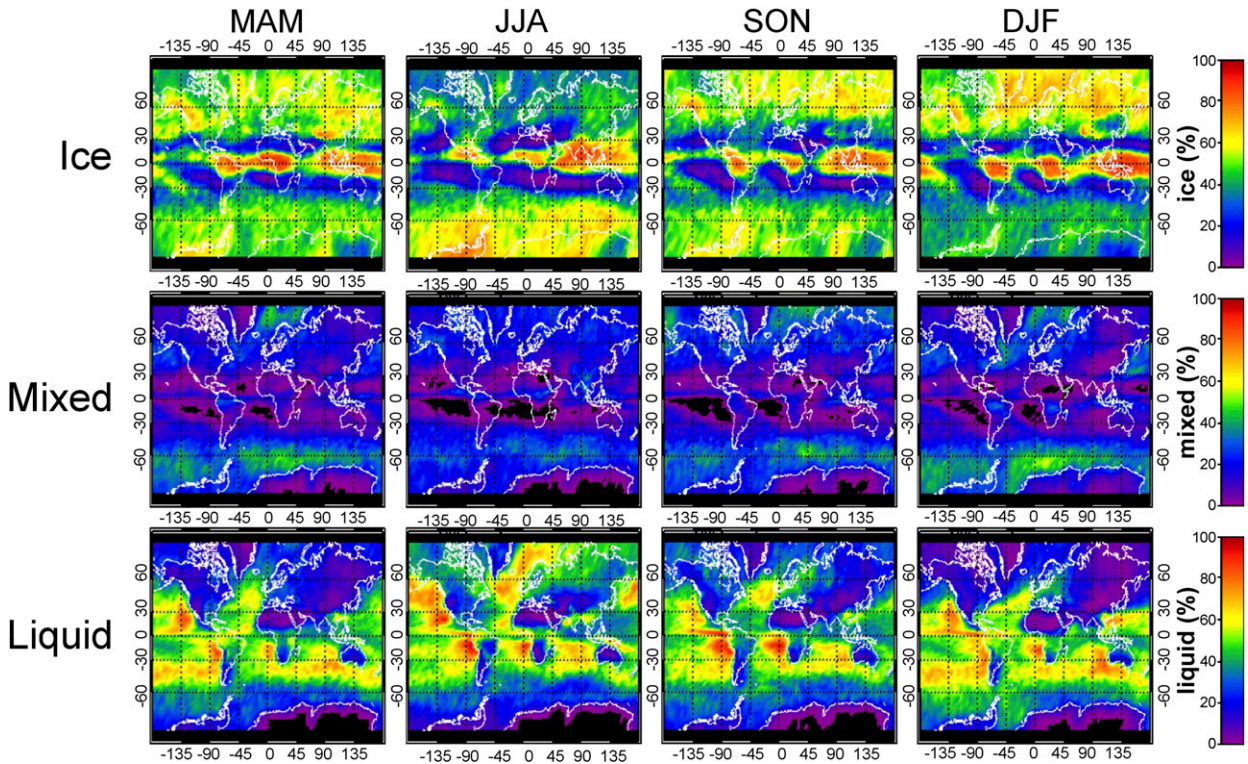
FIG. 5-26. Global cloud-phase (ice, mixed, and liquid) and seasonal (MAM, JJA, SON, and DJF) distributions based on *CloudSat* 2B-CLDCLASS-lidar product during 2006–10. [Adapted from Wang et al. (2013).]

deep convective clouds and midlevel stratiform clouds associated with deep convective clouds. The seasonal shift of mixed-phase clouds is mainly driven by the temperature and large-scale dynamical shifts forced by the annual cycle of solar radiation. These global views of mixed-phase cloud distributions offer important guidance for cloud simulations in climate models.

5. Role of the mixed phase in cloud electrification

The most vigorous manifestation of mixed-phase processes in the atmosphere is found in the updraft regions of thunderstorms. Given the inhospitable environment inside the thunderstorm, the early realization of the importance of the mixed phase for cloud electrification was developed from observations from the outside looking in. Workman and Reynolds (1949) made pioneering radar and electric field observations of the relationship between lightning activity and the vertical development of New Mexico thunderstorms that highlighted the cold (subfreezing) part of the cloud as the origin of the electrification process. Many subsequent radar observations have shown the development of strong radar reflectivity in the cold part of the cloud coincident with the onset of strong electrification (Lhermitte and Williams 1985; Dye et al. 1989; Krehbiel 1986; Stolzenburg

et al. 2015). These early efforts with radar then expanded with the remotely sensed locations of the electric charge participating in intracloud and cloud-to-ground lightning flashes (Reynolds and Neill 1955; Jacobson and Krider 1976; Krehbiel et al. 1979; Krehbiel 1981; Koshak and Krider 1989). These investigations served to confirm the basic positive dipole characterization of the thunderstorm, with the main negative charge over a range of in situ temperatures from $-10°$ to $-20°C$ and with the upper positive charge at $-30°C$ and lower temperatures. The resolution of the lightning charge into individual strokes provided evidence for the lateral extensiveness of the main negative charge region (Krehbiel et al. 1979). These observations isolate the ''mixed phase'' region (bounded by the $0°$ and $-40°C$ isotherms) as the location of the charge separation.

More recent observations with dual-polarization radar (Jameson et al. 1996; Kumjian et al. 2014; Mattos et al. 2017) in this same mixed-phase region have disclosed a transition from supercooled raindrops to graupel, coinciding with the initiation of strong electrification and intracloud lightning. These observations extend support for the idea that, when graupel particles collide with ice crystals, negative charge is selectively transferred to the graupel and positive charge to the rebounding ice crystals so that the main negative charge

region of the thunderstorm dipole is formed. The gravitational descent of the larger negatively charged graupel particles with respect to the positively charged ice crystals serves as the dominant mechanism of charge separation. Measurements of the electric charges carried by precipitation particles inside thunderstorms are consistent with this idea (e.g., Marshall and Winn 1982; Takahashi et al. 1999, 2017).

The insights obtained from the remote sensing of New Mexico thunderclouds led Reynolds et al. (1957) to initiate a laboratory experiment on mixed-phase microphysics. This pioneering experiment set the stage for later laboratory work (Takahashi 1978; Jayaratne et al. 1983; Saunders et al. 1991; Ávila and Pereyra 2000; Berdeklis and List 2001; among others) all with a common goal: to identify the specific mixed-phase conditions linked with the systematic positive and negative charging of simulated graupel and ice crystals.

The challenges of simulating the natural mixed-phase conditions of a thundercloud in a laboratory cold box and making representative measurements of the charge transferred in particle collisions cannot be overstated. This difficulty no doubt has much to do with the differences one finds among published results from different laboratories (Williams 1985; Saunders et al. 1991; Saunders 2008; Takahashi et al. 2017), even when matched mixed-phase conditions are intended.

The usual assumption in the laboratory simulations is that water saturation is maintained, consistent with the presumed condition in a thunderstorm updraft. Later laboratory experiments were aimed at verifying that full-up mixed-phase conditions were needed for substantial charge transfer in ice particle collisions and the production of lightning. More recently this view has changed to some extent because measurable charge separation in laboratory experiments occurs in particle collisions without supercooled water (Keith and Saunders 1990; Luque et al. 2016) and with controlled conditions of relative humidity (with respect to water) less than 100% (Berdeklis and List 2001). This view has changed in the storm context because of the realization that an abundance of ice particles in conditions of weak ascent will deplete the supercooled water concentration by the WBF process. Perhaps the most conspicuous example in the meteorological literature is the trailing stratiform region of squall lines (Williams and Boccippio 1993; Williams and Yair 2006; Hodapp et al. 2008; Takahashi and Suzuki 2010)—the origin location for the laterally extensive "spider" lightning flashes and positive polarity ground flashes that produce sprites in the mesosphere and singlehandedly excite Earth's Schumann resonances (Williams et al. 2010). Deep thunderstorms that extend many kilometers above the −40°C isotherm

(near 10 km MSL altitude in many summertime locations) and above the traditional mixed-phase zone have been documented to produce active lightning discharges there. Yet another situation of documented storm electrification when direct participation of supercooled water is unlikely in promoting charge separation are pyrocumulus clouds (Lang et al. 2014) in which lightning is most prevalent near the −40°C level. Laboratory measurements at low temperatures (Ávila et al. 2011) have also demonstrated appreciable charge separation when ice formed by homogeneous nucleation of supercooled water collides with an ice target.

Mixed-phase conditions lead naturally to asymmetries between hydrometeors. It stands to reason that two identical ice particles will not transfer charge on contact, and that some asymmetry in the physical condition between colliding particles is needed for net charge transfer. Numerous hypotheses have aimed at suggesting a physical basis for why graupel/ice crystals selectively acquire negative/positive charge in collisions. For example, Findeisen (1940) and Findeisen and Findeisen (1943) proposed that ice surfaces undergoing sublimation acquire negative charge and those undergoing vapor deposition charge positively. Baker et al. (1987) generalized this hypothesis in proposing that "the fastest growing ice surface takes on positive charge." Further consideration of these ideas can be found in Saunders (2008), Emersic and Saunders (2010), and Jayaratne and Saunders (2016). Laboratory mixed-phase experiments simulating thunderstorm conditions by Takahashi (1978) were examined in the context of these hypotheses (Williams et al. 1991) with calculations based on heat and mass balance for the rimed particles (Schumann 1938; Ludlam 1951). It was found that simulated graupel particles, accreting supercooled cloud water in a dry growth condition involving sublimation, selectively acquire negative charge, consistent with the characteristic positive thunderstorm dipole. At smaller water contents than needed for sublimation, vapor deposition is prevalent and is enhanced by ventilation effects for the faster-falling larger graupel particles. At larger water contents than needed for sublimation, wet growth in accretion is achieved with a surface temperature near 0°C, with positive charging of the rime in a glaze ice condition (Takahashi 1978; Williams et al. 1991). At still larger liquid water contents and a thick wet water layer, ice crystals may stick to the surface and prevent vigorous charge separation (Saunders and Brooks 1992; Jayaratne and Saunders 2016).

A natural mixed-phase factory is the supercell thunderstorm. The existence of lightning "holes" of 5–10-km diameter in storms of this kind (Krehbiel et al. 2000; Payne

et al. 2010) may provide indirect evidence that hail in wet growth is not an important contributor to charge separation in supercells. Surrounding this hole and the supercell updraft core is a ring of lightning on the edge of the supercell updraft. Lightning is absent in the updraft core, which also often coincides with the radar-identified bounded weak echo region (BWER). Only in the weak ascent in the edges where updraft speeds are typical of ordinary thunderstorms (5–$10\,\mathrm{m\,s^{-1}}$) can there be a balanced condition for graupel growth (Atlas 1966; Lhermitte and Williams 1985), development of a radar echo, and the traditional noninductive ice–ice mechanism for charge separation. In the core of the updraft the ascent is too fast to satisfy this condition for graupel. However, large hail can form at higher levels of the updraft with ascent speeds of many tens of meters per second, above the BWER. Here the supercooled liquid water concentrations are sufficient for wet growth. But, the general absence of VHF emission from this region casts doubt on a primary role for the large hail as an agent for lightning production.

The realization in recent years that thunderstorms in exceptional thermodynamic environments such as Oklahoma (MacGorman and Burgess 1994), eastern Colorado (Rust et al. 2005; Fleenor et al. 2009; Fuchs et al. 2015), the Tibetan Plateau in China (Qie et al. 2009), and the premonsoon phase in India (Pawar et al. 2017) can have their main electrical dipoles reversed with respect to the customary positive-over-negative configuration has spurred new attention to the mixed-phase conditions (and accompanying thermodynamic and aerosol conditions) that might support this polarity change. An exceptionally high cloud base together with substantial convective available potential energy (CAPE) appears to be important in reversing the polarity (Williams et al. 2005; Qie et al. 2009). A greater abundance of ice nucleating particles has also been suggested (Pawar et al. 2017) as an explanation, again pointing to the difficulty in disentangling thermodynamic and aerosol effects (Rosenfeld et al. 2012) on a wide variety of observations. Both the high cloud base (Freud and Rosenfeld 2012) and abundant aerosols can lead to smaller cloud droplet sizes. These smaller cloud droplets are involved in the riming process, with positive charging of rime shown in some laboratory studies (Jayaratne and Saunders 1985; Ávila and Pereyra 2000).

6. Challenges in the study of mixed-phase clouds

Despite recent research on mixed-phase clouds, our understanding of processes governing their life cycle, radiation effects, precipitation formation, and cloud electrification is still far from complete. Below, we provide a list of theoretical and experimental problems related to various aspects of the mixed phase that need to be addressed in future studies.

a. Observations

The statistics of the microphysical properties of mixed-phase clouds in Figs. 5-13–5-14 were obtained for midlatitude frontal and stratiform clouds. At this time, it is not clear whether these distributions are universal or specific to midlatitude frontal and stratiform clouds. One of the important tasks for future in situ observations is to obtain statistically significant data on the microphysics of mixed-phase clouds in other regions and other type of clouds. This specifically refers to mixed-phase statistics in convective clouds, which at the present stage are poorly studied. Global statistics on the microphysical properties of mixed-phase clouds are important for the evaluation of weather and climate models and remote sensing algorithms.

Most previous studies were focused on the characterization of mixed-phase clouds using the ice water fraction IWC/(IWC + LWC) as a metric. Other microphysical characteristics have received significantly less attention. The integral radii of ice particles $N_i\bar{r}_i$ and liquid droplets $N_w\bar{r}_w$ play a fundamental role in the theory of mixed-phase clouds [section 3; Eqs. (5-2)–(5-11)]. Future studies should expand upon the characterization of mixed-phase clouds and include simultaneous measurements of integral radii (or the first moment of particle size distribution) of ice particles $N_i\bar{r}_i$ and liquid droplets $N_w\bar{r}_w$, as well as of relative humidity RH_w, vertical velocity u_z, and extinction coefficient associated with ice β_i and liquid β_w. Measurements of these parameters will help us better understand the direction and rates of partitioning of water, the maintenance of and life cycle of the mixed phase, and their radiative effects.

Examining the spatial inhomogeneity of mixed-phase clouds at small scales down to $10^{-1}\,\mathrm{m}$ is important for understanding how cloud regions with pure ice, liquid, and mixed phase are distributed in space. High-spatial-resolution ($10^{-1}\,\mathrm{m}$) collocated measurements of RH_w and microphysical parameters are also needed to understand ice–vapor–liquid interactions. These measurements and improved understanding of the spatial distribution of ice and liquid are especially important at the early and final stages of mixed-phase clouds. This will help us better understand mechanisms of ice initiation, mixing processes of ice and liquid in mixed-phase clouds, and glaciation. Unfortunately, at present the characterization of the early and final stages of mixed-phase clouds is hindered by instrumentation limitations [sections 4a(i) and 6b].

The observation of ice initiation in liquid and mixed-phase clouds is another long-standing problem within experimental cloud physics. Measurements of ice crystals at the early stage of their formation and identification of the mechanisms of their formation are important for describing the evolution of mixed phase. The measurement of small ice particles remains an unresolved issue (Baumgardner et al. 2017, chapter 9). Size distributions of ice particles and their shapes are key parameters controlling the glaciation of mixed-phase clouds [section 3b; Eqs. (5-5) and (5-6)].

Turbulence is a driving force for mixing liquid droplets, ice particles, and water vapor. Local turbulence determines the intensity of entrainment of out-of-cloud air with its subsequent mixing with the in-cloud environment. The effect of entrainment and mixing in mixed-phase clouds is even less understood and studied than for liquid clouds. Until now no studies on entrainment and mixing in mixed-phase clouds have been conducted. Turbulence is also a key parameter for the maintenance of mixed-phase clouds (section 3d). Observations of the link between mixed-phase cloud microphysics for isotropic and non-isotropic turbulence and its effect on the mixed-phase longevity is an important task for future measurements. This problem also has practical importance for aircraft inflight icing.

Quantifying the role of aerosols in the evolution of mixed-phase clouds is also the subject of ongoing studies. Concentrations of CCN and ice nucleating particles (INPs) and mechanisms of their activation affect the integral radii $N_i \bar{r}_i$ and $N_w \bar{r}_w$, which play a central role in the partitioning of condensed water in mixed-phase clouds and their evolution and radiation properties (section 3). Many aspects of the link between graupel production and CCN concentration remain unexamined. Even though there is a general understanding of how aerosols may affect mixed-phase clouds, more dedicated studies in this direction are required.

The effect of the mixed phase on cloud electrification is probably one of the least understood aspects of mixed-phase clouds (section 5). Observations of electric fields in mixed-phase clouds are difficult to make, and at present they are sparse and not consolidated. Measurements of the electric charges of individual liquid droplets and ice particles in mixed-phase clouds are not routinely performed by research aircraft at the present stage. Such measurements represent a great challenge for airborne measurements. Without such observations, the understanding of charge separation will remain problematic.

b. Instrumental challenges

The major challenge in the microphysical characterization of mixed-phase clouds is to measure simultaneously two different types of cloud particles: ice and liquid, which have concentrations that vary by several orders of magnitude. Typically, in mixed-phase clouds, droplet diameters and concentrations range from 1 to $50 \mu m$ and from 10^1 to $10^3 cm^{-3}$, respectively. Ice particle sizes and concentrations are prevalent within the ranges of 1 to $10^4 \mu m$ and 10^{-6} to $1 cm^{-3}$, respectively. The most complex task is the measurement and segregation of small ice crystals and liquid droplets in the size ranges of $1 < D < 100 \mu m$ (Baumgardner et al. 2017, chapter 9).

Addressing the challenges listed in the previous sections requires improvements to existing instrumentation and developing new techniques for phase discrimination. Below is a list of requirements for the next generation of airborne instrumentation for characterization of the mixed phase:

- Improvement in the accuracy of and ability to discriminate between liquid and solid cloud particles down to the micrometer size range.
- Collocated measurements of water vapor pressure (e) and static air temperature with spatial resolution $10^{-1} m$ in order to determine local relative humidity RH_w. The targeted accuracy of RH_w measurements is 0.1%.
- Developing the ability to make collocated measurements of RH_w and cloud microstructure at high spatial resolution down to 10^{-1}-m scale.
- Improving the accuracy of measurements of IWC and ice particle size distributions in the presence of liquid droplets. This task requires a better definition of the instrumental sample area and minimizing the effect of out-of-focus images on particle sizing.
- Developing a technique for acquiring statistically significant samples of ice particles with concentrations as low as $N_i \sim 1 m^{-3}$ at 1-m spatial resolution.
- Development of new instrumentation for measurements of electric charges on cloud particles.

c. Laboratory studies

Airborne studies do not allow Lagrangian measurements of cloud parcels because of large aircraft true airspeeds. Such measurements would address a great number of questions related to the evolution of the microstructure and the glaciation process in mixed-phase clouds. However, laboratory experiments in cloud-simulating facilities can better address the time evolution of processes that occur in clouds. Experiments with cloud chamber and

wind tunnels could help better understand cycling activation-deactivation of the mixed phase in ice clouds, which is important for the maintenance of the mixed phase (section 3d). Cloud chamber experiments can offer more insight on the collective growth and interaction of ice particles and liquid droplets. A vital set of experiments could be set up to study the WBF process and to compare against theoretical predictions, looking at the change of humidity, ice growth, and liquid evaporation. Existing cloud-simulating laboratory facilities (e.g., Karlsruhe Institute of Technology AIDA aerosol and cloud chamber, University of Manchester Ice Cloud Chamber) have the capability to address these questions.

One of the important evaluations of the theoretical framework of mixed-phase thermodynamics would be a laboratory study of ice particle growth rate under varying conditions. Thus, Eq. (5-2) was obtained under the assumption that ice particles follow Maxwellian growth and evaporation. Past laboratory experiments on ice particle growth were conducted for steady-state environmental conditions (e.g., Fukuta 1969; Ryan et al. 1976; Fukuta and Takahashi 1999; and others). However, in real clouds, environmental conditions (T, RH_w) around individual ice crystals are continuously changing. This will result in changing the growth regime and may result in disruption of the Maxwellian growth. Cloud chamber experiments could also address a number of questions on the dynamic forcing and the role of mixing on the maintenance of the mixed phase.

The greatest single shortcoming in understanding cloud electrification in general is the lack of information about liquid water and ice at the molecular scale in mixed-phase conditions. Even the charge carriers involved with the transfer of charge in ice–ice collisions have not been definitively identified. Methods used to study the molecular structure of surfaces should be exploited to investigate the surface structure of ice when experiencing conditions of both sublimation and vapor deposition, and with and without riming. In these considerations, one should not lose sight of the fundamental dipole moment of the H_2O molecule that is responsible for charge imbalance at a molecular scale in both liquid water and solid ice.

In a laboratory context, more attention is needed on charge separation when ice crystals collide with aggregates (snowflakes). The latter hydrometeors are more prevalent than graupel in mesoscale convective systems undergoing ascent at $1 \, m \, s^{-1}$ or less, but have not yet been considered in laboratory experiments. In the other limit of updraft speed in supercell storms, the connection between the lightning hole (Krehbiel et al. 2000) and the negative hole in differential reflectivity

(Kaltenboeck and Ryzhkov 2013), linked with giant hail, deserves further study. The roles of 1) cloud-base height and 2) enhanced CCN in making positive ground flashes in thunderstorms (Lyons et al. 1998) ingesting forest fire smoke deserve to be disentangled.

d. Theoretical challenges

The set of equations describing the collective growth of liquid and ice particles is based on the assumption that, at each moment of time, all cloud particles are growing under the same background temperature T and water vapor pressure e. It means that local fluctuations of T and e, caused by growing or evaporating cloud particles, are momentarily homogenized over the entire cloud volume. This implies that the coefficient of turbulent diffusion $K_t \rightarrow \infty$. This assumption does not seem realistic. Nevertheless, the assumption about instantaneous spatial averaging of T and e fields is used in all numerical cloud simulations and theoretical considerations of cloudy environments. For mixed-phase clouds, the problem of collective growth is complicated by the fact that the concentrations and sizes of ice and liquid particles are quite different. This results in large differences in the characteristic response times of liquid droplets τ_{pw} and of ice particles τ_{pi}. Thus, the local rates of release and depletion of water vapor and temperature for liquid droplet and ice particles mixed-phase clouds will be quite different across the mixed-phase cloud volume. Thus, the local inhomogeneity of the T and e fields are governed by molecular diffusion inside the Kolmogorov viscous microscale because of the water vapor depletion and release by individual droplets and ice crystals during their growth and evaporation. However, spatial homogenization of T and e is driven by isotropic turbulent mixing and regular dynamics in the inertial subrange. Therefore, the spatial homogenization of the T and e fields occurs through viscous to the inertial subranges. The proof of such a homogenization and characteristic time scales remains unaddressed both theoretically and experimentally. Unfortunately, to this day, there are no theoretical works on the effect of local fluctuations of T and e on the collective growth of cloud particles in mixed-phase clouds.

Another theoretical challenge is the identification of the spatial scale Δx_p (section 2c; Fig. 5-2). This issue is directly linked with the problem of collective growth/evaporation of ice and liquid particles.

e. Challenges of description of the mixed phase in climate and cloud resolving models

Mixed-phase clouds are challenging for climate models to represent. A misrepresentation of mixed-phase clouds has been found to be responsible for

large biases in the reflected shortwave radiation over the Southern Ocean in Cloud Feedback Model Intercomparison Project 2 (CFMIP2) models (Bodas-Salcedo et al. 2014) and for biases in the Arctic wintertime temperature inversion in many CMIP5 models (Pithan et al. 2014). Furthermore, low-lying clouds that are capped by an inversion, such as Arctic mixed-phase clouds, are often underrepresented in GCMs. This can be due to the coarse vertical resolution that does not easily permit the inversion strength to be captured or to a simple mixed-phase cloud representation in some climate and numerical weather prediction models that uses a single prognostic variable to represent cloud condensate mass. In this representation, the condensate is separated into fixed liquid and ice fractions depending on the temperature, and as such this diagnostic representation is unable to characterize the observed variability in liquid and ice partitioning (e.g., mixed-phase clouds with liquid water in the coldest, uppermost cloud levels). More commonly, models use separate prognostic variables to represent the mass of liquid and ice. Most cloud resolving models and state-of-the-art climate and weather forecasting models use double-moment bulk microphysics schemes that have two prognostic variables to represent the bulk mass and number concentration of both liquid and ice. This additional complexity potentially allows cloud microphysics schemes to be coupled to aerosol modules, and also enables models to simulate a wider range of observed variability in mixed-phase cloud properties.

Heterogeneous ice nucleation and secondary ice production are the key processes that control the ice crystal number concentration in mixed-phase clouds. In models, these processes are two of the most uncertain parameterizations due to limitations in measurement capabilities of INPs and ice crystal concentrations that hinder our understanding of the underlying physical mechanisms (see Heymsfield et al. 2017, chapter 2; Field et al. 2017, chapter 7). Many modeling studies have demonstrated a high sensitivity of mixed-phase cloud properties to the ice crystal number concentration. These results have shown that high ice number concentrations tend to reduce the cloud liquid water, which can lead to a rapid glaciation of the cloud (e.g., Rauber and Tokay 1991; Pinto 1998; Jiang et al. 2000; Morrison et al. 2003; Fan et al. 2009; Klein et al. 2009; Lawson and Gettelman 2014; Ovchinnikov et al. 2014; Lawson et al. 2015).

Once ice has formed, the particle growth rates are dependent on the assumed ice crystal shapes and sizes. Uncertainties surrounding the evolution of ice habit impact the capacitance, ventilation, and drag forces acting on the particle, and therefore, the vapor depositional

growth and riming rates (e.g., Sulia and Harrington 2011; Fridlind et al. 2012a,b). Improving the simulation of these ice growth rates is dependent on improving our knowledge of the distribution and evolution of the ice mass, shapes, and sizes under a range of temperature regimes. Simulating the correct ice growth rates and, therefore, the correct partitioning of liquid and ice water, is important for the longevity of persistent mixed-phase clouds, which maintain a delicate balance between the desiccation of supercooled water through ice growth and precipitation, and the generation of liquid water by ascent, radiative cooling, turbulent fluxes, and large-scale moisture advection.

The phase transitions between water vapor and solid condensate are important to represent in models because this process impacts the glaciation times and, therefore, the cloud lifetimes, optical properties, and precipitation. However, this is challenging because of the unresolved temperature and moisture variations that occur within a model grid box, particularly in coarse-resolution climate models. Some climate models include a subgrid distribution of vertical velocity to model the unresolved supersaturation. One approach is to calculate a representative vertical velocity, which is the sum of the grid scale and turbulent velocity, and to compare that to the velocity required for simultaneous growth of cloud droplets and ice crystals u_z^* (Storelvmo et al. 2008b; Lohmann and Hoose 2009). This is consistent with theoretical considerations (Korolev 2007), but shifts the problem to an accurate representation of the vertical velocity.

Another approach is to use the analytic expression for predicting supercooled water (section 3d) where the formation of supercooled water via subgrid turbulence is treated as an additional source term that is added to the liquid water and liquid cloud fraction. This has been applied in a global climate model to improve the frequency of occurrence of supercooled liquid water over the Southern Ocean (Furtado et al. 2016) (Fig. 5-27). Increased amounts of liquid-phase cloud lead to enhanced shortwave reflection reducing the biases in this region.

In addition to unresolved supersaturation, knowledge of how ice and liquid are distributed, homogeneously (Fig. 5-1a) or inhomogeneously (Fig. 5-1b), needs to be represented accurately in order to calculate the correct particle growth rates (e.g., Fan et al. 2011). Many models assume a maximum overlap between the liquid and ice cloud fractions, which results in the maximum amount of supercooled liquid water depletion through the WBF process (e.g., Gettelman et al. 2010). These characterizations of the horizontal and vertical distribution of temperature, moisture,
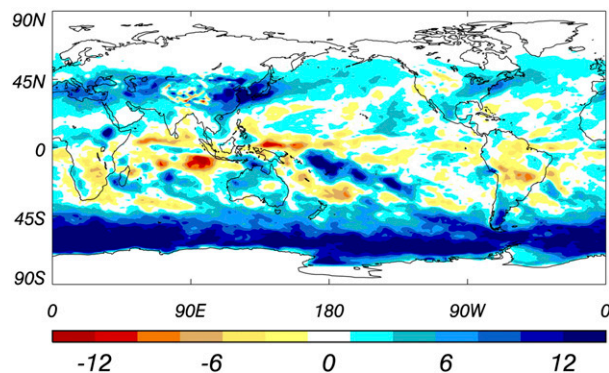
FIG. 5-27. The 20-yr TOA outgoing shortwave flux (W m^{-2}) for December–February from the low-resolution (N96L70) climate simulations. Difference between the experiment with the subgrid turbulent production of liquid water and control models. This shows that the increase in liquid water in clouds over the Southern Ocean leads to an increase in outgoing shortwave flux. [From Furtado et al. (2016).]

and cloud liquid and ice are difficult to obtain because of the mismatch in scales between the models and the measurements.

The above description of cloud parameterizations is applicable for cloud-resolving models and for the stratiform clouds in coarse-resolution models such as climate models. The representation of convective mixed-phase clouds in climate models depends on the assumptions about the phase changes that occur in the parameterized convective plume. The microphysical detail in convection schemes is usually quite crude, with the phase of the convective condensate specified as a function of temperature. Kay et al. (2016) made simple adjustments to increase the amount of water and reduce the amount of ice detrained from shallow convective mixed-phase clouds in a climate model and found a reduction in the errors in radiative flux over the midlatitudes of the Southern Ocean. Greater understanding of the initiation and evolution of ice in convective updrafts [e.g., the in-situ study of Lawson et al. (2015)] is required to be able to more accurately represent the phase partitioning in cumulus convection schemes.

In terms of climate change, Tan et al. (2016) showed that an underrepresentation of the fraction of supercooled liquid water in mixed-phase clouds leads to the overly large negative cloud phase feedback in response to doubling of CO_2 and thus underestimates the temperature in a 2xCO$_2$ climate.

Despite the limited amount of in situ observations, climate models have tried to quantify the climate forcing caused by aerosol indirect effects in mixed-phase clouds. Using different representations of

aerosol effects in the ECHAM5-HAM model (Hoose et al. 2008), Lohmann and Hoose (2009) showed different representations of indirect effects could affect the top of the atmosphere radiation by up to 0.5 W m^{-2}. Storelvmo et al. (2008a) found that depending on the freezing mechanism, the overall aerosol indirect effect in mixed-phase clouds could be reduced by 50%–90%. But, although an increase in ice nucleating particles leads to a decreased lifetime, the smaller particle sizes reflect more solar radiation that partially compensates this effect (Storelvmo et al. 2011). To refine these estimates of mixed-phase indirect effects, additional details about the heterogeneous freezing mechanism and ice nucleating particles are sorely needed.

How mixed-phase clouds respond to anthropogenic aerosol perturbations is still unknown. If the number of ice nucleating particles and ice crystals increases, u_z^* [Eq. (5-8)] would increase and mixed-phase clouds would glaciate more easily (called the glaciation indirect effect; Lohmann 2002). On the contrary, if more ice nuclei were coated by anthropogenic acids (sulfuric acid or nitric acid), their ability to act as INPs would be reduced. This would result in fewer ice crystals that can grow to larger sizes and sediment faster. This deactivation effect was suggested to play an important role for the persistence of Arctic mixed-phase clouds (Girard et al. 2013) and seems to dominate over the glaciation indirect effect in global climate models (Storelvmo et al. 2008a; Hoose et al. 2008).

Decreasing snowfall rates with increasing anthropogenic aerosol loads have been observed in the Rocky Mountains (Borys et al. 2000, 2003) and are caused by a reduction in the collision efficiency of snowflakes with cloud droplets that reduced the riming rate. As riming leads to efficient precipitation formation, a retardation of riming prolongs the development of precipitation to the extent that it can affect the total orographic precipitation budget (Hobbs et al. 1973). In a comparison of different numerical models, a decrease in riming was not a robust result, and an increase in aerosols does not necessarily lead to a reduction in precipitation (Muhlbauer et al. 2010). This is because the effect of anthropogenic aerosols on cloud microphysics and orographic precipitation strongly depends on the large-scale dynamics, cloud dynamics, and the description of aerosol and cloud microphysics in models (e.g., Lynn et al. 2007; Muhlbauer and Lohmann 2009; Lohmann et al. 2016; Fan et al. 2016).

The challenges outlined above for modeling mixed-phase clouds are due to the complicated microphysical and

dynamical interactions that affect the phase-partitioning and glaciation time in these clouds. Uncertainties due to ice initiation, ice particle sizes and shapes, scales of atmospheric variability, and the horizontal and vertical distribution of liquid and ice within clouds limit our ability to accurately model the precipitation and radiative effects of mixed-phase clouds. Given the ubiquitous nature of mixed-phase clouds and their importance in weather and climate, it is important to increase our understanding of these uncertainties through improved measurements to represent these clouds more reliably in atmospheric models.

7. Conclusions

a. Conceptual model of the mixed phase in different types of clouds

It is well established that in-cloud dynamics are closely related to the type of clouds. Since dynamic forcing plays an important role in the formation and maintenance of mixed-phase conditions, it is anticipated that spatial, temporal, and microphysical properties of mixed-phase clouds will also be related to cloud type.

Figure 5-28 shows conceptual diagrams of mixed-phase formation in different types of clouds. In lee-wave clouds, mixed-phase conditions form in the upwind section of the cloud as a result of droplet formation, ice initiation on INP, and droplet freezing (Baker and Lawson 2006; Field et al. 2012) (Fig. 5-28a). The glaciation of the mixed phase occurs downwind via the WBF process. The flow is laminar and no recirculation of ice takes place in wave clouds.

In deep frontal ice clouds, the formation of ice may occur through dynamic forcing resulting from Kelvin–Helmholtz instability (Fig. 5-28b). In this case, the mixed phase forms as a result of activation of liquid droplets inside the preexisting ice cloud, and the role of INPs likely has a limited effect on the formation of the mixed phase. The embedded mixed-phase layer may persist as long as the turbulence is maintained (Hill et al. 2014; Field et al. 2014). However, the lifetime of individual mixed-phase parcels is determined by the characteristic time for turbulent eddy turnover and may be limited by 10–20 min. Persistent turbulence may maintain activation of liquid in ice-only cloud parcels ($u_z > u_z^*$), whereas mixed-phase parcels turn into ice only, when the WBF process is active ($u_z < u_z^*$; section 3c). This process may potentially maintain a steady-state mixed phase over the volume affected by turbulence.

Persistent boundary layer mixed-phase clouds (Fig. 5-28c) form as a balance between dynamic forcing resulting from the boundary layer circulation, radiative

cooling from the cloud top, ice nucleation, and ice precipitating out of the cloud (e.g., Ovchinnikov et al. 2011; Solomon et al. 2014). Liquid droplets go through cycling nucleation and evaporation at the cloud base. Circulating ice, undergoing cycling growth and evaporation, plays an important role in the maintenance of the mixed phase (Korolev and Field 2008; H. Morrison et al. 2011). The characteristic lifetime of mixed-phase parcels inside the cloud layer usually does not exceed 10–15 min, whereas the boundary mixed-phase layers may persist for hours or even days. The WBF process is thought to be active in approximately half of the mixed-phase cloud volume.

The dynamic forcing plays a key role in the maintenance of the mixed phase in convective clouds (Fig. 5-28d). Ice multiplication may be significant in the formation of ice in convective clouds (Field et al. 2017, chapter 7). Recirculation of ice may also contribute in the formation of the mixed-phase microstructure. Recent studies suggest that INPs have a limited role in the initiation of ice in deep convective storms (Ladino et al. 2017). The lifetime of mixed-phase parcels depends on the vertical velocity, ice concentration, and initial LWC. If the vertical velocity is high enough (i.e., $u_z > u_z^*$, section 3c), then the WBF will not be activated and the mixed-phase parcels will be glaciated only after reaching the temperature of homogeneous freezing (Korolev 2007). For moderate vertical velocities, the WBF process may become active, and the characteristic lifetime of the mixed phase will then be determined by Eq. (5-6) (Pinsky et al. 2014).

The above examples demonstrate a multiplicity of mechanisms of mixed-phase formation and maintenance in different types of clouds.

b. Future outlook for studies of mixed-phase clouds

Liquid–ice-phase instability in tropospheric clouds has a significant impact on the global radiation balance, on the hydrological cycle, and on the global electrical circuit. Accordingly, an accurate description of mixed-phase clouds in numerical simulations is required for the improvement of numerical weather prediction and climate models. Yet the current status of our knowledge on droplet-ice interaction in mixed-phase cloud systems is far from complete. Given this chapter's overview of the research and measurement approaches, advancements, and research gaps within mixed-phase cloud investigations, it is our recommendation that future studies of mixed-phase clouds focus on the following directions:

1) Obtaining statistics of microphysical properties from in situ, remote sensing, and satellite measurements on a global scale. These statistics should include ice
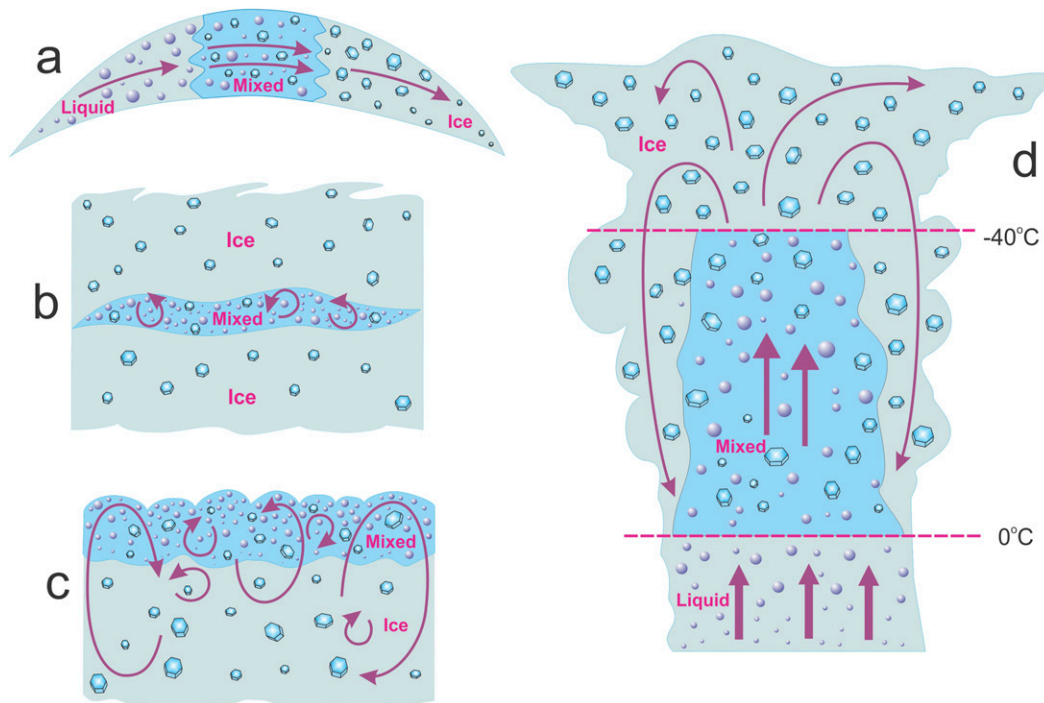
FIG. 5-28. Conceptual model of the effect of dynamic forcing on the formation of the mixed-phase in different types of cloud: (a) Wave clouds, Ac lent; (b) frontal cloud, Cs–Ns; (c) boundary layer clouds, St–Sc; and (d) deep convective clouds, Cb, convective storms.

fraction μ_{ice} for different α metrics (e.g., integral radius, extinction, and mass) and occurrences in different types of clouds in diverse climatic regions at varying altitudes and temperatures.

2) Validating remote sensing and satellite techniques, specifically, their ability to identify the mixed phase, with the help of in situ measurements. Statistical data on the mixed phase (point 1 above) may be used as a part of this validation.

3) Developing new laboratory experiments in cloud chambers and wind tunnels to study mixed-phase clouds. Experimental confirmation of the developed theoretical framework of mixed-phase clouds.

4) Consolidating theoretical efforts to study the behavior of three-phase colloidal systems.

5) Developing new laboratory experiments and collect in situ observations on the effect of the mixed phase on charge separation and cloud electrification.

6) Improved understanding of ice initiation, ice sizes, scales of atmospheric variability, and the horizontal and vertical distribution of liquid and ice within clouds will enable more accurate modeling of mixed-phase clouds.

REFERENCES

Abdelmonem, A., E. Järvinen, D. Duft, E. Hirst, S. Vogt, T. Leisner, and M. Schnaiter, 2016: PHIPS–HALO: The airborne particle habit imaging and polar scattering probe—Part 1: Design and operation. *Atmos. Meas. Tech.*, **9**, 3131–3144, doi:10.5194/amt-9-3131-2016.

Adhikari, L., and Z. Wang, 2013: An A-Train satellite based stratiform mixed-phase cloud retrieval algorithm by combining active and passive sensor measurements. *Br. J. Environ. Climate Change*, **3**, 587–611, doi:10.9734/BJECC/2013/3055.

Albrecht, B. A., 1989: Aerosols, cloud microphysics, and fractional cloudiness. *Science*, **245**, 1227–1230, doi:10.1126/science.245.4923.1227.

Atlas, D., 1966: The balance level in convective storms. *J. Atmos. Sci.*, **23**, 635–651, doi:10.1175/1520-0469(1966)023<0635:TBLICS>2.0.CO;2.

Ávila, E. A., and R. G. Pereyra, 2000: Charge transfer during crystal-graupel collisions for two different cloud droplet size distributions. *Geophys. Res. Lett.*, **27**, 3837–3840, doi:10.1029/2000GL012302.

——, R. E. Bürgesser, N. E. Castellano, R. G. Pereyra, and C. P. R. Saunders, 2011: Charge separation in low-temperature ice cloud regions. *J. Geophys. Res.*, **116**, D14202, doi:10.1029/2010JD015475.

Bachalo, W. D., 2000: Spray diagnostics for the twenty-first century. *Atomization Sprays*, **10**, 439–474, doi:10.1615/AtomizSpr.v10.i3-5.110.

——, and M. J. Houser, 1984: Phase Doppler spray analyzer for simultaneous measurements of drop size and velocity distributions. *Opt. Eng.*, **23**, 583–590, doi:10.1117/12.7973341.

——, J. W. Strapp, E. Biagio, A. Korolev, and M. Wolde, 2015: Performance of the newly developed high speed imaging (HSI) probe for measurements of size and concentration of ice crystals and identification of phase composition of clouds. *SAE 2015 Int. Conf. on Icing of Aircraft, Engines, and Structures*, Prague, Czech Republic, SAE.

Bacon, N. J., M. B. Baker, and B. D. Swanson, 2003: Initial stages in the morphological evolution of vapor-grown ice crystals: A laboratory investigation. *Quart. J. Roy. Meteor. Soc.*, **129**, 1903–1928, doi:10.1256/qj.02.04.

Baker, B. A., and R. P. Lawson, 2006: In situ observations of the microphysical properties of wave, cirrus, and anvil clouds. Part I: Wave clouds. *J. Atmos. Sci.*, **63**, 3160–3185, doi:10.1175/JAS3802.1.

——, M. B. Baker, E. R. Jayaratne, J. Latham, and C. P. R. Saunders, 1987: The influence of diffusional growth rates on the charge transfer accompanying rebounding collisions between ice crystals and soft hailstones. *Quart. J. Roy. Meteor. Soc.*, **113**, 1193–1215, doi:10.1002/qj.49711347807.

Baum, B. A., P. F. Soulen, K. I. Strabala, M. D. King, S. A. Ackerman, and W. P. Menzel, 2000: Remote sensing of cloud properties using MODIS airborne simulator imagery during SUCCESS: 2. Cloud thermodynamic phase. *J. Geophys. Res.*, **105**, 11 781–11 792, doi:10.1029/1999JD901090.

——, R. A. Frey, G. G. Mace, M. K. Harkey, and P. Yang, 2003: Nighttime multilayered cloud detection using MODIS and ARM data. *J. Appl. Meteor.*, **42**, 905–919, doi:10.1175/1520-0450(2003)042<0905:NMCDUM>2.0.CO;2.

——, W. P. Menzel, R. A. Frey, D. C. Tobin, R. E. Holz, S. A. Ackerman, A. K. Heidinger, and P. Yang, 2012: MODIS cloud-top property refinements for collection 6. *J. Appl. Meteor. Climatol.*, **51**, 1145–1163, doi:10.1175/JAMC-D-11-0203.1.

Baumgardner, D., and A. Rodi, 1989: Laboratory and wind tunnel evaluations of the Rosemount Icing Detector. *J. Atmos. Oceanic Technol.*, **6**, 971–979, doi:10.1175/1520-0426(1989)006<0971:LAWTEO>2.0.CO;2.

——, H. Jonsson, W. Dawson, D. O'Connor, and R. Newton, 2001: The cloud, aerosol and precipitation spectrometer (CAPS): A new instrument for cloud investigations. *Atmos. Res.*, **59–60**, 251–264.

——, J. F. Gayet, H. Gerber, A. Korolev, and C. Twohy, 2002: Clouds: Measurement techniques in-situ. *Encyclopedia of Atmospheric Science*, J. Curry, J. Holton, and J. Pyle, Eds., Academic Press, 489–498.

——, R. Newton, M. Kramer, J. Meyer, A. Beyer, M. Wendisch, and P. Vochezer, 2014: The cloud particle spectrometer with polarization detection (CPSPD): A next generation open-path cloud probe for distinguishing liquid cloud droplets from ice crystals. *Atmos. Res.*, **142**, 2–14, doi:10.1016/j.atmosres.2013.12.010.

——, and Coauthors, 2017: Cloud ice properties: In situ measurement challenges. *Ice Formation and Evolution in Clouds and Precipitation: Measurement and Modeling Challenges*, Meteor. Monogr., No. 58, Amer. Meteor. Soc., doi:10.1175/AMSMONOGRAPHS-D-16-0011.1.

Berdeklis, P., and R. List, 2001: The ice crystal–graupel collision charging mechanism of thunderstorm electrification. *J. Atmos. Sci.*, **58**, 2751–2770, doi:10.1175/1520-0469(2001)058<2751:TICGCC>2.0.CO;2.

Bergeron, T., 1928: Über die dreidimensional verknüpfende Wetteranalyse. *Geophys. Norv.*, **5** (6), 1–111.

——, 1935: On the physics of clouds and precipitation. *Proces Verbaux de l'Association de Météorologie,* International Union of Geodesy and Geophysics, 156–178.

Biter, C. J., J. E. Dye, D. Huffman, and W. D. King, 1987: The dropsize response of the CSIRO liquid water probe. *J. Atmos. Oceanic Technol.*, **4**, 359–367, doi:10.1175/1520-0426(1987)004<0359:TDSROT>2.0.CO;2.

Bodas-Salcedo, A., and Coauthors, 2014: Origins of the solar radiation biases over the Southern Ocean in CFMIP2 models. *J. Climate*, **27**, 41–56, doi:10.1175/JCLI-D-13-00169.1.

——, P. G. Hill, K. Furtado, K. D. Williams, P. R. Field, J. C. Manners, P. Hyder, and S. Kato, 2016: Large contribution of supercooled liquid clouds to the solar radiation budget of the Southern Ocean. *J. Climate*, **29**, 4213–4228, doi:10.1175/JCLI-D-15-0564.1.

Boers, R., and R. M. Mitchell, 1994: Absorption feedback in stratocumulus clouds: Influence on cloud top albedo. *Tellus*, **46A**, 229–241, doi:10.3402/tellusa.v46i3.15476.

Borovikov, A. M., I. I. Gaivoronskii, E. G. Zak, V. V. Kostarev, I. P. Mazin, V. E. Minervin, A. K. Khrgian, and S. M. Shmeter,

1963: *Cloud Physics*. Israel Program for Scientific Translations, 392 pp.

Borrmann, S., B. Luot, and M. Mishchenko, 2000: Application of the T-matrix method to the measurement of aspherical (ellipsoidal) particles with forward scattering optical particle counters. *J. Aerosol Sci.*, **31**, 789–799, doi:10.1016/S0021-8502(99)00563-7.

Borys, R. D., D. H. Lowenthal, and D. L. Mitchell, 2000: The relationships among cloud microphysics, chemistry, and precipitation rate in cold mountain clouds. *Atmos. Environ.*, **34**, 2593–2602, doi:10.1016/S1352-2310(99)00492-6.

——, ——, S. A. Cohn, and W. O. J. Brown, 2003: Mountaintop and radar measurements of anthropogenic aerosol effects on snow growth and snowfall rate. *Geophys. Res. Lett.*, **30**, 1538, doi:10.1029/2002GL016855.

Brenguier, J. L., T. Bourrianne, A. Coelho, J. Isbert, R. Peytavi, D. Trevarin, and P. Wechsler, 1998: Improvements of droplet size distribution measurements with the Fast-FSSP (Forward Scattering Spectrometer Probe). *J. Atmos. Oceanic. Technol.*, **15**, 1077–1090, doi:10.1175/1520-0426(1998)015<1077:IODSDM>2.0.CO;2.

——, and Coauthors, 2013: In situ measurements of cloud and precipitation particles. *Airborne Measurements for Environmental Research: Methods and Instruments*, M. Wendisch and J. L. Brenguier, Eds., Wiley, 225–302, doi:10.1002/9783527653218.ch5.

Buriez, J. C., and Coauthors, 1997: Cloud detection and derivation of cloud properties from POLDER. *Int. J. Remote Sens.*, **18**, 2785–2813, doi:10.1080/014311697217332.

Byers, H. R., and R. R. Braham, 1949: *The Thunderstorm*. U.S. Government Printing Office, 287 pp.

Cadeddu, M. P., J. C. Liljegren, and D. D. Turner, 2013: The Atmospheric Radiation Measurement (ARM) program network of microwave radiometers: Instrumentation, data, and retrievals. *Atmos. Meas. Tech.*, **6**, 2359–2372, doi:10.5194/amt-6-2359-2013.

Castellano, N. E., E. E. Avila, and C. P. R. Saunders, 2004: Theoretical model of the Bergeron–Findeisen mechanism of ice crystal growth in clouds. *Atmos. Environ.*, **38**, 6751–6761, doi:10.1016/j.atmosenv.2004.09.003.

——, ——, and ——, 2008: Vapour density field of mixed-phase clouds. *Atmos. Res.*, **88**, 56–65, doi:10.1016/j.atmosres.2007.10.002.

Cesana, G., D. E. Waliser, X. Jiang, and J.-L. F. Li, 2015: Multimodel evaluation of cloud phase transition using satellite and reanalysis data. *J. Geophys. Res. Atmos.*, **120**, 7871–7892, doi:10.1002/2014JD022932.

Cess, R. D., and G. L. Potter, 1988: A methodology for understanding and intercomparing atmospheric climate feedback processes in general circulation models. *J. Geophys. Res.*, **93**, 8305–8314, doi:10.1029/JD093iD07p08305.

Chylek, P., and C. Borel, 2004: Mixed-phase cloud water/ice structure from high spatial resolution satellite data. *Geophys. Res. Lett.*, **31**, L14104, doi:10.1029/2004GL020428.

Cober, S. G., G. A. Isaac, and A. V. Korolev, 2001a: Assessing the Rosemount Icing Detector with in situ measurements. *J. Atmos. Oceanic Technol.*, **18**, 515–528, doi:10.1175/1520-0426(2001)018<0515:ATRIDW>2.0.CO;2.

——, ——, ——, and J. W. Strapp, 2001b: Assessing cloud phase conditions. *J. Appl. Meteor.*, **40**, 1967–1983, doi:10.1175/1520-0450(2001)040<1967:ACPC>2.0.CO;2.

Costa, A., and Coauthors, 2017: Classification of Arctic, midlatitude and tropical clouds in the mixed-phase temperature regime. *Atmos. Chem. Phys. Discuss.*, doi:10.5194/acp-2017-226.

Cotton, R., S. Osborne, Z. Ulanowski, E. Hirst, P. H. Kaye, and R. S. Greenaway, 2010: The ability of the Small Ice Detector (SID-2) to characterize cloud particle and aerosol morphologies obtained during flights of the FAAM BAe-146 research aircraft. *J. Atmos. Oceanic Technol.*, **27**, 290–303, doi:10.1175/2009JTECHA1282.1.

Davison, C. R., T. Rutke, J. W. Strapp, T. P. Ratvasky, and E. F. Emery, 2012: Naturally aspirating isokinetic total water content probe: Pre-flight wind tunnel testing and design modifications. *Fourth AIAA Atmospheric and Space Environments Conf.*, New Orleans, LA, AIAA, 2012-3040, doi:10.2514/6.2012-3040.

Delanoë, J., and R. J. Hogan, 2008: A variational scheme for retrieving ice cloud properties from combined radar, lidar, and infrared radiometer. *J. Geophys. Res.*, **113**, D07204, doi:10.1029/2007JD009000.

Deng, M., G. G. Mace, Z. Wang, and H. Okamoto, 2010: Tropical Composition, Cloud and Climate Coupling Experiment validation for cirrus cloud profiling retrieval using CloudSat radar and CALIPSO lidar. *J. Geophys. Res.*, **115**, D00J15, doi:10.1029/2009JD013104.

——, ——, ——, and R. P. Lawson, 2013: Evaluation of several A-Train ice cloud retrieval products with in situ measurements collected during the SPARTICUS campaign. *J. Appl. Meteor. Climatol.*, **52**, 1014–1030, doi:10.1175/JAMC-D-12-054.1.

Dong, X., and G. G. Mace, 2003: Arctic stratus cloud properties and radiative forcing derived from ground-based data collected at Barrow, Alaska. *J. Climate*, **16**, 445–461, doi:10.1175/1520-0442(2003)016<0445:ASCPAR>2.0.CO;2.

Dye, J. E., W. P. Winn, J. J. Jones, and D. W. Breed, 1989: The electrification of New Mexico thunderstorms 1. Relationship between precipitation development and the onset of electrification. *J. Geophys. Res.*, **94**, 8643–8656, doi:10.1029/JD094iD06p08643.

Ehrlich, A., E. Bierwirth, M. Wendisch, J.-F. Gayet, G. Mioche, A. Lampert, and J. Heintzenberg, 2008: Cloud phase identification of Arctic boundary-layer clouds from airborne spectral reflection measurements: Test of three approaches. *Atmos. Chem. Phys.*, **8**, 7493–7505, doi:10.5194/acp-8-7493-2008.

Emersic, C., and C. P. R. Saunders, 2010: Further laboratory investigations into the relative diffusional growth rate theory of thunderstorm electrification. *Atmos. Res.*, **98**, 327–340, doi:10.1016/j.atmosres.2010.07.011.

Emery, E. F., D. R. Miller, S. R. Plaskon, J. W. Strapp, and L. Lilie, 2004: Ice particle impact on cloud water content instrumentation. Preprints, *42nd AIAA Aerospace Sciences Meeting and Exhibit*, Reno, NV, AIAA, 2004-0731, doi:10.2514/6.2004-731.

Fahrenheit, D. G., 1724: Experimenta & observationes de congelatione aquæ in vacuo factæ. *Philos. Trans.*, **33**, 78–84, doi:10.1098/rstl.1724.0016.

Fan, J., M. Ovtchinnikov, J. M. Comstock, S. A. McFarlane, and A. Khain, 2009: Ice formation in Arctic mixed-phase clouds: Insights from a 3-D cloud-resolving model with size-resolved aerosol and cloud microphysics. *J. Geophys. Res.*, **114**, D04205, doi:10.1029/2008JD010782.

——, S. Ghan, M. Ovchinnikov, X. Liu, P. Rasch, and A. Korolev, 2011: Representation of Arctic mixed-phase clouds and the Wegener-Bergeron-Findeisen process in climate models: Perspectives from a cloud-resolving study. *J. Geophys. Res.*, **116**, D00T07, doi:10.1029/2010JD015375.

——, Y. Wang, D. Rosenfeld, and X. Liu, 2016: Review of aerosol–cloud interactions: Mechanisms, significance, and challenges. *J. Atmos. Sci.*, **73**, 4221–4252, doi:10.1175/JAS-D-16-0037.1.

Farrington, R., and Coauthors, 2016: Discriminating between liquid and ice particles measured in mixed-phase cloud during the INUPIAQ campaign. *Int. Conf. on Clouds and Precipitation*, Manchester, UK, P16.18.

Field, P. R., and A. J. Heymsfield, 2015: Importance of snow to global precipitation. *Geophys. Res. Lett.*, **42**, 9512–9520, doi:10.1002/2015GL065497.

——, R. Wood, P. R. Brown, P. H. Kaye, E. Hirst, R. Greenaway, and J. A. Smith, 2003: Ice particle interarrival times measured with a Fast FSSP. *J. Atmos. Oceanic Technol.*, **20**, 249–261, doi:10.1175/1520-0426(2003)020<0249:IPITMW>2.0.CO;2.

——, R. J. Hogan, P. R. A. Brown, A. J. Illingworth, T. W. Choularton, P. H. Kaye, E. Hirst, and R. Greenaway, 2004: Simultaneous radar and aircraft observations of mixed-phase cloud at the 100 m-scale. *Quart. J. Roy. Meteor. Soc.*, **130**, 1877–1904, doi:10.1256/qj.03.102.

——, A. J. Heymsfield, B. J. Shipway, P. J. DeMott, K. A. Pratt, D. C. Rogers, J. Stith, and K. A. Prather, 2012: Ice in Clouds Experiment–Layer Clouds. Part II: Testing characteristics of heterogeneous ice formation in lee wave clouds. *J. Atmos. Sci.*, **69**, 1066–1079, doi:10.1175/JAS-D-11-026.1.

——, A. A. Hill, K. Furtado, and A. Korolev, 2014: Mixed-phase clouds in a turbulent environment. Part 2: Analytic treatment. *Quart. J. Roy. Meteor. Soc.*, **140**, 870–880. doi:10.1002/qj.2175.

——, and Coauthors, 2017: Secondary ice production: Current state of the science and recommendations for the future. *Ice Formation and Evolution in Clouds and Precipitation: Measurement and Modeling Challenges*, *Meteor. Monogr.*, No. 58, Amer. Meteor. Soc., doi:10.1175/AMSMONOGRAPHS-D-16-0014.1.

Findeisen, W., 1938: Kolloid-meteorologische Vorgänge bei Niederschlags-bildung. *Meteor. Z.*, **55**, 121–133.

——, 1940: On the origin of thunderstorm electricity. *Meteor. Z.*, **57**, 201–215.

——, 1942: Results of cloud and precipitation observations in weather reconnaissance flights over sea. *Forsch. Erfahr. Reichsamt Wetterdienst*, **8B**, 1–12.

——, and E. Findeisen, 1943: Investigations on the ice splinter formation on rime layers (A contribution to the origin of storm electricity and to the microstructure of cumulonimbi). *Meteor. Z.*, **60** (5), 145–154.

Fleenor, S. A., C. J. Biagi, K. L. Cummins, E. P. Krider, and X.-M. Shao, 2009: Characteristics of cloud-to-ground lightning in warm-season thunderstorms in the Central Great Plains. *Atmos. Res.*, **91**, 333–352, doi:10.1016/j.atmosres.2008.08.011.

Fleishauer, R. P., V. E. Larson, and T. H. Vonder Haar, 2002: Observed microphysical structure of midlevel, mixed-phase clouds. *J. Atmos. Sci.*, **59**, 1779–1804, doi:10.1175/1520-0469(2002)059<1779:OMSOMM>2.0.CO;2.

Fowler, L. D., D. A. Randall, and S. A. Rutledge, 1996: Liquid and ice cloud microphysics in the CSU general circulation model. Part I: Model description and simulated microphysical processes. *J. Climate*, **9**, 489–529, doi:10.1175/1520-0442(1996)009<0489:LAICMI>2.0.CO;2.

Freer, M., D. Baumgardner, M. W. Gallagher, A. Dean, A. Petzold, and J. Dorsey, 2014: Droplets, ice crystal or ash? Real time detection using the next generation Backscatter Cloud Probe. *14th Conf. on Cloud Physics*, Boston, MA, Amer. Meteor. Soc., P2.20. [Available online at https://ams.confex.com/ams/14CLOUD14ATRAD/webprogram/Paper249408.html.]

Freud, E., and D. Rosenfeld, 2012: Linear relation between convective cloud drop number concentration and depth for rain initiation. *J. Geophys. Res.*, **117**, D02207, doi:10.1029/2011JD016457.

Fridlind, A. M., and Coauthors, 2012a: A comparison of TWP-ICE observational data with cloud-resolving model results. *J. Geophys. Res.*, **117**, D05204, doi:10.1029/2011JD016595.

——, B. van Diedenhoven, A. S. Ackerman, A. Avramov, A. Morrie, H. Morrison, P. Zuidema, and M. D. Snipe, 2012b: A FIRE-ACE/SHEBA case study of mixed-phase Arctic boundary layer clouds: Entrainment rate limitations on rapid primary ice nucleation processes. *J. Atmos. Sci.*, **69**, 365–389, doi:10.1175/JAS-D-11-052.1.

Fu, Q., and S. Hollars, 2004: Testing mixed-phase cloud water vapor parameterizations with SHEBA/FIRE–ACE observations. *J. Atmos. Sci.*, **61**, 2083–2091, doi:10.1175/1520-0469(2004)061<2083:TMCWVP>2.0.CO;2.

Fuchs, B. R., and Coauthors, 2015: Environmental controls on storm intensity and charge structure in multiple regions of the continental United States. *J. Geophys. Res. Atmos.*, **120**, 6575–6596, doi:10.1002/2015JD023271.

Fugal, J. P., and R. A. Shaw, 2009: Cloud particle size distributions measured with an airborne digital in-line holographic instrument. *Atmos. Meas. Tech.*, **2**, 259–271, doi:10.5194/amt-2-259-2009.

——, T. J. Schultz, and R. A. Shaw, 2009: Practical methods for automated reconstruction and characterization of particles in digital in-line holograms. *Meas. Sci. Technol.*, **20**, 075501, doi:10.1088/0957-0233/20/7/075501.

Fukuta, N., 1969: Experimental studies on the growth of small ice crystals. *J. Atmos. Sci.*, **26**, 522–531, doi:10.1175/1520-0469(1969)026<0522:ESOTGO>2.0.CO;2.

——, and T. Takahashi, 1999: The growth of atmospheric ice crystals: A summary of findings in vertical supercooled cloud tunnel studies. *J. Atmos. Sci.*, **56**, 1963–1979, doi:10.1175/1520-0469(1999)056<1963:TGOAIC>2.0.CO;2.

Furtado, K., P. R. Field, I. A. Boutle, C. J. Morcrette, and J. M. Wilkinson, 2016: A physically based subgrid parameterization for the production and maintenance of mixed-phase clouds in a general circulation model. *J. Atmos. Sci.*, **73**, 279–291, doi:10.1175/JAS-D-15-0021.1.

Gao, B.-C., and A. F. H. Goetz, 1990: Column atmospheric water vapor and vegetation liquid water retrievals from Airborne Imaging Spectrometer data. *J. Geophys. Res.*, **95**, 3549–3564, doi:10.1029/JD095iD04p03549.

Gardiner, B. A. and J. Hallett, 1985: Degradation of in-cloud forward scattering spectrometer probe measurements in the presence of ice particles. *J. Atmos. Oceanic Technol.*, **2**, 171–180, doi:10.1175/1520-0426(1985)002<0171:DOICFS>2.0.CO;2.

Gayet, J.-F., S. Asano, A. Yamazaki, A. Uchiyama, A. Sinyuk, O. Jourdan, and F. Auriol, 2002: Two case studies of winter continental-type water and mixed-phase stratocumuli over the sea. 1: Microphysical and optical properties. *J. Geophys. Res.*, **107**, 4569, doi:10.1029/2001JD001106.

Gettelman, A., X. Liu, S. J. Ghan, H. Morrison, S. Park, and A. J. Conley, 2010: Global simulations of ice nucleation and ice supersaturation with an improved cloud scheme in the Community Atmosphere Model. *J. Geophys. Res.*, **115**, D18216, doi:10.1029/2009JD013797.

Girard, E., G. Dueymes, P. Du, and A. K. Bertram, 2013: Assessment of the effects of acid-coated ice nuclei on the Arctic cloud microstructure, atmospheric dehydration, radiation and temperature during winter. *Int. J. Climatol.*, **33**, 599–614, doi:10.1002/joc.3454.

Gliki, N. V., and A. A. Eliseev, 1962: Effect of supersaturation and temperature of the development of the initial growth forms on a sphere of ice. *Kristallografia*, **7**, 802–804.

——, ——, and N. M. Marchenko, 1962: The growth of spherical ice crystals. *Kristallografia*, **7**, 609–612.

Goloub, P., M. Herman, H. Chepfer, J. Riedi, G. Brogniez, P. Couvert, and G. Séze, 2000: Cloud thermodynamical phase classification from the POLDER spaceborne instrument. *J. Geophys. Res.*, **105**, 14 747–14 759, doi:10.1029/1999JD901183.

Gonda, T., and T. Yamazaki, 1984: Initial growth forms of snow crystals growing from frozen droplets. *J. Meteor. Soc. Japan*, **62**, 190–192, doi:10.2151/jmsj1965.62.1_190.

Green, R. O., T. H. Painter, D. A. Roberts, and J. Dozier, 2006: Measuring the expressed abundance of the three phases of water with an imaging spectrometer over melting snow. *Water Resour. Res.*, **42**, W10402, doi:10.1029/2005WR004509.

Gregory, D., and D. Morris, 1996: The sensitivity of climate simulations to the specification of mixed-phase clouds. *Climate Dyn.*, **12**, 641–651, doi:10.1007/BF00216271.

Hansen, J., M. Sato, and R. Ruedy, 1997: Radiative forcing and climate response. *J. Geophys. Res.*, **102**, 6831–6864, doi:10.1029/96JD03436.

Harrington, J. Y., and P. Q. Olsson, 2001: On the potential influence of ice nuclei on surface-forced marine stratocumulus cloud dynamics. *J. Geophys. Res.*, **106**, 27 473–27 484, doi:10.1029/2000JD000236.

——, T. Reisin, W. R. Cotton, and S. M. Kreidenweis, 1999: Cloud resolving simulation of Arctic stratus: Part II: Transition-season clouds. *Atmos. Res.*, **51**, 45–75, doi:10.1016/S0169-8095(98)00098-2.

Heidinger, A. K., and M. J. Pavolonis, 2009: Gazing at cirrus clouds for 25 years through a split window. Part I: Methodology. *J. Appl. Meteor. Climatol.*, **48**, 1100–1116, doi:10.1175/2008JAMC1882.1.

Heymsfield, A. J., 1977: Precipitation development in stratiform ice clouds: A microphysical and dynamical study. *J. Atmos. Sci.*, **34**, 367–381, doi:10.1175/1520-0469(1977)034<0367:PDISIC>2.0.CO;2.

——, and L. M. Miloshevich, 1989: Evaluation of liquid water measuring instruments in cold clouds sampled during FIRE. *J. Atmos. Oceanic Technol.*, **6**, 378–388, doi:10.1175/1520-0426(1989)006<0378:EOLWMI>2.0.CO;2.

——, and ——, 1993: Homogeneous ice nucleation and super-cooled liquid water in orographic wave clouds. *J. Atmos. Sci.*, **50**, 2335–2353, doi:10.1175/1520-0469(1993)050<2335:HINASL>2.0.CO;2.

——, and G. M. McFarquhar, 1996: High albedos of cirrus in the tropical Pacific warm pool: Microphysical interpretations from CEPEX and from Kwajalein, Marshall Islands. *J. Atmos. Sci.*, **53**, 2424–2451, doi:10.1175/1520-0469(1996)053<2424:HAOCIT>2.0.CO;2.

——, and Coauthors, 2017: Cirrus clouds. *Ice Formation and Evolution in Clouds and Precipitation: Measurement and Modeling Challenges*, Meteor. Monogr., No. 58, Amer. Meteor. Soc., doi:10.1175/AMSMONOGRAPHS-D-16-0010.1.

Hill, A. A., P. R. Field, K. Furtado, A. Korolev, and B. J. Shipway, 2014: Mixed-phase clouds in a turbulent environment. Part 1: Large-eddy simulation experiments. *Quart. J. Roy. Meteor. Soc.*, **140**, 855–869, doi:10.1002/qj.2177.

Hobbs, P. V., and L. F. Radke, 1975: The nature of winter clouds and precipitation in the Cascade Mountains and their modification by artificial seeding. Part II: Techniques for the physical evaluation of seeding. *J. Appl. Meteor.*, **14**, 805–818, doi:10.1175/1520-0450(1975)014<0805:TNOWCA>2.0.CO;2.

——, and A. L. Rangno, 1998: Microstructures of low and middle-level clouds over the Beaufort Sea. *Quart. J. Roy. Meteor. Soc.*, **124**, 2035–2071, doi:10.1002/qj.49712455012.

——, R. C. Easter, and A. B. Fraser, 1973: A theoretical study of the flow of air and fallout of solid precipitation over mountainous terrain: Part II. Microphysics. *J. Atmos. Sci.*, **30**, 813–823, doi:10.1175/1520-0469(1973)030<0813:ATSOTF>2.0.CO;2.

Hodapp, C. L., L. D. Carey, and R. E. Orville, 2008: Evolution of radar reflectivity and total lightning structure of the 21 April 2006 mesoscale convective system over Texas. *Atmos. Res.*, **89**, 113–137, doi:10.1016/j.atmosres.2008.01.007.

Hogan, R. J., P. R. Field, A. J. Illingworth, R. J. Cotton, and T. W. Choularton, 2002: Properties of embedded convection in warm-frontal mixed-phase cloud from aircraft and polarimetric radar. *Quart. J. Roy. Meteor. Soc.*, **128**, 451–476, doi:10.1256/003590002321042054.

——, P. N. Francis, H. Flentje, A. J. Illingworth, M. Quante, and J. Pelon, 2003a: Characteristics of mixed-phase clouds. I: Lidar, radar and aircraft observations from CLARE98. *Quart. J. Roy. Meteor. Soc.*, **129**, 2089–2116, doi:10.1256/rj.01.208.

——, A. J. Illingworth, E. J. O'Connor, and J. P. V. Poiares Baptista, 2003b: Characteristics of mixed-phase clouds. II: A climatology from ground-based lidar. *Quart. J. Roy. Meteor. Soc.*, **129**, 2117–2134, doi:10.1256/qj.01.209.

Hoose, C., U. Lohmann, P. Steir, B. Verheggen, and E. Weingartner, 2008: Aerosol processing in mixed-phase clouds in ECHAM5-HAM: Model description and comparison to observations. *J. Geophys. Res.*, **113**, D07210, doi:10.1029/2007JD009251.

Hu, Y., and Coauthors, 2007: The depolarization–attenuated backscatter relation: CALIPSO lidar measurements vs. theory. *Opt. Express*, **15**, 5327–5332, doi:10.1364/OE.15.005327.

——, S. Rodier, K.-M. Xu, W. Sun, J. Huang, B. Lin, P. Zhai, and D. Josset, 2010: Occurrence, liquid water content and fraction of supercooled water clouds from combined CALIOP/IIR/MODIS measurements. *J. Geophys. Res.*, **115**, D00H34, doi:10.1029/2009JD012384.

Huang, D., K. Johnson, Y. Liu, and W. Wiscombe, 2009: High-resolution retrieval of liquid water vertical distributions using collocated Ka-band and W-band cloud radars. *Geophys. Res. Lett.*, **36**, L24807, doi:10.1029/2009GL041364.

Huang, Y., S. T. Siems, M. J. Manton, A. Protat, and J. Delanöe, 2012: A study on the low-altitude clouds over the Southern Ocean using the DARDAR-MASK. *J. Geophys. Res.*, **117**, D18204, doi:10.1029/2012JB009424.

Intrieri, J. M., M. D. Shupe, T. Uttal, and B. J. McCarty, 2002: An annual cycle of Arctic cloud characteristics observed by radar and lidar at SHEBA. *J. Geophys. Res.*, **107**, 8030, doi:10.1029/2000jc000423.

Isaac, G. A., and R. S. Schemenauer, 1979: Large particles in super-cooled regions of northern Canadian cumulus clouds. *J. Appl. Meteor.*, **18**, 1056–1065, doi:10.1175/1520-0450(1979)018<1056:LPISRO>2.0.CO;2.

Iwabuchi, T., and C. Magono, 1975: A laboratory experiment on the freezing electrification of freely falling water droplets. *J. Meteor. Soc. Japan*, **53**, 393–401, doi:10.2151/jmsj1965.53.6_393.

Jackson, R. C., and Coauthors, 2012: The dependence of Arctic mixed-phase stratus ice cloud microphysics on aerosol concentration using observations acquired during ISDAC and M-PACE. *J. Geophys. Res.*, **117**, D15207, doi:10.1029/2012JD017668.

Jacobson, E. A., and E. P. Krider, 1976: Electrostatic field changes produced by Florida lightning. *J. Atmos. Sci.*, **33**, 103–117, doi:10.1175/1520-0469(1976)033<0103:EFCPBF>2.0.CO;2.

Jäkel, E., J. Walter, and M. Wendisch, 2013: Thermodynamic phase retrieval of convective clouds: Impact of sensor viewing geometry and vertical distribution of cloud properties. *Atmos. Meas. Tech.*, **6**, 539–547, doi:10.5194/amt-6-539-2013.

Jakob, C., 2002: Ice clouds in numerical weather prediction models: Progress, problems, and prospects. *Cirrus,* D. K. Lynch et al., Eds., Oxford University Press, 327–345.

Jameson, A. R., M. J. Murphy, and E. P. Krider, 1996: Multiple-parameter radar observations of isolated Florida thunderstorms during the onset of electrification. *J. Appl. Meteor.*, **35**, 343–354, doi:10.1175/1520-0450(1996)035<0343:MPROOI>2.0.CO;2.

Järvinen, E., and Coauthors, 2016: Quasi-spherical ice in convective clouds. *J. Atmos. Sci.*, **73**, 3885–3910, doi:10.1175/JAS-D-15-0365.1.

Jayaratne, E. R., and C. P. R. Saunders, 1985: Thunderstorm electrification: The effect of cloud droplets. *J. Geophys. Res.*, **90**, 13 063–13 066, doi:10.1029/JD090iD07p13063.

——, and ——, 2016: The interaction of ice crystals with hailstones in wet growth and its possible role in thunderstorm electrification. *Quart. J. Roy. Meteor. Soc.*, **142**, 1809–1815, doi:10.1002/qj.2777.

——, ——, and J. Hallett, 1983: Laboratory studies of the charging of soft-hail during ice crystal interactions. *Quart. J. Roy. Meteor. Soc.*, **109**, 609–630, doi:10.1002/qj.49710946111.

Jiang, H., W. R. Cotton, J. Pinto, J. Curry, and M. J. Weissbluth, 2000: Cloud resolving simulations of mixed-phase Arctic stratus observed during BASE: Sensitivity to concentration of ice crystals and large-scale heat and moisture advection. *J. Atmos. Sci.*, **57**, 2105–2117, doi:10.1175/1520-0469(2000)057<2105:CRSOMP>2.0.CO;2.

Johnson, A., S. Lasher-Trapp, A. Bansemer, Z. Ulanowski, and A. J. Heymsfield, 2014: Difficulties in early ice detection with the Small Ice Detector-2 HIAPER (SID-2H) in maritime cumuli. *J. Atmos. Oceanic Technol.*, **31**, 1263–1275, doi:10.1175/JTECH-D-13-00079.1.

Kaltenboeck, R., and A. Ryzhkov, 2013: Comparison of hail signatures of hail at S and C bands for different hail sizes. *Atmos. Res.*, **123**, 323–336, doi:10.1016/j.atmosres.2012.05.013.

Kanitz, T., P. Seifert, A. Ansmann, R. Engelmann, D. Althausen, C. Casiccia, and E. G. Rohwer, 2011: Contrasting the impact of aerosols at northern and southern midlatitudes on heterogeneous ice formation. *Geophys. Res. Lett.*, **38**, L17802, doi:10.1029/2011GL048532.

Kay, J. E., C. Wall, V. Yettella, B. Medeiros, C. Hannay, P. Caldwell, and C. Bitz, 2016: Global climate impacts of fixing the Southern Ocean shortwave radiation bias in the Community Earth System Model. *J. Climate*, **29**, 4617–4636, doi:10.1175/JCLI-D-15-0358.1.

Keeler, R. J., J. Lutz, and J. Vivekanandan, 2000: S-Pol: NCAR's polarimetric Doppler research radar. *Proc. Int. Geoscience and Remote Sensing Symp.*, Honolulu, HI, IEEE, 1570–1573.

Keith, W. D., and C. P. R. Saunders, 1990: Further laboratory studies of the charging of graupel during ice crystal interactions. *Atmos. Res.*, **25**, 445–464, doi:10.1016/0169-8095(90)90028-B.

Key, J. R., and J. M. Intrieri, 2000: Cloud particle phase determination with AVHRR. *J. Appl. Meteor.*, **39**, 1797–1804, doi:10.1175/1520-0450-39.10.1797.

King, W. D., D. A. Parkin, and R. J. Handsworth, 1978: A hot-wire liquid water device having fully calculable response

characteristics. *J. Appl. Meteor.*, **17**, 1809–1813, doi:10.1175/1520-0450(1978)017<1809:AHWLWD>2.0.CO;2.

Klein, S. A., and Coauthors, 2009: Intercomparison of model simulations of mixed-phase clouds observed during the ARM Mixed-Phase Arctic Cloud Experiment. I: Single layer cloud. *Quart. J. Roy. Meteor. Soc.*, **135**, 979–1002, doi:10.1002/qj.416.

Knollenberg, R. G., 1970: The optical array: An alternative to scattering or extinction for airborne particle size determination. *J. Appl. Meteor.*, **9**, 86–103, doi:10.1175/1520-0450(1970)009<0086:TOAAAT>2.0.CO;2.

——, 1981: Techniques for probing cloud microstructure. *Clouds, Their Formation, Optical Properties and Effects*, P. V. Hobbs and A. Deepak, Eds., Academic Press, 15–89.

Kollias, P., E. E. Clothiaux, M. A. Miller, B. A. Albrecht, G. L. Stephens, and T. P. Ackerman, 2007: Millimeter-wavelength radars—New frontier in atmospheric cloud and precipitation research. *Bull. Amer. Meteor. Soc.*, **88**, 1608–1624, doi:10.1175/BAMS-88-10-1608.

Komurcu, M., and Coauthors, 2014: Intercomparison of the cloud water phase among global climate models. *J. Geophys. Res. Atmos.*, **119**, 3372–3400, doi:10.1002/2013JD021119.

Korolev, A. V., 2007: Limitations of the Wegener–Bergeron–Findeisen mechanism in the evolution of mixed-phase clouds. *J. Atmos. Sci.*, **64**, 3372–3375, doi:10.1175/JAS4035.1.

——, 2008: Rates of phase transformations in mixed-phase clouds. *Quart. J. Roy. Meteor. Soc.*, **134**, 595–608, doi:10.1002/qj.230.

——, and J. W. Strapp, 2002: Accuracy of measurements of cloud ice water content by the Nevzorov probe. *40th Aerospace Science Meeting and Exhibit*, Reno, NV, AIAA, AIAA 2002-0679. [Available online at https://www.eol.ucar.edu/homes/dcrogers/C130/Probes/Nevzorov/IWC_AIAA.pdf.]

——, and G. A. Isaac, 2003: Phase transformation of mixed-phase clouds. *Quart. J. Roy. Meteor. Soc.*, **129**, 19–38, doi:10.1256/qj.01.203.

——, and I. P. Mazin, 2003: Supersaturation of water vapor in clouds. *J. Atmos. Sci.*, **60**, 2957–2974, doi:10.1175/1520-0469(2003)060<2957:SOWVIC>2.0.CO;2.

——, and G. A. Isaac, 2006: Relative humidity in liquid, mixed-phase and ice clouds. *J. Atmos. Sci.*, **63**, 2865–2880, doi:10.1175/JAS3784.1.

——, and P. R. Field, 2008: The effect of dynamics on mixed-phase clouds: Theoretical considerations. *J. Atmos. Sci.*, **65**, 66–86, doi:10.1175/2007JAS2355.1.

——, and G. A. Isaac, 2008: The effect of spatial averaging on the relative humidity and phase composition of clouds. *Int. Conf. on Clouds and Precipitation*, Cancun, Mexico, ICCP, P1.3. [Available online at http://cabernet.atmosfcu.unam.mx/ICCP-2008/abstracts/Program_on_line/Poster_01/Korolev&Isaac_extended.pdf.]

——, J. W. Strapp, G. A. Isaac, and A. N. Nevzorov, 1998: The Nevzorov airborne hot-wire LWC-TWC probe: Principle of operation and performance characteristics. *J. Atmos. Oceanic Technol.*, **15**, 1495–1510, doi:10.1175/1520-0426(1998)015<1495:TNAHWL>2.0.CO;2.

——, G. A. Isaac, S. Cober, J. W. Strapp, and J. Hallett, 2003: Microphysical characterization of mixed-phase clouds. *Quart. J. Roy. Meteor. Soc.*, **129**, 39–66, doi:10.1256/qj.01.204.

——, M. P. Bailey, J. Hallett, and G. A. Isaac, 2004: Laboratory and in situ observation of deposition growth of frozen drops. *J. Appl. Meteor.*, **43**, 612–622, doi:10.1175/1520-0450(2004)043<0612:LAISOO>2.0.CO;2.

——, E. F. Emery, J. W. Strapp, S. G. Cober, G. A. Isaac, M. Wasey, and D. Marcotte, 2011: Small ice particles in tropospheric clouds:

Fact or artifact? Airborne Icing Instrumentation Evaluation Experiment. *Bull. Amer. Meteor. Soc.*, **92**, 967–973, doi:10.1175/2010BAMS3141.1.

——, ——, and K. Creelman, 2013a: Modification and tests of particle probe tips to mitigate effects of ice shattering. *J. Atmos. Oceanic Technol.*, **30**, 690–708, doi:10.1175/JTECH-D-12-00142.1.

——, ——, J. W. Strapp, S. G. Cober, and G. A. Isaac, 2013b: Quantification of the effects of shattering on airborne ice particle measurements. *J. Atmos. Oceanic Technol.*, **30**, 2527–2553, doi:10.1175/JTECH-D-13-00115.1.

——, J. W. Strapp, G. A. Isaac, and E. Emery, 2013c: Improved airborne hot-wire measurements of ice water content in clouds. *J. Atmos. Oceanic Technol.*, **30**, 2121–2131, doi:10.1175/JTECH-D-13-00007.1.

Koshak, W. J., and E. P. Krider, 1989: Analysis of lightning field changes during active Florida thunderstorms. *J. Geophys. Res.*, **94**, 1165–1186, doi:10.1029/JD094iD01p01165.

Kou, L., D. Labrie, and P. Chylek, 1993: Refractive indices of water and ice in the 0.65- to 2.5-μm spectral range. *Appl. Opt.*, **32**, 3531–3540, doi:10.1364/AO.32.003531.

Krämer, M., and Coauthors, 2009: Ice supersaturations and cirrus cloud crystal numbers. *Atmos. Chem. Phys.*, **9**, 3505–3522, doi:10.5194/acp-9-3505-2009.

Krehbiel, P. R., 1981: *An Analysis of the Electric Field Change Produced by Lightning.* Vols. I and II, New Mexico Mining and Technology Rep. T-11, 490 pp.

——, 1986: The electrical structure of thunderstorms. *The Earth's Electrical Environment*, National Academy Press, 90–113.

——, M. Brook, and R. A. McCrory, 1979: An analysis of the charge structure of lightning discharges to ground. *J. Geophys. Res.*, **84**, 2432–2456, doi:10.1029/JC084iC05p02432.

——, R. J. Thomas, W. Rison, T. Hamlin, J. Harlin, and M. Davis, 2000: Lightning mapping observations in central Oklahoma. *Eos, Trans. Amer. Geophys. Union*, **81**, 21–25, doi:10.1029/00EO00014.

Kumjian, M. R., A. P. Khain, N. Benmoshe, E. Ilotoviz, A. V. Ryzhkov, and V. T. J. Phillips, 2014: The anatomy and physics of ZDR columns: Investigating a polarimetric radar signature with a spectral bin microphysical model. *J. Appl. Meteor. Climatol.*, **53**, 1820–1843, doi:10.1175/JAMC-D-13-0354.1.

Ladino, L. A., A. Korolev, I. Heckman, M. Wolde, A. M. Fridlind, and A. S. Ackerman, 2017: On the role of ice-nucleating aerosol in the formation of ice particles in tropical mesoscale convective systems. *Geophys. Res. Lett.*, **44**, 1574–1582, doi:10.1002/2016GL072455.

Lance, S., C. A. Brock, D. Rogers, and J. A. Gordon, 2010: Water droplet calibration of the Cloud Droplet Probe (CDP) and in-flight performance in liquid, ice and mixed-phase clouds during ARCPAC. *Atmos. Meas. Tech.*, **3**, 1683–1706, doi:10.5194/amt-3-1683-2010.

Lang, T. J., S. A. Rutledge, B. Dolan, P. Krehbiel, W. Rison, and D. T. Lindsey, 2014: Lightning in wildfire smoke plumes observed in Colorado during summer 2012. *Mon. Wea. Rev.*, **142**, 489–507, doi:10.1175/MWR-D-13-00184.1.

Lawson, P., C. Gurganus, S. Woods, and R. Bruintjes, 2017: Aircraft observations of cumulus microphysics ranging from the tropics to midlatitudes: Implications for a "new" secondary ice process. *J. Atmos. Sci.*, **174**, 2899–2920, doi:10.1175/JAS-D-17-0033.

Lawson, R. P., and A. Gettelman, 2014: Impact of Antarctic mixed-phase clouds on climate. *Proc. Natl. Acad. Sci. USA*, **111**, 18 156–18 161, doi:10.1073/pnas.1418197111.

——, B. A. Baker, C. G. Schmitt, and T. L. Jensen, 2001: An overview of microphysical properties of Arctic clouds

observed in May and July 1998 during FIRE ACE. *J. Geophys. Res.*, **106**, 14 989–15 014, doi:10.1029/2000JD900789.

——, D. O'Connor, P. Zmarzly, K. Weaver, B. Baker, Q. Mo, and H. Jonsson, 2006: The 2D-S (stereo) probe: Design and preliminary tests of a new airborne, high-speed, high-resolution particle imaging probe. *J. Atmos. Oceanic Technol.*, **23**, 1462–1477, doi:10.1175/JTECH1927.1.

——, S. Woods, and H. Morrison, 2015: The microphysics of ice and precipitation development in tropical cumulus clouds. *J. Atmos. Sci.*, **72**, 2429–2445, doi:10.1175/JAS-D-14-0274.1.

LeBlanc, S. E., P. Pilewskie, K. S. Schmidt, and O. Coddington, 2015: A spectral method for discriminating thermodynamic phase and retrieving cloud optical thickness and effective radius using transmitted solar radiance spectra. *Atmos. Meas. Tech.*, **8**, 1361–1383, doi:10.5194/amt-8-1361-2015.

Leon, D. C., and Coauthors, 2016: The Convective Precipitation Experiment (COPE): Investigating the origins of heavy precipitation in the southwestern United Kingdom. *Bull. Amer. Meteor. Soc.*, **97**, 1003–1020, doi:10.1175/BAMS-D-14-00157.1.

Lhermitte, R., 1987: A 94-GHz Doppler radar for cloud observations. *J. Atmos. Oceanic Technol.*, **4**, 36–48, doi:10.1175/1520-0426(1987)004<0036:AGDRFC>2.0.CO;2.

——, and E. Williams, 1985: Thunderstorm electrification: A case study. *J. Geophys. Res.*, **90**, 6071–6078, doi:10.1029/JD090iD04p06071.

Li, Z.-X., and H. Le Treut, 1992: Cloud-radiation feedbacks in a general circulation model and their dependence on cloud modeling assumptions. *Climate Dyn.*, **7**, 133–139, doi:10.1007/BF00211155.

Lohmann, U., 2002: A glaciation indirect aerosol effect caused by soot aerosols. *Geophys. Res. Lett.*, **29**, doi:10.1029/2001GL014357.

——, and C. Hoose, 2009: Sensitivity studies of different aerosol indirect effects in mixed-phase clouds. *Atmos. Chem. Phys.*, **9**, 8917–8934, doi:10.5194/acp-9-8917-2009.

——, J. Henneberger, O. Henneberg, J. P. Fugal, J. Bühl, and Z. A. Kanji, 2016: Persistence of orographic mixed-phase clouds. *Geophys. Res. Lett.*, **43**, 10 512–10 519, doi:10.1002/2016GL071036.

López, M. L., and E. E. Ávila, 2012: Deformations of frozen droplets formed at −40°C. *Geophys. Res. Lett.*, **39**, L01805, doi:10.1029/2011GL050185.

Lord, S. J., H. E. Willoughby, and J. M. Piotrowicz, 1984: Role of a parameterized ice-phase microphysics in an axisymmetric, non-hydrostatic tropical cyclone model. *J. Atmos. Sci.*, **41**, 2836–2848, doi:10.1175/1520-0469(1984)041<2836:ROAPIP>2.0.CO;2.

Lubin, D., 2004: Thermodynamic phase of maritime Antarctic clouds from FTIR and supplementary radiometric data. *J. Geophys. Res.*, **109**, D04204, doi:10.1029/2003JD003979.

Ludlam, F. H., 1951: The heat economy of a rimed cylinder. *Quart. J. Roy. Meteor. Soc.*, **77**, 663–666, doi:10.1002/qj.49707733410.

Luke, E. P., P. Kollias, and M. D. Shupe, 2010: Detection of supercooled liquid in mixed-phase clouds using radar Doppler spectra. *J. Geophys. Res.*, **115**, D19201, doi:10.1029/2009JD012884.

Luque, M. Y., R. Burgesser, and E. Avila, 2016: Thunderstorm graupel charging in the absence of supercooled water droplets. *Quart. J. Roy. Meteor. Soc.*, **142**, 2418–2423, doi:10.1002/qj.2834.

Lynn, B., A. Khain, D. Rosenfeld, and W. L. Woodley, 2007: Effects of aerosols on precipitation from orographic clouds. *J. Geophys. Res.*, **112**, D10225, doi:10.1029/2006JD007537.

Lyons, W. A., T. E. Nelson, E. R. Williams, J. Cramer, and T. Turner, 1998: Enhanced positive cloud-to-ground lightning

in thunderstorms ingesting smoke. *Science*, **282**, 77–81, doi:10.1126/science.282.5386.77.

MacGorman, D. R., and D. W. Burgess, 1994: Positive cloud-to-ground lightning in tornadic storms and hailstorms. *Mon. Wea. Rev.*, **122**, 1671–1697, doi:10.1175/1520-0493(1994)122<1671:PCTGLI>2.0.CO;2.

Marshall, T. C., and W. P. Winn, 1982: Measurements of charged precipitation in a New Mexico thunderstorm: Lower positive charge centers. *J. Geophys. Res.*, **87**, 7141–7157, doi:10.1029/JC087iC09p07141.

Mattos, E. V., L. A. T. Machado, E. R. Williams, S. J. Goodman, R. J. Blakeslee, and J. C. Bailey, 2017: Electrification life cycle of incipient thunderstorms. *J. Geophys. Res. Atmos.*, **122**, 4670–4697, doi:10.1002/2016JD025772.

Matus, A. V., and T. S. L'Ecuyer, 2017: The role of cloud phase in Earth's radiation budget. *J. Geophys. Res. Atmos.*, **122**, 2559–2578, doi:10.1002/2016JD025951.

Mazin, I. P., 1986: Relation of clouds phase structure to vertical motion. *Sov. Meteor. Hydrol.*, **11**, 27–35.

——, A. V. Korolev, A. Heymsfield, G. A. Isaac, and S. G. Cober, 2001: Thermodynamics of icing cylinder for measurements of liquid water content in supercooled clouds. *J. Atmos. Oceanic Technol.*, **18**, 543–558, doi:10.1175/1520-0426(2001)018<0543:TOICFM>2.0.CO;2.

McCoy, D. T., D. L. Hartmann, and D. P. Grosvenor, 2014: Observed Southern Ocean cloud properties and shortwave reflection. Part I: Calculation of SW flux from observed cloud properties. *J. Climate*, **27**, 8836–8857, doi:10.1175/JCLI-D-14-00287.1.

——, ——, M. D. Zelinka, P. Ceppi, and D. P. Grosvenor, 2015: Mixed-phase cloud physics and Southern Ocean cloud feedback in climate models. *J. Geophys. Res. Atmos.*, **120**, 9539–9554, doi:10.1002/2015JD023603.

——, I. Tan, D. L. Hartmann, M. D. Zelinka, and T. Storelvmo, 2016: On the relationships among cloud cover, mixed-phase partitioning, and planetary albedo in GCMs. *J. Adv. Model. Earth Syst.*, **8**, 650–668, doi:10.1002/2015MS000589.

McFarquhar, G. M., and S. G. Cober, 2004: Single-scattering properties of mixed-phase Arctic clouds at solar wavelengths: Impacts on radiative transfer. *J. Climate*, **17**, 3799–3813, doi:10.1175/1520-0442(2004)017<3799:SPOMAC>2.0.CO;2.

——, G. Zhang, M. R. Poellot, G. L. Kok, R. McCoy, T. Tooman, and A. J. Heymsfield, 2007: Ice properties of single layer stratocumulus during the Mixed-Phase Arctic Cloud Experiment (MPACE). Part I: Observations. *J. Geophys. Res.*, **112**, D24202, doi:10.1029/2007JD008633.

——, and Coauthors, 2011: Indirect and Semi-Direct Aerosol Campaign: The impact of Arctic aerosols on clouds. *Bull. Amer. Meteor. Soc.*, **92**, 183–201, doi:10.1175/2010BAMS2935.1.

——, J. Um, and R. Jackson, 2013: Small particle shape in mixed-phase clouds. *J. Appl. Meteor. Climatol.*, **52**, 1277–1293, doi:10.1175/JAMC-D-12-0114.1.

Meyer, J., 2013: *Ice Crystal Measurements with the New Particle Spectrometer NIXE-CAPS*. Forschungszentrum Jülich, 132 pp.

Miller, S. D., Y.-J. Noh, and A. K. Heidinger, 2014: Liquid-top mixed-phase cloud detection from shortwave-infrared satellite radiometer observations: A physical basis. *J. Geophys. Res. Atmos.*, **119**, 8245–8267, doi:10.1002/2013JD021262.

Mioche, G., O. Jourdan, M. Ceccaldi, and J. Delanoë, 2015: Variability of mixed-phase clouds in the Arctic with a focus on the Svalbard region: A study based on spaceborne active remote sensing. *Atmos. Chem. Phys.*, **15**, 2445–2461, doi:10.5194/acp-15-2445-2015.

Moran, K. P., B. E. Martner, M. J. Post, R. A. Kropfli, D. C. Welsh, and K. B. Widener, 1998: An unattended cloud-profiling radar for use in climate research. *Bull. Amer. Meteor. Soc.*, **79**, 443–455, doi:10.1175/1520-0477(1998)079<0443:AUCPRF>2.0.CO;2.

Morrison, A. E., S. T. Siems, and M. J. Manton, 2011: A three-year climatology of cloud-top phase over the Southern Ocean and North Pacific. *J. Climate*, **24**, 2405–2418, doi:10.1175/2010JCLI3842.1.

Morrison, H., M. D. Shupe, and J. A. Curry, 2003: Modeling clouds observed at SHEBA using a bulk parameterization implemented into a single-column model. *J. Geophys. Res.*, **108**, 4255, doi:10.1029/2002JD002229.

——, and Coauthors, 2009: Intercomparison of model simulations of mixed-phase clouds observed during the ARM Mixed-Phase Arctic Cloud Experiment. II: Multilayered cloud. *Quart. J. Roy. Meteor. Soc.*, **135**, 1003–1019, doi:10.1002/qj.415.

——, and Coauthors, 2011: Intercomparison of cloud model simulations of Arctic mixed-phase boundary layer clouds observed during SHEBA/FIRE-ACE. *J. Adv. Model. Earth Syst.*, **3**, M05001, doi:10.1029/2011MS000066.

——, G. de Boer, G. Feingold, J. Harrington, M. D. Shupe, and K. Sulia, 2012: Resilience of persistent Arctic mixed-phase clouds. *Nat. Geosci.*, **5**, 11–17, doi:10.1038/ngeo1332.

Moss, S. J., and D. W. Johnson, 1994: Aircraft measurements to validate and improve numerical model parametrization of ice to water ratios in clouds. *Atmos. Res.*, **34**, 1–25, doi:10.1016/0169-8095(94)90078-7.

Mossop, S. C., A. Ono, and E. R. Wishart, 1970: Ice particles in maritime clouds near Tasmania. *Quart. J. Roy. Meteor. Soc.*, **96**, 487–508, doi:10.1002/qj.49709640910.

Muhlbauer, A., and U. Lohmann, 2009: Sensitivity studies of aerosol–cloud interactions in mixed-phase orographic precipitation. *J. Atmos. Sci.*, **66**, 2517–2538, doi:10.1175/2009JAS3001.1.

——, T. Hashino, L. Xue, A. Teller, U. Lohmann, R. M. Rasmussen, I. Geresdi, and Z. Pan, 2010: Intercomparison of aerosol-cloud-precipitation interactions in stratiform orographic mixed-phase clouds. *Atmos. Chem. Phys.*, **10**, 8173–8196, doi:10.5194/acp-10-8173-2010.

Mülmenstädt, J., O. Sourdeval, J. Delanoë, and J. Quaas, 2015: Frequency of occurrence of rain from liquid-, mixed-, and ice-phase clouds derived from A-Train satellite retrievals. *Geophys. Res. Lett.*, **42**, 6502–6509, doi:10.1002/2015GL064604.

Murakami, M., and T. Matsuo, 1990: Development of the hydrometeor videosonde. *J. Atmos. Oceanic Technol.*, **7**, 613–620, doi:10.1175/1520-0426(1990)007<0613:DOTHV>2.0.CO;2.

Murphy, A., R. M. Rauber, G. M. McFarquhar, B. F. Jewett, D. M. Plummer, J. A. Finlon, and A. A. Rosenow, 2017: Microphysical structure of elevated convection in winter cyclones. *J. Atmos. Sci.*, **74**, 69–91, doi:10.1175/JAS-D-16-0204.1.

Nasiri, S. L., and B. H. Kahn, 2008: Limitations of bispectral infrared cloud phase determination and potential for improvement. *J. Appl. Meteor. Climatol.*, **47**, 2895–2910, doi:10.1175/2008JAMC1879.1.

Naud, C., J. F. Booth, and A. D. Del Genio, 2014: Evaluation of ERA-Interim and MERRA cloudiness in the Southern Ocean. *J. Climate*, **27**, 2109–2124, doi:10.1175/JCLI-D-13-00432.1.

Neel, C. B., 1955: Heated-wire-liquid-water content instrument and results of initial flight tests in icing conditions. National Advisory Committee for Aeronautics Research Memo. RMA54123, 33 pp.

Nichman, L., and Coauthors, 2016: Phase transition observations and discrimination of small cloud particles by light polarization in expansion chamber experiments. *Atmos. Chem. Phys.*, **16**, 3651–3664, doi:10.5194/acp-16-3651-2016.

Nicholls, S., J. Leighton, and R. Barker, 1990: A new fast response instrument for measuring total water content from aircraft. *J. Atmos. Oceanic Technol.*, **7**, 706–718, doi:10.1175/1520-0426(1990)007<0706:ANFRIF>2.0.CO;2.

Noh, Y. J., C. J. Seaman, T. H. Vonder Haar, and G. Liu, 2013: In situ aircraft measurements of the vertical distribution of liquid and ice water content in midlatitude mixed-phase clouds. *J. Appl. Meteor.*, **52**, 269–279, doi:10.1175/JAMC-D-11-0202.1.

Noone, K. J., J. A. Ogren, J. Heintzenberg, R. J. Charlson, and D. S. Covert, 1988: Design and calibration of a counterflow virtual impactor for sampling of atmospheric fog and cloud droplets. *J. Aerosol. Sci. Technol.*, **8**, 235–244, doi:10.1080/02786828808959186.

O'Connor, D., B. Baker, and R. P. Lawson, 2008: Upgrades to the FSSP-100 electronics. *Proc. 15th Int. Conf. on Clouds and Precipitation*, Cancun, Mexico, P13.6. [Available online at http://cabernet.atmosfcu.unam.mx/ICCP-2008/abstracts/Program_on_line/Poster_13/O-Connor_extended_final.pdf.]

Okamoto, H., K. Sato, and Y. Hagihara, 2010: Global analysis of ice microphysics from CloudSat and CALIPSO: Incorporation of specular reflection in lidar signals. *J. Geophys. Res.*, **115**, D22209, doi:10.1029/2009JD013383.

Ovchinnikov, M., A. Korolev, and J. Fan, 2011: Effects of ice number concentration on dynamics of a shallow mixed-phase stratiform cloud. *J. Geophys. Res.*, **116**, D00T06, doi:10.1029/2011JD015888.

——, and Coauthors, 2014: Intercomparison of large-eddy simulations of Arctic mixed-phase clouds: Importance of ice size distribution assumptions. *J. Adv. Model. Earth Syst.*, **6**, 223–248, doi:10.1002/2013MS000282.

Pavolonis, M. J., and A. K. Heidinger, 2004: Daytime cloud overlap detection from AVHRR and VIIRS. *J. Appl. Meteor.*, **43**, 762–778, doi:10.1175/2099.1.

Pawar, S. D., V. Gopalakrishnan, P. Murugavel, N. E. Veremey, and A. A. Sinkevich, 2017: Possible role of aerosols in the charge structure of isolated thunderstorms. *Atmos. Res.*, **183**, 331–340, doi:10.1016/j.atmosres.2016.09.016.

Payne, C. D., T. J. Schuur, D. R. MacGorman, K. M. Kuhlman, and W. D. Rust, 2010: Polarimetric and electrical characteristics of a lightning ring in a supercell storm. *Mon. Wea. Rev.*, **138**, 2405–2425, doi:10.1175/2009MWR3210.1.

Peppler, W., 1940: Unterkühle Wasserwolken und Eiswolken. *Forsch. Erfahr. Reichsamt Wetterdienst*, **1B**, 3–68.

Pilewskie, P., and S. Twomey, 1987: Cloud phase discrimination by reflectance measurements near 1.6 and 2.2 μm. *J. Atmos. Sci.*, **44**, 3419–3420, doi:10.1175/1520-0469(1987)044<3419:CPDBRM>2.0.CO;2.

Pincus, R., and M. B. Baker, 1994: Effect of precipitation on the albedo susceptibility of clouds in the marine boundary layer. *Nature*, **372**, 250–252, doi:10.1038/372250a0.

Pinsky, M., A. Khain, and A. Korolev, 2014: Analytical investigation of glaciation time in mixed-phase adiabatic cloud volumes. *J. Atmos. Sci.*, **71**, 4143–4157, doi:10.1175/JAS-D-13-0359.1.

——, ——, and ——, 2015: Phase transformations in an ascending adiabatic mixed-phase cloud volume. *J. Geophys. Res.*, **120**, 3329–3353.

Pinto, J. O., 1998: Autumnal mixed-phase cloudy boundary layers in the Arctic. *J. Atmos. Sci.*, **55**, 2016–2037, doi:10.1175/1520-0469(1998)055<2016:AMPCBL>2.0.CO;2.

Pithan, F., B. Medeiros, and T. Mauritsen, 2014: Mixed-phase clouds cause climate model biases in Arctic wintertime temperature inversions. *Climate Dyn.*, **43**, 289–303, doi:10.1007/s00382-013-1964-9.

Platnick, S., and Coauthors, 2017: The MODIS cloud optical and microphysical products: Collection 6 updates and examples from Terra and Aqua. *IEEE Trans. Geosci. Remote Sens.*, **55**, 502–505, doi:10.1109/TGRS.2016.2610522.

Plummer, D. M., S. Goeke, R. M. Rauber, and L. DiGirolamo, 2010: Discrimination of mixed- versus ice-phase clouds using dual-polarization radar with application to detection of aircraft icing regions. *J. Appl. Meteor. Climatol.*, **49**, 920–935, doi:10.1175/2009JAMC2267.1.

——, G. M. McFarquhar, R. M. Rauber, B. F. Jewett, and D. C. Leon, 2014: Structure and statistical analysis of the microphysical properties of generating cells in the comma head region of continental winter cyclones. *J. Atmos. Sci.*, **71**, 4181–4203, doi:10.1175/JAS-D-14-0100.1.

——, ——, ——, ——, and ——, 2015: Microphysical structure of fall streaks in stratiform areas within winter cyclones. *J. Atmos. Sci.*, **72**, 2465–2483, doi:10.1175/JAS-D-14-0354.1.

Qie, X., T. Zhang, G. Zhang, T. Zhang, and Z. Kong, 2009: Electrical characteristics of thunderstorms in different plateau regions of China. *Atmos. Res.*, **91**, 244–249, doi:10.1016/j.atmosres.2008.04.014.

Rangno, A. L., and P. V. Hobbs, 2001: Ice particles in stratiform clouds in the Arctic and possible mechanisms for the production of high ice concentrations. *J. Geophys. Res.*, **106**, 15 065–15 075, doi:10.1029/2000JD900286.

Rauber, R. M., and L. O. Grant, 1986: The characteristics and distribution of cloud water over the mountains of Northern Colorado during wintertime storms. Part II: Spatial distribution and microphysical characteristics. *J. Climate Appl. Meteor.*, **25**, 489–504, doi:10.1175/1520-0450(1986)025<0489:TCADOC>2.0.CO;2.

——, and A. Tokay, 1991: An explanation for the existence of supercooled water at the tops of cold clouds. *J. Atmos. Sci.*, **48**, 1005–1023, doi:10.1175/1520-0469(1991)048<1005:AEFTEO>2.0.CO;2.

Reynolds, S. E., and H. W. Neill, 1955: The distribution and discharge of thunderstorm charge centers. *J. Meteor.*, **12**, 1–12, doi:10.1175/1520-0469(1955)012<0001:TDADOT>2.0.CO;2.

——, M. Brook, and M. F. Gourley, 1957: Thunderstorm charge separation. *J. Meteor.*, **14**, 426–436, doi:10.1175/1520-0469(1957)014<0426:TCS>2.0.CO;2.

Riedi, J., and Coauthors, 2010: Cloud thermodynamic phase inferred from merged POLDER and MODIS data. *Atmos. Chem. Phys.*, **10**, 11 851–11 865, doi:10.5194/acp-10-11851-2010.

Rollins, A. W., T. D. Thornberry, R. S. Gao, S. Woods, R. P. Lawson, T. P. Bui, E. J. Jensen, and D. W. Fahey, 2016: Observational constraints on the efficiency of dehydration mechanisms in the tropical tropopause layer. *Geophys. Res. Lett.*, **43**, 2912–2918, doi:10.1002/2016GL067972.

Rosenfeld, D., and W. L. Woodley, 2000: Deep convective clouds with sustained supercooled liquid water down to −37.5°C. *Nature*, **405**, 440–442, doi:10.1038/35013030.

——, E. Williams, M. O. Andreae, E. Freud, U. Pöschl, and N. O. Rennó, 2012: The scientific basis for a satellite mission to retrieve CCN concentrations and their impacts on convective clouds. *Atmos. Meas. Tech.*, **5**, 2039–2055, doi:10.5194/amt-5-2039-2012.

Rosenow, A. A., D. M. Plummer, R. M. Rauber, G. M. McFarquhar, B. F. Jewett, and D. Leon, 2014: Vertical velocity and physical structure of generating cells and convection

in the comma head region of continental winter cyclones. *J. Atmos. Sci.*, **71**, 1538–1558, doi:10.1175/JAS-D-13-0249.1.

Rust, W. D., and Coauthors, 2005: Inverted-polarity electrical structures in thunderstorms in the Severe Thunderstorm Electrification and Precipitation Study (STEPS). *Atmos. Res.*, **76**, 247–271, doi:10.1016/j.atmosres.2004.11.029.

Ryan, B. F., E. R. Wishart, and D. E. Shaw, 1976: The growth rates and densities of ice crystals between −3°C and −21°C. *J. Atmos. Sci.*, **33**, 842–850, doi:10.1175/1520-0469(1976)033<0842:TGRADO>2.0.CO;2.

Sassen, K., 1991: The polarization lidar technique for cloud research: A review and current assessment. *Bull. Amer. Meteor. Soc.*, **72**, 1848–1866, doi:10.1175/1520-0477(1991)072<1848:TPLTFC>2.0.CO;2.

Saunders, C. P. R., 2008: Charge separation mechanisms in clouds. *Space Sci. Rev.*, **137**, 335–353, doi:10.1007/s11214-008-9345-0.

——, and I. Brooks, 1992: The effects of high liquid water content on thunderstorm charging. *J. Geophys. Res.*, **97**, 14 671–14 676, doi:10.1029/92JD01186.

——, W. D. Keith, and R. P. Mitzeva, 1991: The effect of liquid water content on thunderstorm charging. *J. Geophys. Res.*, **96**, 11 007–11 017, doi:10.1029/91JD00970.

Schlenczek, O., J. Fugal, G. Lloyd, K. N. Bower, T. W. Choularton, M. Flynn, J. Crosier, and S. Borrmann, 2017: Microphysical properties of ice crystal precipitation and surface-generated ice crystals in a high Alpine environment in Switzerland. *J. Appl. Meteor. Climatol.*, **56**, 433–453, doi:10.1175/JAMC-D-16-0060.1.

Schmitt, C. G., and A. J. Heymsfield, 2009: The size distribution and mass-weighted terminal velocity of low-latitude tropopause cirrus crystal populations. *J. Atmos. Sci.*, **66**, 2013–2028, doi:10.1175/2009JAS3004.1.

Schnaiter, M., E. Järvinen, A. Abdelmonem, and T. Leisner, 2017: PHIPS-HALO: The airborne Particle Habit Imaging and Polar Scattering probe—Part 2: Characterization and first results. *Atmos. Meas. Tech. Discuss.*, doi:10.5194/amt-2017-304.

Schumann, T. E. W., 1938: The theory of hail formation. *Quart. J. Roy. Meteor. Soc.*, **64**, 3–21, doi:10.1002/qj.49706427303.

Shifrin, K. S., and A. Y. Perelman, 1960: The kinetics of distillation of supercooled systems (in Russian). *Dokl. Akad. Nauk SSSR*, **132**, 1148–1151.

Shupe, M. D., 2007: A ground-based multisensor cloud phase classifier. *Geophys. Res. Lett.*, **34**, L22809, doi:10.1029/2007GL031008.

——, T. Uttal, S. Y. Matrosov, and A. S. Rrisch, 2001: Cloud water contents and hydrometeor sizes during the FIRE Arctic clouds experiment. *J. Geophys. Res.*, **106**, 15 015–15 028, doi:10.1029/2000JD900476.

——, ——, and ——, 2005: Arctic cloud microphysics retrievals from surface-based remote sensors at SHEBA. *J. Appl. Meteor.*, **44**, 1544–1562, doi:10.1175/JAM2297.1.

——, S. Y. Matrosov, and T. Uttal, 2006: Arctic mixed-phase cloud properties derived from surface-based sensors at SHEBA. *J. Atmos. Sci.*, **63**, 697–711, doi:10.1175/JAS3659.1.

——, and Coauthors, 2008: A focus on mixed-phase clouds: The status of ground-based observational methods. *Bull. Amer. Meteor. Soc.*, **89**, 1549–1562, doi:10.1175/2008BAMS2378.1.

——, V. P. Walden, E. Eloranta, T. Uttal, J. R. Campbell, S. M. Starkweather, and M. Shiobara, 2011: Clouds at Arctic atmospheric observatories. Part I: Occurrence and macrophysical properties. *J. Appl. Meteor. Climatol.*, **50**, 626–644, doi:10.1175/2010JAMC2467.1.

——, D. D. Turner, A. Zwink, M. M. Theimann, M. J. Mlawer, and T. R. Shippert, 2015: Deriving Arctic cloud microphysics at

Barrow: Algorithms, results, and radiative closure. *J. Appl. Meteor. Climatol.*, **54**, 1675–1689, doi:10.1175/JAMC-D-15-0054.1.

Solomon, A., M. D. Shupe, P. O. G. Persson, H. Morrison, T. Yamaguchi, P. M. Caldwell, and G. de Boer, 2014: The sensitivity of springtime Arctic mixed-phase stratocumulus clouds to surface layer and cloud-top inversion layer moisture sources. *J. Atmos. Sci.*, **71**, 574–595, doi:10.1175/JAS-D-13-0179.1.

Steen, L. C. E., R. F. Ide, and J. F. Van Zante, 2016: An assessment of the icing blade and the SEA multi-element sensor for liquid water content calibration of the NASA GRC Icing Research Tunnel. *Eighth AIAA Atmospheric and Space Environments Conf.*, Washington, DC, AIAA, 2016-4051. [Available online at https://doi.org/10.2514/6.2016-4051.]

Stephens, G. L., and Coauthors, 2002: The CloudSat Mission and the A-Train: A new dimension of space-based observations of clouds and precipitation. *Bull. Amer. Meteor. Soc.*, **83**, 1771–1790, doi:10.1175/BAMS-83-12-1771.

Stith, J. L., J. A. Haggerty, A. Heymsfield, and C. A. Grainger, 2004: Microphysical characteristics of tropical updrafts in clean conditions. *J. Appl. Meteor.*, **43**, 779–794, doi:10.1175/2104.1.

Stolzenburg, M., T. C. Marshall, and P. R. Krehbiel, 2015: Initial electrification to the first lightning flash in New Mexico thunderstorms. *J. Geophys. Res. Atmos.*, **120**, 11 253–11 276, doi:10.1002/2015JD023988.

Storelvmo, T., J. E. Kristjánsson, and U. Lohmann, 2008a: Aerosol influence on mixed-phase clouds in CAM-Oslo. *J. Atmos. Sci.*, **65**, 3214–3230, doi:10.1175/2008JAS2430.1.

——, J. E. Kristjansson, U. Lohmann, T. Iversen, A. Kirkevag, and O. Seland, 2008b: Modeling of the Wegener–Bergeron–Findeisen process—Implications for aerosol indirect effects. *Environ. Res. Lett.*, **3**, 045001, doi:10.1088/1748-9326/3/4/045001.

——, C. Hoose, and P. Eriksson, 2011: Global modeling of mixed-phase clouds: The albedo and lifetime effect of aerosols. *J. Geophys. Res.*, **116**, D05207, doi:10.1029/2010JD014724.

Strangeways, I., 2006: *Precipitation: Theory, Measurement and Distribution.* Cambridge University Press, 302 pp.

Strapp, J. W., and Coauthors, 2003: Wind tunnel measurements of the response of hot-wire liquid water content instruments to large droplets. *J. Atmos. Oceanic Technol.*, **20**, 791–806, doi:10.1175/1520-0426(2003)020<0791:WTMOTR>2.0.CO;2.

Stubenrauch, C. J., and Coauthors, 2013: Assessment of global cloud datasets from satellites: Project and database initiated by the GEWEX Radiation Panel. *Bull. Amer. Meteor. Soc.*, **94**, 1031–1049, doi:10.1175/BAMS-D-12-00117.1.

Sulia, K. J., and J. Y. Harrington, 2011: Ice aspect ratio influences on mixed-phase clouds: Impacts on phase partitioning in parcel models. *J. Geophys. Res.*, **116**, D21309, doi:10.1029/2011JD016298.

Sun, Z., and K. P. Shine, 1994: Studies of the radiative properties of ice and mixed-phase clouds. *Quart. J. Roy. Meteor. Soc.*, **120**, 111–137, doi:10.1002/qj.49712051508.

Takahashi, C., 1975: Deformations of frozen water drops and their frequencies. *J. Meteor. Soc. Japan*, **53**, 402–411, doi:10.2151/jmsj1965.53.6_402.

——, 1979: Formation of poly-crystalline snow crystals by riming process. *J. Meteor. Soc. Japan*, **57**, 458–464, doi:10.2151/jmsj1965.57.5_458.

Takahashi, T., 1978: Riming electrification as a charge generation mechanism in thunderstorms. *J. Atmos. Sci.*, **35**, 1536–1548, doi:10.1175/1520-0469(1978)035<1536:REAACG>2.0.CO;2.

——, and K. Suzuki, 2010: Development of negative dipoles in a stratiform cloud layer in Okinawa "Baiu" MCS system. *Atmos. Res.*, **98**, 317–326, doi:10.1016/j.atmosres.2010.07.013.

——, T. Tajiri, and Y. Sonoi, 1999: Charges on graupel and snow crystals and the electrical structure of winter thunderstorms. *J. Atmos. Sci.*, **56**, 1561–1578, doi:10.1175/1520-0469(1999)056<1561:COGASC>2.0.CO;2.

——, S. Sugimoto, T. Kawano, and K. Suzuki, 2017: Riming electrification in Hokuriku winter clouds and comparison with laboratory observations. *J. Atmos. Sci.*, **74**, 431–447, doi:10.1175/JAS-D-16-0154.1.

Tan, I., T. Storelvmo, and Y.-S. Choi, 2014: Spaceborne lidar observations of the ice-nucleating potential of dust, polluted dust, and smoke aerosols in mixed-phase clouds. *J. Geophys. Res. Atmos.*, **119**, 6653–6665, doi:10.1002/2013JD021333.

——, ——, and M. D. Zelinka, 2016: Observational constraints on mixed-phase clouds imply higher climate sensitivity. *Science*, **352**, 224–227, doi:10.1126/science.aad5300.

Taylor, J. W., and Coauthors, 2016: Observations of cloud microphysics and ice formation during COPE. *Atmos. Chem. Phys.*, **16**, 799–826, doi:10.5194/acp-16-799-2016.

Tessendorf, S. A., and Coauthors, 2012: The Queensland Cloud Seeding Research Program. *Bull. Amer. Meteor. Soc.*, **93**, 75–90, doi:10.1175/BAMS-D-11-00060.1.

——, B. Boe, B. Geerts, M. J. Manton, S. Parkinson, and R. Rasmussen, 2015: The future of winter orographic cloud seeding: A view from scientists and stakeholders. *Bull. Amer. Meteor. Soc.*, **96**, 2195–2198, doi:10.1175/BAMS-D-15-00146.1.

Thompson, D. R., B.-C. Gao, R. O. Green, D. A. Roberts, P. E. Dennison, and S. Lundeen, 2015: Atmospheric correction for global mapping spectroscopy: ATREM advances for the HyspIRI preparatory campaign. *Remote Sens. Environ.*, **167**, 64–77, doi:10.1016/j.rse.2015.02.010.

——, and Coauthors, 2016: Measuring cloud thermodynamic phase with shortwave infrared imaging spectroscopy. *J. Geophys. Res. Atmos.*, **121**, 9174–9190, doi:10.1002/2016JD024999.

Tremblay, A., A. Glazer, W. Yu, and R. Benoit, 1996: A mixed-phase cloud scheme based on a single prognostic equation. *Tellus*, **48A**, 483–500, doi:10.1034/j.1600-0870.1996.t01-3-00001.x

Tsushima, Y., and Coauthors, 2006: Importance of the mixed-phase cloud distribution in the control climate for assessing the response of clouds to carbon dioxide increase: A multi-model study. *Climate Dyn.*, **27**, 113–126, doi:10.1007/s00382-006-0127-7.

Turner, D. D., S. A. Ackerman, B. A. Baum, H. E. Revercomb, and P. Yang, 2003: Cloud phase determination using ground-based AERI observations at SHEBA. *J. Appl. Meteor.*, **42**, 701–715, doi:10.1175/1520-0450(2003)042<0701:CPDUGA>2.0.CO;2.

——, S. A. Clough, J. C. Liljegren, E. E. Clothiaux, K. E. Cady-Pereira, and K. L. Gaustad, 2007: Retrieving liquid water path and precipitable water vapor from the Atmospheric Radiation Measurement (ARM) microwave radiometers. *IEEE Trans. Geosci. Remote Sens.*, **45**, 3680–3690, doi:10.1109/TGRS.2007.903703

Twomey, S., 1974: Pollution and planetary albedo. *Atmos. Environ.*, **8**, 1251–1256, doi:10.1016/0004-6981(74)90004-3.

van der Hage, J. C. H., 1995: A parameterization of the Wegener-Bergeron-Findeisen effect. *Atmos. Res.*, **39**, 201–214, doi:10.1016/0169-8095(95)00013-H.

Verlinde, J., and Coauthors, 2007: The Mixed-Phase Arctic Cloud Experiment. *Bull. Amer. Meteor. Soc.*, **88**, 205–221, doi:10.1175/BAMS-88-2-205.

Vivekanandan, J., B. E. Martner, M. K. Politovich, and G. Zhang, 1999: Retrieval of atmospheric liquid and ice characteristics using dual-wavelength radar observations. *IEEE Trans. Geosci. Remote Sens.*, **37**, 2325–2334, doi:10.1109/36.789629.

Vochezer, P., E. Järvinen, R. Wagner, P. Kupiszewski, T. Leisner, and M. Schnaiter, 2016: In situ characterization of mixed-phase clouds using the Small Ice Detector and the Particle Phase Discriminator. *Atmos. Meas. Tech.*, **9**, 159–177, doi:10.5194/amt-9-159-2016.

Wallace, J. M., and P. V. Hobbs, 1975: *Atmospheric Science: An Introductory Survey.* Academic Press, 467 pp.

Wang, Z., 2007: A refined two-channel microwave radiometer liquid water path retrieval for cold regions by using multiple-sensor measurements. *IEEE Geosci. Remote Sens. Lett.*, **4**, 591–595, doi:10.1109/LGRS.2007.900752.

——, and K. Sassen, 2001: Cloud type and macrophysical property retrieval using multiple remote sensors. *J. Appl. Meteor.*, **40**, 1665–1682, doi:10.1175/1520-0450(2001)040<1665:CTAMPR>2.0.CO;2.

——, and ——, 2002: Cirrus cloud microphysical property retrieval using lidar and radar measurements. Part I: Algorithm description and comparison with in situ data. *J. Appl. Meteor.*, **41**, 218–229, doi:10.1175/1520-0450(2002)041<0218:CCMPRU>2.0.CO;2.

——, ——, D. N. Whiteman, and B. B. Demoz, 2004: Studying altocumulus with ice virga using ground-based active and passive remote sensors. *J. Appl. Meteor.*, **43**, 449–460, doi:10.1175/1520-0450(2004)043<0449:SAWIVU>2.0.CO;2.

——, P. Wechsler, W. Kuestner, J. French, A. Rodi, B. Glover, M. Burkhart, and D. Lukens, 2009: Wyoming Cloud Lidar: Instrument description and applications. *Opt. Express*, **17**, 13 576–13 587, doi:10.1364/OE.17.013576.

——, and Coauthors, 2012: Single aircraft integration of remote sensing and in situ sampling for the study of cloud microphysics and dynamics. *Bull. Amer. Meteor. Soc.*, **93**, 653–668, doi:10.1175/BAMS-D-11-00044.1.

——, and Coauthors, 2013: CloudSat Project: Level 2 combined radar and lidar cloud scenario classification product process description and interface control document. California Institute of Technology JPL, 61 pp.

Wegener, A., 1911: *Thermodynamik der Atmosphäre.* J. A. Barth, 331 pp.

Weickmann, H., 1945: Formen und Bildung atmosphärischer Eiskristalle. *Beitr. Phys. Freien Atmos.*, **28**, 12–52.

Williams, E. R., 1985: Large-scale charge separation in thunderclouds. *J. Geophys. Res.*, **90**, 6013–6025, doi:10.1029/JD090iD04p06013.

——, and D. J. Boccippio, 1993: Dependence of cloud microphysics and electrification on mesoscale vertical air motions in stratiform precipitation. *Conf. on Atmospheric Electricity*, St. Louis, MO, Amer. Meteor. Soc., 825–831.

——, and Y. Yair, 2006: The microphysical and electrical properties of sprite-producing thunderstorms. *Sprites, Elves and Intense Lightning Discharges*, M. Füllekrug, E. A. Mareev, and M. J. Rycroft, Eds., NATO Science Series II: Mathematics, Physics and Chemistry, Springer, 225 pp.

——, R. Zhang, and J. Rydock, 1991: Mixed-phase microphysics and cloud electrification. *J. Atmos. Sci.*, **48**, 2195–2203, doi:10.1175/1520-0469(1991)048<2195:MPMACE>2.0.CO;2.

——, V. C. Mushtak, D. Rosenfeld, S. J. Goodman, and D. J. Boccippio, 2005: Thermodynamic conditions favorable to superlative thunderstorm updraft, mixed phase microphysics and lightning flash rate. *Atmos. Res.*, **76**, 288–306, doi:10.1016/j.atmosres.2004.11.009.

——, and Coauthors, 2010: Ground-based detection of sprites and their parent lightning flashes over Africa during the 2006 AMMA campaign. *Quart. J. Roy. Meteor. Soc.*, **136**, 257–271, doi:10.1002/qj.489.

Williams, J. K., and J. Vivekanandan, 2007: Sources of error in dual-wavelength radar remote sensing of cloud liquid water content. *J. Atmos. Oceanic Technol.*, **24**, 1317–1336, doi:10.1175/JTECH2042.1.

Wood, R., and P. R. Field, 2000: Relationships between total water, condensed water, and cloud fraction in stratiform clouds examined using aircraft data. *J. Atmos. Sci.*, **57**, 1888–1905, doi:10.1175/1520-0469(2000)057<1888:RBTWCW>2.0.CO;2.

Workman, E. J., and S. E. Reynolds, 1949: Electrical activity as related to thunderstorm growth. *Bull. Amer. Meteor. Soc.*, **30**, 142–144.

Yang, F., M. Ovchinnikov, and R. A. Shaw, 2013: Minimalist model of ice microphysics in mixed-phase stratiform clouds. *Geophys. Res. Lett.*, **40**, 3756–3760, doi:10.1002/grl.50700.

——, ——, and ——, 2014: Microphysical consequences of the spatial distribution of ice nucleation in mixed-phase stratiform clouds. *Geophys. Res. Lett.*, **41**, 5280–5287, doi:10.1002/2014GL060657.

Yu, G., J. Verlinde, E. E. Clothiaux, and Y.-S. Chen, 2014: Mixed-phase cloud phase partitioning using millimeter wavelength cloud radar Doppler velocity spectra. *J. Geophys. Res. Atmos.*, **119**, 7556–7576, doi:10.1002/2013JD021182.

Zak, E. G., 1949: Microstructure of frontal clouds. *Sov. Meteor. Hydrol.*, **6**, 24–33.

Zawadzki, I., F. Fabry, and W. Szyrmer, 2001: Observations of supercooled water and secondary ice generation by a vertically pointing X-band Doppler radar. *Atmos. Res.*, **59–60**, 343–359, doi:10.1016/S0169-8095(01)00124-7.

Zhang, D., Z. Wang, and D. Liu, 2010: A global view of mid-level liquid-layer topped stratiform cloud distribution and phase partition from CALIPSO and CloudSat measurements. *J. Geophys. Res.*, **115**, D00H13, doi:10.1029/2010JD014030.

——, ——, A. J. Heymsfield, J. Fan, D. Liu, and M. Zhao, 2012: Quantifying the impact of dust on heterogeneous ice generation in midlevel supercooled stratiform clouds. *Geophys. Res. Lett.*, **39**, L18805, doi:10.1029/2012GL052831.

Zhao, C., and Coauthors, 2012: Towards understanding of differences in current cloud retrievals of ARM ground-based measurements. *J. Geophys. Res.*, **117**, D10206, doi:10.1029/2011JD016792.

Zhao, M., and Z. Wang, 2010: Comparison of Arctic clouds between European Center for Medium-Range Weather Forecasts simulations and Atmospheric Radiation Measurement Climate Research Facility long-term observations at the North Slope of Alaska Barrow site. *J. Geophys. Res.*, **115**, D23202, doi:10.1029/2010JD014285.

Zuidema, P., E. R. Westwater, C. Fairall, and D. Hazen, 2005: Ship-based liquid water path estimates in marine stratocumulus. *J. Geophys. Res.*, **110**, D20206, doi:10.1029/2005JD005833.